

Technical Report Documentation Page

1. Report No. FHWA/TX-03/2109-1		2. Government Accession No.		3. Recipient's Catalog No.	
4. Title and Subtitle HYDRAULICS OF CHANNEL EXPANSIONS LEADING TO LOW-HEAD CULVERTS				5. Report Date October 2002	
				6. Performing Organization Code	
7. Author(s) Randall J. Charbeneau, Andrew D. Henderson, Ryan C. Murdock, Lee C. Sherman				8. Performing Organization Report No. 2109-1	
9. Performing Organization Name and Address Center for Transportation Research The University of Texas at Austin 3208 Red River, Suite 200 Austin, TX 78705-2650				10. Work Unit No. (TRAIS)	
				11. Contract or Grant No. 0-2109	
12. Sponsoring Agency Name and Address Texas Department of Transportation Research and Technology Implementation Office P.O. Box 5080 Austin, TX 78763-5080				13. Type of Report and Period Covered Research Report	
				14. Sponsoring Agency Code	
15. Supplementary Notes Project conducted in cooperation with the U.S. Department of Transportation, Federal Highway Administration, and the Texas Department of Transportation.					
16. Abstract Channel improvements involving channel expansion upstream of culverts may result in increased sediment deposition near the structure, which in turn may result in decreased hydraulic performance and safety. These conditions are investigated through physical and numerical modeling. An improved understanding of the hydraulic performance of channel expansions is developed, improved performance curves for multiple-barrel box culverts are presented, design guidance for new structures are provided, and potential remedies for existing structures are suggested.					
17. Key Words Box culverts, channel expansions, performance curves, physical modeling, numerical modeling				18. Distribution Statement No restrictions. This document is available to the public through the National Technical Information Service, Springfield, Virginia 22161.	
19. Security Classif. (of report) Unclassified		20. Security Classif. (of this page) Unclassified		21. No. of pages 114	
22. Price					



Hydraulics of Channel Expansions Leading to Low-Head Culverts

Randall J. Charbeneau
Andrew D. Henderson
Ryan C. Murdock
Lee C. Sherman

CTR Research Report: 2109-1
Report Date: October 2002
Research Project: 0-2109
Research Project Title: *Evaluate the Effects of Channel Improvements,
Especially Channel Transitions, on Culverts and Bridges*

This research was conducted for the Texas Department of Transportation in cooperation with the U.S. Department of Transportation, Federal Highway Administration by the Center for Transportation Research, Bureau of Engineering Research, The University of Texas at Austin.

Center for Transportation Research
The University of Texas at Austin
3208 Red River
Austin, TX 78705

www.utexas.edu/research/ctr

Copyright © 2003
Center for Transportation Research
The University of Texas at Austin

All rights reserved
Printed in the United States of America

Disclaimers

Authors' Disclaimer: The contents of this report reflect the views of the authors, who are responsible for the facts and the accuracy of the data presented herein. The contents do not necessarily reflect the official view or policies of the Federal Highway Administration or the Texas Department of Transportation. This report does not constitute a standard, specification, or regulation.

Patent Disclaimer: There was no invention or discovery conceived or first actually reduced to practice in the course of or under this contract, including any art, method, process, machine manufacture, design or composition of matter, or any new useful improvement thereof, or any variety of plant, which is or may be patentable under the patent laws of the United States of America or any foreign country.

Engineering Disclaimer

NOT INTENDED FOR CONSTRUCTION, BIDDING, OR PERMIT PURPOSES.

Project Engineer: Randall J. Charbeneau, P.E.
Professional Engineer License Number: Texas No. 56662
P. E. Designation: "Research Supervisor"

Acknowledgments

The authors would like to express appreciation to George (Rudy) Herrmann, TxDOT project director for this study, for his guidance, support, and continued interest in this research. The authors also wish to thank Edward R. Holley and Ben Hodges for their technical support.

Table of Contents

1. Introduction	1
1.1 Background and Significance of Work	1
1.2 Study Objectives.....	3
1.3 Overview	4
2. Literature Review	5
2.1 Energy Losses in Open Channel Flow	5
2.2 Hydraulics of Channel Expansions	5
2.3 Hydraulics of (Box) Culverts	9
2.3.1 Previous Investigations of Culvert Hydraulics	10
2.3.2 Unsubmerged Entrance Under Inlet Control	13
2.3.3 Submerged Entrance Under Inlet Control.....	16
2.4 Hydraulic Similitude	17
2.5 Numerical Modeling of Culvert Hydraulics.....	19
2.5.1 FESWMS for Two-Dimensional Hydraulic Modeling.....	19
2.5.2 Governing Equations.....	21
2.5.3 Application of Two-Dimensional Models	24
3. Physical Model System and Experiment Procedures	27
3.1 Overview	27
3.2 Design of Physical Model	27
3.3 Description of the Physical Model	28
3.3.2 Water Supply and Upstream Channel Section.....	28
3.3.3 Channel Expansion Section	30
3.3.4 Tailgate Section.....	32
3.3.5 Culvert Model	32
3.3.6 Rails and Trolleys	33
3.4 Data Acquisition.....	34
3.4.1 Channel Discharge	34
3.4.2 Water Depth	37
3.4.3 Water Velocity with ADV	37
3.4.4 Water Velocity with Pitot Tubes.....	39
3.4.5 Depth-Averaged Velocities.....	39
3.4.6 Specific Energy	40
4. Physical Model Experiment Results	41
4.1 Overview	41
4.2 Distribution of Velocity.....	41
4.2.1 Vertical Velocity Distribution.....	41
4.2.2 Distribution of Velocity with Cross Section.....	43

4.3	Distribution of Specific Energy Upstream of the Culvert System	45
4.3.1	Variation of Specific Energy with Distance Upstream of the Culvert System	45
4.3.2	Variation of Specific Energy with Cross-Section	48
4.4	Performance Curves for Box Culverts	50
4.4.1	Development of Performance Curve Equations.....	50
4.4.2	Fitting of the Performance Curves.....	53
5.	FESWMS Modeling.....	61
5.1	Introduction	61
5.2	Data Collection	61
5.3	Numerical Model Network Design	63
5.3.1	Network Development Process.....	64
5.3.2	Culvert Representation in FESWMS	66
5.4	Model Debugging.....	68
5.5	Model Testing/Calibration/Validation.....	71
5.5.1	Overview	71
5.5.2	Eddy Viscosity Model.....	71
5.5.3	Calibration Process	73
5.5.4	Model Validation	78
5.6	Model Application to Expansion Ratio Effects.....	79
6.	Design Procedures and Remedies	85
6.1	Introduction	85
6.2	Design of Box Culverts for Inlet Control	85
6.2.1	Development of Design Equations	85
6.2.2	Example Problem.....	86
6.3	Use of Gabions as Remedy for Hydraulic Performance	87
6.3.1	Physical Model Experiments	87
6.3.2	Numerical Model Experiments	90
7.	Summary and Conclusions	93
7.1	Summary.....	93
7.2	Conclusions and Recommendations.....	94
	References.....	97

List of Figures

Figure 1.1 Approximate centerline of approach channel of multiple-barrel box culvert near San Angelo, Texas	2
Figure 1.2 Upstream view from culvert showing poorly defined channel	2
Figure 1.3 Downstream view showing wide channel with no obstructions	3
Figure 1.4 Sediment accumulation within the culvert boxes	3
Figure 2.1 Schematic plan view of flow at bridge openings.....	7
Figure 2.2 (a) Front view of box culvert with span B and rise D . (b) Profile view of box culvert showing energy grade line (dashed), water surface profile (solid), and control section located distance L' downstream from culvert entrance.....	14
Figure 2.3 Comparison of performance curves for the FHWA model (equations (2.27) and (2.31)) as the solid curves and the model equations of Henderson (equations (2.29) and (2.32)) as the dashed curves.....	17
Figure 3.1 Schematic view of the physical model	28
Figure 3.2 Schematic view of the water distribution system	29
Figure 3.3 Channel headbox and flow straighteners.....	29
Figure 3.4 Abrupt channel expansion looking upstream towards the headbox	30
Figure 3.5 Modified channel expansion.....	31
Figure 3.6 Six-barrel culvert model with headwall and wingwalls	33
Figure 3.7 Measurement trolley.....	34
Figure 3.8 Propeller meter	35
Figure 3.9 Large reservoir used for propeller meter calibration.....	36
Figure 3.10 Propeller meter calibration	36
Figure 3.11 Down-looking ADV probe.....	38
Figure 3.12 ADV velocity output for down-looking probe	38
Figure 3.13 Logarithmic velocity profile extrapolation for estimation of the average velocity.....	40
Figure 4.1 Typical velocity profile at 1.22 meters upstream of the channel expansion, where the depth is 24.5 cm and the average velocity is 65 cm/s	42
Figure 4.2 Vertical velocity distribution at a centerline location 1.22 meters downstream of the channel expansion where the depth is 23.5 cm and the average velocity is 71.2 cm/s	42

Figure 4.3 Cross-section distribution of depth-averaged velocity as a function of distance downstream of the abrupt channel expansion for a discharge of 6.05 cfs.....	43
Figure 4.4 Cross-section distribution of depth-averaged velocity as a function of downstream distance from the channel expansion (channel discharge = 6.21 ft ³ /s), with the culvert in place at a distance 20 ft downstream of the expansion.....	44
Figure 4.5 Lateral distribution of velocity for a range of channel discharge values with unsubmerged inlet conditions (Q in ft ³ /s).....	45
Figure 4.6 Variation of specific energy with distance upstream of the culvert for different discharge values (Q in ft ³ /s) and number of barrels.....	46
Figure 4.7 Variation of E/D with upstream distance for transverse locations across the channel cross section. Channel centerline is at 134 ft.	47
Figure 4.8 Variation in specific energy with transverse location for data set of Figure 4.7	47
Figure 4.9 Lateral variation of specific energy for unsubmerged inlet experiments (Q in ft ³ /s).....	48
Figure 4.10 Lateral variation of specific energy for submerged inlet conditions with 4 and 6 barrels open.....	49
Figure 4.11 Standing wave at culvert inlet	50
Figure 4.12 Culvert entrance acting as a submerged sluice gate	53
Figure 4.13 Box culvert performance data	55
Figure 4.14 Performance curve plus/minus one standard error	56
Figure 4.15 Constrained ($C_b = 1$) performance curve with standard error	57
Figure 4.16 Comparison of performance curves.....	58
Figure 4.17 Performance data showing depth versus specific energy and that data includes both subcritical and supercritical flow conditions.....	59
Figure 5.1 Calibration point locations in physical model.....	62
Figure 5.2 Velocity component comparisons for physical model data.....	63
Figure 5.3 Example of a two-dimensional finite element with node points	63
Figure 5.4 Setup of conceptual model	65
Figure 5.5 Coons Patch and Tessellation mesh generation techniques	65
Figure 5.6 Completed version of finite element network	68
Figure 5.7 Closed boundary slip conditions	70
Figure 5.8 Calibration of velocity magnitude (ft/s) values.....	74

Figure 5.9 Velocity vectors near abrupt expansion in calibration solution, with the upper boundary of the figure representing the channel centerline.....	75
Figure 5.10 Comparison of water depths (feet) in the calibration solution	75
Figure 5.11 Varying expansion ratio schematic	80
Figure 5.12 Velocity vectors and contours for abrupt expansion	80
Figure 5.13 Stagnation zone for abrupt expansion	81
Figure 5.14 Velocity vectors and contours for 4:1 expansion ratio.....	81
Figure 5.15 Basis functions and weights for calculation of barrel discharge	83
Figure 5.16 Flow distribution through culvert boxes for all expansion ratios.....	83
Figure 6.1 Specific energy distribution across culvert barrels (discharge in ft ³ /s).....	88
Figure 6.2 Distribution of specific energy with and without gabions present	89
Figure 6.3 Lack of impact of gabions on flow distribution	90
Figure 6.4 Gabion located along the channel centerline.....	91
Figure 6.5 Gabion pair located off-center.....	91
Figure 6.6 Flow distribution from FESWMS model simulations with and without gabions present	92

List of Tables

Table 5.1 Calibration results for water depth magnitudes (CL = centerline)	76
Table 5.2 Calibration results for water velocity magnitudes	77
Table 5.3 Froude number comparison for calibration model	78
Table 5.4 Validation results for water depth and velocity (CL = centerline)	79

1. Introduction

1.1 Background and Significance of Work

Channel improvements involving channel expansion upstream of culverts and bridges may result in increased sediment deposition near the structure, which in turn may result in decreased hydraulic performance. The purpose of this research is to evaluate the hydraulic performance of channel expansions upstream of highway structures. The research emphasis is placed on highway culverts. This evaluation includes literature review, physical modeling experiments, and numerical modeling experiments.

Highway construction and improvements require consideration of natural drainage patterns of small streams. Bridges and culverts (box and pipe) are constructed to allow the passage of natural and storm flows through highway embankments. Design criteria are based on allowing passage of design flows while maintaining a minimum freeboard upstream of the embankment. These criteria dictate structure size, and may require multiple barrels when culverts are used. The normal design of channel improvements for culverts and bridges involves contraction of the channel upstream of the openings, and expansion to the natural channel width on the downstream side. A significant body of experience and literature exists for these conditions, especially with regard to backwater effects and use of backwater stage to estimate channel discharge for flood analyses. In cases where the design procedure suggests that required size and geometry extend beyond the width of the natural channel, artificial channel transitions are also required to convey water to and from the structure openings. These transitions disturb the natural channel regime, and may have undesirable consequences.

Figure 1.1 shows a multiple-barrel box culvert located near San Angelo, Texas, as viewed from the upstream side. The culvert has six barrels, each of which is 6 feet (1.8 meters) high (rise) and 10 feet (3 meters) wide (span). The location from which the picture was taken is roughly in the middle of the approach channel. Conditions resulting from channel erosion are visible in this location and downstream. In Figure 1.1, the entrance to each barrel appears to be clear of debris. However, this picture was taken following maintenance by the Texas Department of Transportation (TxDOT) where the entrance section was cleared of debris and sediment. While it is not apparent from the figure, the width of the upstream channel section is much narrower than the culvert span. Such an expansion upstream of a culvert or bridge is contrary to normal design, and a focus of this research is to determine the hydraulic effects of upstream channel expansions on culvert performance.



Figure 1.1 Approximate centerline of approach channel of multiple-barrel box culvert near San Angelo, Texas

Figure 1.2 provides two views looking upstream from the culvert. The approach channel is poorly defined and is significantly narrower than the multiple-barrel culvert width. The channel transition occurs within the highway right-of-way.



Figure 1.2 Upstream view from culvert showing poorly defined channel

Figure 1.3 shows a view looking downstream from the culvert section. The channel remains wide and is poorly defined. There are no obstructions to retard the flow and cause backwater effects. Figure 1.4 shows sediment accumulation within the culvert boxes. This accumulation remained after TxDOT maintenance was performed at the culvert entrance.



Figure 1.3 Downstream view showing wide channel with no obstructions



Figure 1.4 Sediment accumulation within the culvert boxes

This case near San Angelo, Texas, suggests that widening a channel upstream of culverts and bridges can lead to increased local sediment accumulation within and upstream of the structures. Due to this accumulation and loss of capacity, wide culvert systems and bridges may not perform according to design, resulting in decreased safety and increased costs for maintenance.

1.2 Study Objectives

The overall goals of this research are to develop an improved understanding of the hydraulics of channel transitions and associated sediment movement and/or deposition, especially related to channel expansions leading to wide culverts and bridges; to develop improved design procedures that will aid in avoiding performance characteristics seen

within the case studied above; and to identify remedies for existing culverts. These overall goals are to be achieved through use of physical and numerical simulation models.

The specific objectives that are addressed through this research are as follows:

1. Evaluate the hydraulic performance of the channel expansion from a trapezoidal (nonrectangular) channel.
2. Determine the hydraulic performance of box culverts for single and multiple-barrel systems.
3. Determine the distribution of discharge and specific energy through different barrels of a multiple-barrel culvert system.
4. Calibrate the numerical model, FESWMS, to existing physical model conditions.
5. Apply the calibrated model to investigate and identify potential remedies for existing culvert systems.
6. Evaluate the applicability of FESWMS for practical application to the class of problems addressed through this research.

1.3 Overview

There is extensive literature dealing with culvert performance, with much emphasis placed on different types of end treatments for different barrel shapes. However, there is scant literature dealing with the hydraulic performance of channel expansions leading to wide multiple-barrel culverts. Relevant literature and background material is presented in Chapter 2. Chapter 3 describes the physical model system, equipment used, and experiment procedures. In Chapter 4, the experiment results are presented and discussed. Chapter 5 describes the FESWMS model and its application. Chapter 6 addresses design procedures and possible remedies for existing culvert systems, while Chapter 7 provides a summary and conclusions.

2. Literature Review

2.1 Energy Losses in Open Channel Flow

The analysis of open channel flow is based on the continuity principle, the energy equation, and occasionally the momentum equation from fluid mechanics. Steady, nonuniform (varied) open channel flow is analyzed assuming gradually varied flow conditions, while channel transitions frequently have rapidly varied flow. The standard procedure for analysis of gradually varied flow hydraulics is the one-dimensional energy equation, which may be written between two stations in a flow (Chow, 1959)

$$z_1 + y_1 + \alpha_1 \frac{v_1^2}{2g} = z_2 + y_2 + \alpha_2 \frac{v_2^2}{2g} + h_f + h_e \quad (2.1)$$

In equation (2.1) z is the elevation of the channel bottom (invert), y is the depth of water at the cross section, v is the average velocity (discharge/area), α is a velocity weighting coefficient that accounts for the nonuniform kinetic energy distribution across the channel section, h_f is the friction loss between the two sections, and h_e is the eddy loss associated with channel expansions and contractions. The friction loss is calculated from Manning's equation, which may be written for the channel discharge Q in the form

$$Q = K S_f^{1/2} \quad (2.2)$$

In equation (2.2), K is called the conveyance ($K = \phi A R_h^{2/3}/n$; where $\phi = 1.486$ in standard English units and $\phi = 1$ in metric units, A is the cross-section area, R_h is the hydraulic radius, and n is the Manning's roughness coefficient), and S_f is the friction slope ($S_f = h_f/L$, for effective channel length L between stations 1 and 2). With Manning's equation (2.2), the friction loss between the stations is calculated from

$$h_f = L \frac{Q^2}{K^2} \quad (2.3)$$

For gradually varied flow with possible changes in channel discharge, there are alternative ways to estimate effective Q 's and K 's to calculate the friction loss (see for example HEC, 1998). Expansion and contraction losses are discussed in the following section that considers the hydraulics of channel transitions.

2.2 Hydraulics of Channel Expansions

A channel transition is a change in the direction, slope, or cross section of an open channel that produces a change in the state of the flow (Henderson, 1966). Transitions frequently have rapidly varied flow. This research is primarily concerned with channel expansions, which generally include a change in channel cross-section geometry. Issues

involved in design of channel transitions (expansions) depend on whether flow is subcritical or supercritical, or whether the transition acts as a control with the flow passing through critical stage. The focus of this research is on flow conditions that remain subcritical upstream and downstream of the culvert system. Froude numbers (Fr) are less than one. The *primary function of design* of channel transitions has usually been to avoid excessive energy losses and to eliminate cross-waves, which may be a significant problem in supercritical flow (Chow, 1959; Henderson, 1966). While major energy losses due to bed friction and turbulence will occur within channel transitions, additional losses are associated with expansion and contraction of the flow.

Approaches for quantification of these expansion and contraction losses vary. Even with the assumption of one-dimensional flow, exact solutions are not available except for the simplest of conditions. As an example, for an *abrupt-rectangular expansion* with no change in elevation of the channel base, Henderson (1966) presents the following approximate result for change in specific energy (good for small Froude numbers, neglecting terms of order Fr_1^4)

$$\Delta E = \frac{v_1^2}{2g} \left[\left(1 - \frac{b_1}{b_2} \right)^2 + \frac{2Fr_1^2 b_1^3 (b_2 - b_1)}{b_2^4} \right] \quad (2.4)$$

In equation (2.4) the subscript 1 refers to upstream conditions and subscript 2 refers to downstream conditions, b is the channel width, and Fr_1 is the Froude number at section 1. The first term within the brackets of equation (2.4) is what one would obtain for closed-conduit energy losses through an abrupt expansion. The second term accounts for open channel flow effects. In the limit for small Froude numbers, equation (2.4) becomes

$$\Delta E = \frac{(v_1 - v_2)^2}{2g} \quad (2.5)$$

Equation (2.5), along with a multiplying coefficient, suggests an appropriate form for calculation of energy losses through expansions. Abrupt expansions are not often used because of excessive energy losses. Instead, smooth transitions are usually used between differing prismatic channel cross sections.

The hydraulic performance of more general channel transitions may be analyzed numerically using either one-dimensional or two-dimensional flow models. While two-dimensional models are better capable of capturing flow phenomena in channel expansions that relate to cross-section shape, channel roughness, and flow distribution, there is a significant overhead (learning time) in their use, and they are unlikely to become standard tools for application during design in the near future. Furthermore, it is difficult to integrate the results from two-dimensional flow models with one-dimensional hydraulics models such as HEC-RAS (HEC, 1998) or WSPRO (FHWA, 1986) that are regularly used for analysis of water levels along the channel length. Physical models can also be used to study the flow phenomena.

Empirical models are used to estimate transition losses in one-dimensional models. Within the HEC-RAS model, these additional eddy losses are calculated from

$$h_e = C \left| \alpha_1 \frac{v_1^2}{2g} - \alpha_2 \frac{v_2^2}{2g} \right| \quad (2.6)$$

In equation (2.6) C is the expansion or contraction loss coefficient. For gradually varying expansions in natural channels, C will vary from approximately 0.2 (Chow, 1959) to 0.3 (HEC, 1998). For more rapid expansions, such as those near wide bridge or culvert system openings, the expansion coefficient will be larger (0.5 or larger). The HEC-RAS total energy loss in the expansion reach downstream from a bridge or culvert opening is the sum of the major loss plus the expansion loss from equation (2.6). This total loss depends on the expansion length L and the expansion coefficient C in equation (2.6).

Transition energy losses are calculated differently in the FHWA-WSPRO model. The computational setup for a bridge opening is shown in Figure 2.1, and is the same as used in HEC-RAS. Four cross sections delineate the computation reaches, numbered from downstream to upstream. Taken in the downstream direction, the flow first contracts to pass through the confined opening. A contracted reach exists between sections 3 and 2. On the downstream side of the opening, the flow expands to the full channel width. This is the configuration expected under normal design conditions (contrary to those studied in this research).

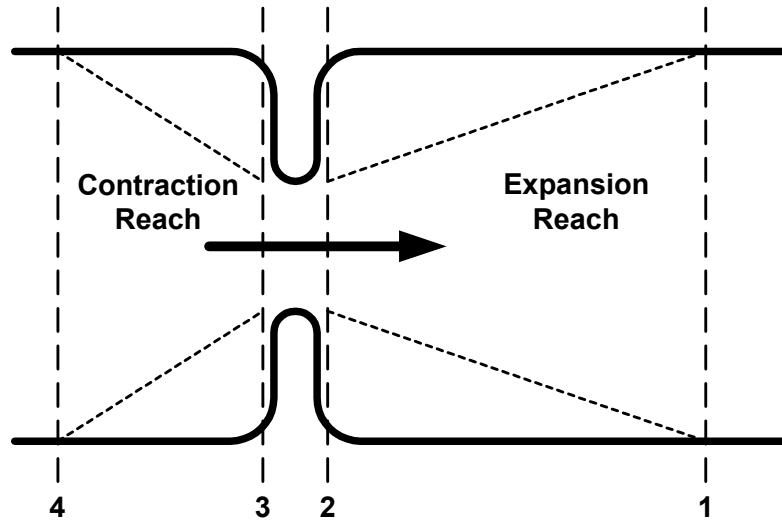


Figure 2.1 Schematic plan view of flow at bridge openings

With reference to Figure 2.1, if K_q is the portion of the total section 4 conveyance contained within the bridge width and K_c is the smaller of the conveyances K_2 and K_q , then the friction losses through the expansion reach are calculated in WSPRO from

$$h_{f(2 \rightarrow 1)} = \frac{b Q^2}{K_1 K_c} \quad (2.7)$$

In equation (2.7) b is the bridge opening width. The corresponding flow expansion losses are calculated from

$$h_e = \frac{Q^2}{2gA_1^2} \left[2(\beta_1 - \alpha_1) - 2\beta_2 \frac{A_1}{A_2} + \alpha_2 \left(\frac{A_1}{A_2} \right)^2 \right] \quad (2.8)$$

In equation (2.8) β_1 and β_2 are the momentum correction factors that account for nonuniform distribution of momentum across the channel section in a one-dimensional model. Derivation of equation (2.8) has not been presented in the literature, and in an investigation of flow transitions for bridge openings, the form of equation (2.8) has been questioned (HEC, 1995).

There are a number of difficulties in applying equation (2.1) with equations (2.3) and (2.6) for HEC-RAS, or with equations (2.7) and (2.8) for WSPRO, to design of channel transitions leading to wide culverts. The distance upstream from the culvert to which the transition effects are insignificant is uncertain. It is not clear how C will vary with distance upstream from the culvert. One-dimensional flow models may fail due to separation of flow within the expansion section. Also, the spatial distribution of the velocity at the cross section immediately upstream of the culvert is difficult to estimate from the average velocity, though this velocity distribution is crucial in determining culvert flows (and design).

Issues associated with the geometry and energy losses through channel expansions have been investigated by a number of researchers. Ippen (1950) states that “wedge and warped transitions produce recovery of 80 to 90 per cent of the velocity-head difference, provided the expansions are of such length that a line connecting the water surfaces at the channel sides between entrance and exit sections forms an angle not larger than $12^\circ 30'$ with the channel axis,” and he references the work of Hinds (1928) and Scobey (1933). This corresponds to an expansion ratio of approximately $4\frac{1}{2}:1$. Albertson et al. (1950) investigated diffusion of submerged jets into a fluid at rest (using air as the fluid) and found that the natural expansion ratio was approximately 4:1. More recent investigations by HEC (1995) focused on the lengths of channel contractions and expansions associated with bridges, according to the geometry shown in Figure 2.1, and with channel contraction and expansion energy loss coefficients C_c and C_e , according to equation (2.6), all of which were to be used in one-dimensional models. One of the preliminary conclusions of the study is that when the traditional expansion ratio of 4:1 (longitudinal to transverse distances) is used in one-dimensional models compared with actual measured water levels, the energy loss in the expansion reach is over-predicted.

In the HEC investigation, the channel lengths and energy loss coefficients were determined through use of a two-dimensional hydrodynamic model, RMA-2 (King, 1994), to simulate flow through a large number of idealized floodplain and bridge geometries. The lengths of transition reaches were estimated from output velocity vector plots. On these plots, lines were subjectively drawn across the floodplain that separate zones of significant lateral flow from the zones of predominantly streamwise flow, and these lines were used to determine the expansion and contraction ratios. With the expansion and contraction lengths determined, the simulations also provided the water surface elevation

along the channel length. Separate HEC-RAS simulations were performed to fit these elevations by adjusting energy loss coefficients C_e and C_c . The resulting expansion/contraction ratios and energy loss coefficients were fit to various regression equations based on flow and geometry parameters.

For all simulations in the HEC (1995) study the floodplain width was 1000 feet. Different combinations of bridge opening width, slope abutment type, total discharge, and overbank roughness were used. From 76 simulations, the average expansion reach length was 564 feet, with values ranging from 260 to 1600 feet. The best-fitting equation for the expansion reach length presented is

$$L_e = -298 + 257 \frac{F_{c2}}{F_{c1}} + 0.918 \bar{L}_{obs} + 0.00479 Q \quad (2.9)$$

In equation (2.9) L_e is the length (in feet) of the expansion reach, F_{c1} and F_{c2} are the main channel Froude numbers at sections 1 and 2 in Figure 2.1, respectively, \bar{L}_{obs} is the average length (in feet) of the obstruction caused by the bridge approaches, and Q is the total discharge (in cfs). The adjusted determination coefficient and standard error of estimate of equation (2.9) are $R^2 = 0.84$ and $S_e = 96$ feet. Similarly, the regression equation for the expansion ratio was found to be

$$ER = \frac{L_e}{\bar{L}_{obs}} = 0.421 + 0.485 \frac{F_{c2}}{F_{c1}} + 0.000018 Q \quad (2.10)$$

with $R^2 = 0.71$ and $S_e = 0.26$ (the standard error is dimensionless in equation 2.10).

The developed regression equations for the energy loss coefficients are not as useful as the expansion ratio equation, partly due to the fact that the velocity head differences were small in many cases. The best regression relationship for the expansion energy loss coefficient is

$$C_e = -0.092 + 0.570 \frac{D_{ob}}{D_c} + 0.075 \frac{F_{c2}}{F_{c1}} \quad (2.11)$$

In equation (2.11) D_{ob} is the hydraulic depth (flow area divided by top width) for the overbank at the normal flow section (section 1) in feet, and D_c is the hydraulic depth (feet) for the main channel at the normal flow section. The coefficient of determination and standard error are $R^2 = 0.55$ and $S_e = 0.10$ (dimensionless). Calibrated values of C_e ranged from 0.10 to 0.65, with a median value of 0.30.

2.3 Hydraulics of (Box) Culverts

A culvert is a covered channel of comparatively short length that is installed to drain water through highway, railroad, and other embankments (Chow, 1959). From a hydraulic point of view, the defining feature of a culvert is that it may or may not run full (Henderson, 1966). A culvert that runs full with both its inlet and outlet submerged

functions as a pressurized conduit, and its hydraulic analysis is straightforward. However, under design conditions, a culvert may have either its inlet or outlet unsubmerged, and the conduit may run partially or totally under unsubmerged conditions; that is, as an open channel. The range of potential operating conditions makes hydraulic analysis and design of culverts challenging. Nevertheless, the hydraulic performance of culverts has been extensively studied, and design guidance exists within the technical literature.

Culverts may operate under either inlet or outlet control conditions. Inlet control occurs when the culvert barrel is capable of conveying more flow than the inlet will accept. The control section of a culvert operating under inlet control is located just inside the entrance. Critical depth occurs at or near this location, and the flow regime immediately downstream is supercritical (Normann et al., 2001, p. 7). Only the headwater and the inlet configuration affect the culvert performance. Important factors include the headwater depth, the inlet area, the barrel shape and the inlet edge configuration (Herr and Bossy, 1965). Use of beveled or grooved inlets may improve culvert performance by decreasing entrance losses and increasing effective inlet area. Outlet control flow occurs when the culvert barrel is not capable of conveying as much discharge as the inlet opening will accept. Under outlet control, in addition to the same factors for inlet control, the barrel length, barrel roughness, barrel slope, and tailwater depth determine culvert performance. The design procedures and equations differ for inlet and outlet control. In design, both conditions are analyzed separately, and that which predicts the largest headwater value is assumed to govern.

Following a brief review of studies of culvert hydraulics, the basic equations for design and analysis of culverts operating under inlet control will be presented. The primary emphasis is on inlet control conditions with small headwater (unsubmerged) because these conditions are most relevant to design of highway culverts with limited culvert rise and unobstructed downstream area. However, submerged inlets operating under inlet control are also considered.

2.3.1 Previous Investigations of Culvert Hydraulics

Among the earliest investigations of culvert hydraulics are the observations on the Miami Flood Control Project reported by S. M. Woodward in 1920 (Mavis, 1943). Woodward presented two hypotheses to describe culvert hydraulics:

1. The culvert flows partly full and the inlet serves as a control section. For a given culvert the discharge is accordingly a function of the elevation of the headwater pond above the invert of the culvert at the inlet.
2. The culvert flows entirely full and for a given culvert the discharge is a function only of the difference between headwater and tailwater levels.

Yarnell et al. (1926) reported on the first exhaustive set of experiments based on these hypotheses. While they included some tests on culverts flowing partly full, most tests were of full culverts. The most significant contributions from these tests were the evaluation under actual operating conditions of roughness factors for concrete, corrugated metal, and vitrified clay pipe culverts and box concrete culverts, and a preliminary evaluation of the effect of entrance conditions on the flow of water through culverts of various types.

Mavis (1943) recognized that there is a significant gap between the set of conditions proposed by Woodward to describe culvert hydraulics, and reports on a series of experiments using circular pipe culverts. He identified five categories of culvert flow. These include part-full and full conduits with free outfall and partially submerged outfall conditions. Mavis recognized that discharge of culverts flowing part-full could be represented through a function of $Q/D^{5/2}$ versus H/D , where Q is the discharge, D the culvert diameter, and H the elevation of headwater pool above inlet invert, though he was not able to identify an analytical basis for this function using the rational of critical flow in culvert segments. However, he did present a nomograph based on empirical data for circular pipe culvert discharge under inlet conditions that is similar to the nomograph developed for FHWA that is in current use.

Metzler and Rouse (1959) provide a review of hydraulics as it applies to box culverts. Experimentally, they consider only square box culverts. For perspective, they note that hydraulic measurements can be made with an accuracy of 1% to 10% in the laboratory and field, while hydrologic estimates involve uncertainties as much as 200%. Thus precision in culvert design is unnecessary, though it is important to understand the performance of different culvert attributes for a range of flows that can exceed design discharge, and an appreciation of hydraulic principles is essential for this understanding. Metzler and Rouse divide their discussion of culvert hydraulics into cases with mild or steep slope, based on the depth of flow just before the culvert begins to flow full. For a mild slope culvert, they state that the control is located at the downstream end “either in the form of the free overfall at critical depth, if the outlet is unsubmerged, or as the beginning of a backwater curve if the tailwater is of sufficient depth.” This does not recognize conditions of inlet control where the barrel characteristics do not play a significant role in culvert performance. For unsubmerged inlet conditions they present the discharge function in the form

$$\frac{Q}{\sqrt{g} b^{5/2}} = K \left(\frac{H}{b} \right)^{3/2} \quad (2.12)$$

In equation (2.12), Q is the culvert barrel discharge, g is the gravitational constant, b is the square-barrel size (span and rise), H is the depth of the inlet pool above the barrel invert, and K is a factor that depends on culvert characteristics. The equation (2.12) is similar in form to the equations for flow over a weir. While Metzler and Rouse do not give a specific value, their experimental data (presented in their Figure 15) suggest that K has a value of about 0.465 for both square and rounded inlets. For conditions of inlet submergence, Metzler and Rouse (1959) suggest that the discharge function takes the form

$$\frac{Q}{\sqrt{g} b^{5/2}} = K \left(\frac{H + \Delta h}{b} \right)^{1/2} \quad (2.13)$$

In equation (2.13) Δh is the further change in head over the length of the barrel, and K is a different factor that depends on culvert characteristics. Equation (2.13) is similar in form to the orifice equation. Their Figure 16 shows that for a sharp-edged inlet, K has an

approximate value $K = 1/\sqrt{2} \cong 0.707$. For a rounded inlet, there is a larger discharge for the same head difference, with values also depending on the barrel length. Metzler and Rouse also discuss culvert performance on steep slopes, culverts with tapered and hooded inlets, and culverts with discontinuous slope (“broken-back” type).

Under the sponsorship of the Bureau of Public Roads (now the Federal Highway Administration, FHWA), the National Bureau of Standards (now the National Institute of Science and Technology, NIST) conducted an extensive series of experiments to better define the performance of culverts. This research was performed during the 1950’s and 60’s, and forms the basis for many culvert design procedures and computer programs. French (1955) outlines the general scope of the investigations and presents hydraulic characteristics for circular and pipe-arch barrel shapes. French (1966) considered box culverts with nonenlarged (not tapered) inlets and constant barrel size operating under conditions of entrance control, with the objective of identifying the hydraulic performance of different leading edge geometries. For unsubmerged entrance conditions he suggests that the culvert rating-curve may be expressed as the function

$$\frac{Q}{\sqrt{g}BH_t^{3/2}} = f\left(\frac{H}{B}, \beta_s, S\right) \quad (2.14)$$

In equation (2.14) B is the culvert barrel width, H is the upstream pool depth referenced to the inlet invert elevation at the downstream edge of the side bevels, β_s is the sidewall bevel angle, if one is present, and S is the barrel slope. For tapered inlets he presents results that approach the theoretical value based on critical flow at the culvert entrance that is given by

$$\frac{Q}{BH^{3/2}} = \left(\frac{2}{3}\right)^{3/2} \sqrt{g} \quad (2.15)$$

In US Customary units ($g = 32.2 \text{ ft}^2/\text{s}$) the theoretical value is 3.09.

For a submerged entrance French (1955, 1966) uses the energy equation to develop the following model form for the culvert performance curve.

$$\frac{H}{D} + S\frac{L'}{D} = \frac{1}{2gC_d^2} \left(\frac{Q^2}{A_b^2 D} \right) + k_d \quad (2.16)$$

In equation (2.16) H is the elevation of the upstream pool with respect to the inlet invert at the face section, D is the culvert rise, S the culvert slope, L' is the distance from the inlet face to the control section, A_b is the barrel area, and C_d and k_d are constants for a given inlet. During the NBS investigations of culvert hydraulics, French (1955) found that while the influence of culvert slope was small under conditions of inlet control, it was consistent, and he retained the slope term and suggests (see French, 1955, Figure 16)

$$\frac{L'}{D} \approx 0.5 \quad (2.17)$$

This estimate has been used in all FHWA culvert models for all barrel shapes.

2.3.2 Unsubmerged Entrance Under Inlet Control

Inlet control exists when the headwater and culvert entrance conditions determine culvert performance. The culvert entrance may be either unsubmerged or submerged. The transition between these conditions is not well defined. If the entrance is unsubmerged, then the culvert hydraulic performance may be considered to be similar to weir flow (Normann et al., 2001; ASCE/WEF, 1992), and the hydraulic performance may be described by an equation of the form

$$Q = C_w L (h)^{3/2} \quad (2.18)$$

In equation (2.18), Q is the discharge (ft^3/s), C_w is a weir (discharge) coefficient, L is the transverse length of weir (feet), and h is the driving head above the weir crest (feet). With US Customary units, Streeter and Wylie (1985) suggest $C_w = 3.33$ for a rectangular sharp-crested weir. When applied to a culvert, the coefficient C_w will have to be evaluated using laboratory experiments for each inlet configuration, and the effective culvert length may be modified to take into account the effects of end contractions that may be significant for sharp-edge culvert entrances.

Based on the assumption of critical flow within the culvert barrel near the entrance, Henderson (1966) presents the performance equation in the following form

$$Q = \frac{2}{3} C_b B H \sqrt{\frac{2}{3} g H} \quad (2.19)$$

In equation (2.19), B is the width of the culvert and C_b is a coefficient expressing the effective width contraction in the flow. Henderson states that if the vertical edges are rounded to a radius of $0.1 B$ or more, that there is no side contraction and $C_b = 1$. If the vertical edges are left square, he gives $C_b = 0.9$. According to Henderson, H is the height of pool level above the invert (that is, it does not include the approach velocity head). According to equation (2.19), the theoretical discharge coefficient is given by

$$C_w = \frac{2}{3} \sqrt{\frac{2}{3} g} \quad (2.20)$$

Using US Customary units, this coefficient has a value $C_w = 3.09$.

French (1966) also presents experimental data supporting equation (2.19), also with use of the headwater depth rather than specific energy. For square and rectangular box culverts with square-edges, he finds discharge coefficients that range from 2.68 to 2.80, with an average value near 2.73. This value is very close to Henderson's $C_b = 0.9$ [$C_b = 2.73/3.09 = 0.88$]. The data presented by French supports the conclusion that the reduction

in discharge coefficient for square-edged box culverts is associated with width contraction. Data from his Table 12 show that for tapered inlets that will not have width contractions, the discharge coefficients average 3.08 (compared with the theoretical value of 3.09).

Application of the energy equation between the upstream section and the control section of Figure 2.2 gives

$$\frac{v_a^2}{2g} + y_a = HW = E_c + \Delta H_L - S_o L' \quad (2.21)$$

In equation (2.21), v_a and y_a are the upstream approach velocity and depth, and HW is the headwater measured from the culvert upstream invert elevation. Equation (2.21) may be normalized by dividing by the culvert rise, D , which gives

$$\frac{HW}{D} = \frac{E_c}{D} + \frac{\Delta H_L}{D} - S_o \frac{L'}{D} \quad (2.22)$$

According to equation (2.17), $L'/D = 0.5$.

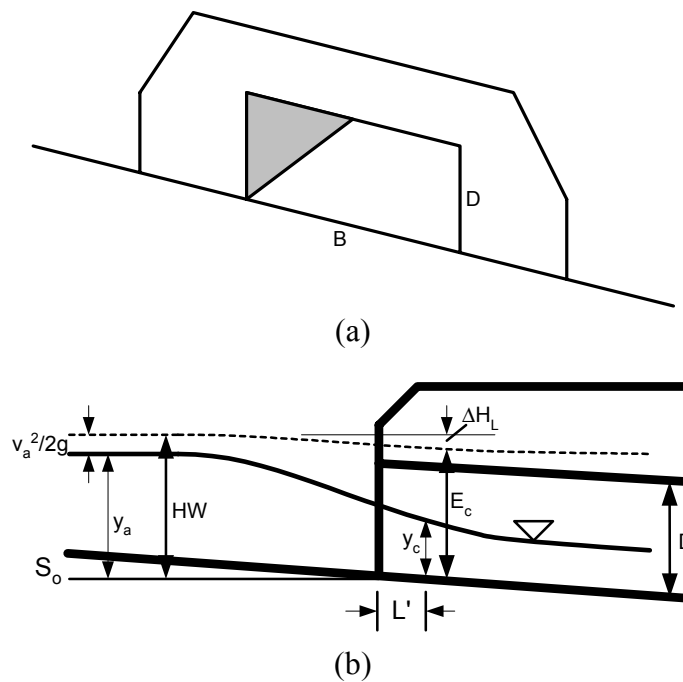


Figure 2.2 (a) Front view of box culvert with span B and rise D . (b) Profile view of box culvert showing energy grade line (dashed), water surface profile (solid), and control section located distance L' downstream from culvert entrance.

Based on the studies performed by the National Bureau of Standards (now NIST), the Bureau of Public Roads (now FHWA) developed a series of performance curves and nomographs for calculation of culvert performance under both inlet and outlet control for

many commonly used entrance configurations and culvert materials. For unsubmerged inlet conditions, FHWA presents the following relationship for the performance curve (see Normann et al., 2001)

$$\frac{HW}{D} = \frac{E_c}{D} + K \left[\frac{Q}{AD^{0.5}} \right]^M - 0.5S \quad (2.23)$$

In equation (2.23), HW is the headwater depth above inlet invert (ft), D is the interior height of culvert barrel (ft), E_c is the specific (head) energy at critical depth (ft), Q is the culvert barrel discharge (cfs), A is the full cross-sectional area of culvert barrel (ft²), S is the culvert barrel slope (ft/ft), and K and M are constants. For 90° wingwall flares the coefficients are K = 0.061 and M = 0.75 (Normann et al., 2001). This equation was used to develop nomographs to predict culvert performance, and in the nomograph development a slope of 0.02 was assumed (Herr and Bossy, 1965). By comparison, equations (2.22) and (2.23) show that the second term on the right of equation (2.23) accounts for head losses between the headwater and control sections.

At the control section in Figure 2.2 the depth and velocity are critical (Froude number, Fr = 1 so $v_c = (g y_c)^{1/2}$) and the theoretical discharge may be calculated from

$$Q = B y_c v_c = B \sqrt{g} y_c^{3/2} \quad (2.24)$$

Also, for critical flow, the specific energy is given by

$$E_c = \frac{v_c^2}{2g} + y_c = \left(\frac{1}{2} \frac{v_c^2}{g y_c} + 1 \right) y_c = \frac{3}{2} y_c \quad (2.25)$$

Combining equations (2.24) and (2.25) one finds

$$Q = \sqrt{g} \left(\frac{2}{3} \right)^{3/2} B E_c^{3/2} \quad (2.26)$$

Using equation (2.26) in the first term on the right side of equation (2.23) gives (where A is again the full cross-section area of the culvert barrel)

$$\frac{HW}{D} = \frac{3}{2g^{1/3}} \left[\frac{Q}{AD^{0.5}} \right]^{2/3} + K \left[\frac{Q}{AD^{0.5}} \right]^M - 0.5S \quad (2.27)$$

Equation (2.27) is the FHWA performance curve for a rectangular box culvert with square edges, when K = 0.061 and M = 0.75, and US Customary units are used.

For comparison purposes, one may write equation (2.19) as

$$\frac{HW}{D} = \frac{3}{2} \left(\frac{1}{\sqrt{g} C_b} \right)^{2/3} \left[\frac{Q}{AD^{0.5}} \right]^{2/3} \quad (2.28)$$

In transforming equation (2.19) to equation (2.28), it has been assumed that the velocity head is negligible so that the headwater HW is the same as the upstream water depth above the culvert inlet invert.

2.3.3 Submerged Entrance Under Inlet Control

When the culvert entrance is submerged, then the culvert acts either as an orifice (Normann et al., 2001; ASCE/WEF, 1992) or as a sluice gate (Henderson, 1966). To represent the culvert performance as an orifice, the performance equation takes the form

$$Q = C_d A \sqrt{2gh} = C_d BD \sqrt{2g(H - D/2)} \quad (2.29)$$

In equation (2.29), C_d is a discharge coefficient that must be evaluated for different inlet conditions, A is the culvert inlet full area, h is the head on the culvert centroid, and H is the upstream headwater. The discharge coefficient is approximately equal to $C_d = 0.6$ for square-edge entrance conditions. The equation resulting when the culvert acts as a sluice gate is similar. For a sluice gate the performance equation is (Henderson, 1966)

$$Q = C_c BD \sqrt{2g(H - C_c D)} \quad (2.30)$$

In equation (2.30), C_c is a contraction coefficient that has a value of $C_c = 0.6$ for sharp-edged entrance conditions and $C_c = 0.8$ for rounded soffit and vertical edges.

For submerged inlet conditions, the data from experiments performed by National Bureau of Standards for the FHWA have been fit to an equation of the form

$$\frac{HW}{D} = c \left[\frac{Q}{AD^{0.5}} \right]^2 + Y - 0.5S \quad (2.31)$$

In equation (2.31), c and Y are coefficients that depend on the culvert inlet conditions. For a sharp-edged inlet with 90° wingwalls, $c = 0.040$ and $Y = 0.80$. For comparison purposes with equation (2.31), equation (2.30) may be written in the form

$$\frac{H}{D} = \frac{1}{2gC_c^2} \left[\frac{Q}{AD^{0.5}} \right]^2 + C_c \quad (2.32)$$

This discussion has reviewed various forms for culvert performance equations under inlet control for both submerged and unsubmerged conditions. Figure 2.3 compares the FHWA performance curves (solid line) with the models presented in Henderson (1966). As expected, there is great similarity between the shapes of the curves, with the FHWA model generally predicting a smaller culvert discharge for a given headwater. The FHWA curves for unsubmerged and submerged conditions do not intersect. The Henderson curves cross, but have a discontinuous slope at the crossing point.

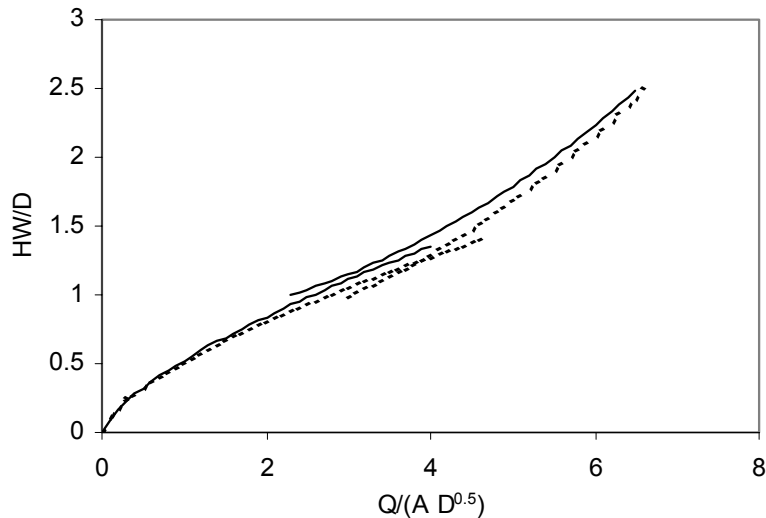


Figure 2.3 Comparison of performance curves for the FHWA model (equations (2.27) and (2.31)) as the solid curves and the model equations of Henderson (equations (2.29) and (2.32)) as the dashed curves

2.4 Hydraulic Similitude

Modern hydraulic analysis utilizes field observation, mathematical analysis (differential or control volume), and experimental study to develop an understanding of complex fluid flow phenomena. Experimental study utilizes the principle of hydraulic similitude, which is the establishment of correspondence between the behavior of a model and that of its prototype (Warnock, 1950). *Geometric similarity* exists between two objects or systems if the ratios of corresponding linear dimensions are equal. For an undistorted model with model-to-prototype scale ratio $L_r = L_m:L_p$, the corresponding areas and volume ratios scale as

$$A_r = \frac{A_m}{A_p} = L_r^2 \quad (2.33)$$

$$V_r = \frac{V_m}{V_p} = L_r^3 \quad (2.34)$$

Kinematic similarity is similarity of motion. This requires that the ratios of velocity components at homologous points in the geometrically similar model and prototype are equal. Kinematic similarity follows from the requirement of *dynamic similarity*, where the ratios of homologous forces in the two systems are equal. Force ratios are expressed through dimensionless numbers, the most important of which for engineering hydraulics are the Reynolds number

$$Re = \frac{\text{inertial force}}{\text{viscous force}} = \frac{vL}{\nu} \quad (2.35)$$

which is the ratio of inertial to viscous forces and is expressed in terms of characteristic velocity v , length L , and kinematic viscosity ν values; and the Froude number

$$Fr = \frac{\text{inertial force}}{\text{gravitational force}} = \frac{v}{\sqrt{gL}} \quad (2.36)$$

which is the ratio of inertial to gravitational forces and is expressed in terms of characteristic velocity v , length L , and gravitational constant g values. For open channel flow the appropriate length scale is frequently the hydraulic depth and the denominator of equation (2.36) is the shallow water wave celerity. Dynamic similarity requires that these and other force ratios are equal; that is, the dimensionless numbers are the same for the model and prototype.

Fortunately, all forces are not necessarily significant for describing the essential hydraulic characteristics of each system. For flow through open channels, channel transitions, and culverts and bridges, the most important forces are those that determine the behavior of the free surface: inertial and gravitational forces. Froude number similarity is required. For geometrically similar systems with Froude number similarity, the model-to-prototype velocity ratio is

$$v_r = \frac{v_m}{v_p} = L_r^{1/2} \quad (2.37)$$

while the model-to-prototype discharge ratio is

$$Q_r = \frac{Q_m}{Q_p} = L_r^{5/2} \quad (2.38)$$

For example, with a 1:9 scale model, a velocity $v_m = 2$ ft/s in the model will correspond to a prototype velocity $v_p = 6$ ft/s, while a model discharge of $Q_m = 9$ cfs will correspond to a prototype discharge $Q_p = 2,200$ cfs.

The effect of the ratio of inertial to viscous forces becomes independent of Re if Re is sufficiently large. This conclusion is familiar from the Moody diagram and drag

coefficient diagrams that are provided in textbooks on fluid mechanics. For prototype conditions of interest in this research, the flow Reynolds number is very large. For model conditions we expect velocity and length scales that are on the order of 10 ft/s and 10 feet, and since for water $\nu = 10^{-5}$ ft²/s, $Re \sim 10^7$ which is sufficiently large to expect that Reynolds number effects on channel flow behavior will be small.

2.5 Numerical Modeling of Culvert Hydraulics

The performance of many culverts has been modeled with the use of computers. The studies that are first mentioned in this section did not use two-dimensional finite element models (as in the present research), but the summary of these computer applications will be helpful in looking at other methods used in analyzing culverts.

Saleh and Hwang (1992) presented a computer model with an analytical methodology that simulates a wide range of flow phenomena in culverts and is intended to replace the use of nomographs and other hand calculation methodologies. Their flow classification was based on actual field conditions instead of inlet/outlet control, and was verified in a physical model study. Ferguson and Deak (1994) found that the area upstream of a culvert acts as a reservoir, which retains incoming runoff while earlier runoff is passing through the culvert opening. They use a computer model of a culvert entrance based on the orifice equation ($C_d = 0.8$) to route storm hydrographs with different flow volumes and peak rates through culverts in studying the increase in upstream stage with increase in flow volume.

Langlinsais (1992) discussed a computer aided design tool called DRAINCALC, which performs drainage runoff calculations and open channel, culvert, or storm drainage design calculations, eliminating the need for cumbersome charts, tables, data sets, and nomographs. With this tool, culverts may be designed as flowing under full flow conditions or partial flow conditions. The software has been successfully field-tested. Liriano and Day (2001) compared current prediction equations for scour at culvert outlets with results from two Artificial Neural Network models (ANN) using a training algorithm with data collected from published studies and their own experiments. The ANN results successfully predicted the scour depth with more accuracy than existing empirical equations and over a broader range of conditions.

Widely used one-dimensional open channel flow models such as HEC-RAS and WSPRO have the capability of analyzing culvert performance within the framework of one-dimensional flow calculations using the energy and momentum equations. Within HEC-RAS, the culvert equations developed for FHWA are utilized (HEC, 1998). Along with specifying the shape, size, material type, and location of the culvert system within the cross section, the user must specify the appropriate chart number and scale number so that appropriate coefficients (see equations (2.23) and (2.31)) are selected for computation.

2.5.1 FESWMS for Two-Dimensional Hydraulic Modeling

The hydraulic modeling code used in this research is the Finite Element Surface Water Modeling System (FESWMS). It is a two-dimensional modeling code originally developed in 1978 for the Federal Highway Administration (FHWA) and the US Geological Survey (USGS) Water Resource Division to evaluate complex hydraulic conditions at highway river crossings (Froehlich, 1996).

The FESWMS two-dimensional model is vertically averaged, as opposed to a one-dimensional model that is cross-section averaged (laterally and vertically averaged), and is

applied where the vertical component of velocity is small compared to the horizontal components. FESWMS solves for the depth-averaged velocities and water depth at each node point and can also represent the effects of bed friction and turbulent stresses using empirical relationships. Steady or unsteady flow may be modeled. Flow through culverts or bridges can be modeled as one- or two-dimensional flow. Froehlich (1996) provides examples of surface water bodies where two-dimensional simulations can provide a good representation of flow motion: shallow rivers, flood plains, estuaries, harbors, and coastal seas. Water density is assumed constant in FESWMS. If stratification were significant, estuaries and harbors would not be appropriately modeled with FESWMS since the density would not be constant and depth-averaged velocities would not be accurate.

A two-dimensional model is more appropriate than a one-dimensional model when the system has ineffective flow area(s), recirculation zones, or flow separation (ASCE, 2001). Ports and South (1995) found that two-dimensional modeling yields more accurate velocity magnitudes and represents depth changes better than one-dimensional modeling, especially when the river to be modeled contains a bend. Two-dimensional hydraulic models allow transverse variation in water surface elevation along a cross section (Froehlich, 1996; HEC, 1995; and Thompson and James, 1988). One-dimensional models represent a flat water-surface elevation along a cross section. FESWMS could also be applied to model flow at a multiple opening bridge crossing, flow around islands, and flow near a harbor entrance (Thompson and James, 1988).

Flow through culverts can be modeled as either one-dimensional or two-dimensional in FESWMS. One-dimensional culvert flow is computed by equations with empirical coefficients (see Section 5.3.2). Lee and Froehlich (1989) note that two-dimensional flow through a culvert should be modeled the same as open channel flow when the water is not in contact with the top of the culvert. When the water is in contact with the culvert soffit, the model computes a pressure head instead of depth through the culvert. The soffit of the culvert is modeled by specifying a *ceiling elevation* at all of the nodes within the culvert. When such pressure flow conditions exist, the governing equations are modified, as described below.

The finite element method is a numerical procedure for solving differential equations. FESWMS uses the Galerkin Finite Element Method to solve the governing system of hydraulic differential equations. This method weights the governing equations over the modeling domain. The weighting process applies numerical integration using Gaussian quadrature for each element, resulting in a system of nonlinear algebraic equations and requiring an iterative solution procedure. A variation of the Newton-iteration method is used, producing a system of equations that is then solved using an “efficient frontal solution scheme” (Froehlich, 1996).

The physical region of interest is divided into subregions, which are called *elements*. Elements are the building blocks of a finite element network. The method of weighted residuals is applied to the governing differential equations to form a set of equations for each element. The element (local) equations are assembled to obtain the complete (global) system of equations, and then the global set of algebraic equations is solved simultaneously (Froehlich, 1996). The values of velocity and water depth at the node points are the unknowns.

The FESWMS model was applied in the graphical user interface package called the Surface Water Modeling System (SMS). Jones et al. (1995) describe SMS as a pre- and

post-processor for a variety of finite element and finite difference surface water flow modeling codes. The Engineering Computer Graphics Laboratory at Brigham Young University developed SMS in cooperation with the US Army Engineer Waterways Experiment Station and FHWA. SMS includes tools that facilitate creating a finite element network. The finite element network represents the system being modeled. SMS also includes capabilities that allow the user to view velocity vectors and contours of velocity magnitude, water depth, or water surface elevation displayed on the finite element network. FESWMS supports analysis of both subcritical and supercritical flows, as well as transitions between subcritical and supercritical flow.

2.5.2 Governing Equations

To derive the depth-averaged surface water flow equations, the three-dimensional mass and momentum transport equations are integrated with respect to the z (vertical) coordinate from the bed to the water surface. Vertical accelerations are assumed to be negligible, which leads to the hydrostatic approximation. The physics of flow are assumed to obey differential equations including several empirical coefficients (Froehlich, 1996). The momentum principle (Newton's Second Law), as applied to a column of water, states the sum of the forces acting on the column equals the sum of net momentum transport and accumulations in the column. The forces acting on the water column are 1) body forces, which have no direct contact with the column, and 2) surface forces, which have direct contact. The body forces are gravity and Coriolis. The Coriolis force is due to the rotation of the earth and is neglected in the present scenario because the rotation of the earth does not have a significant effect in the flows in such a shallow and narrow channel and culvert. The surface forces are hydrostatic pressure, and drag on the top and bottom of the water column. The continuity principle requires the time rate of change of mass in the water column to equal the net flux of mass entering the column. The governing equations presented below (and the form of these equations) are taken from Froehlich (1996).

The vertically integrated momentum equation for flow (neglecting Coriolis and wind stress) in the x -direction (+ x is downstream) is

$$\begin{aligned} \frac{\partial(HU)}{\partial t} + \frac{\partial}{\partial x} \left(\beta H U U + (\cos \alpha_x \cos \alpha_z)^2 \frac{1}{2} g H^2 \right) + \frac{\partial}{\partial y} (\beta H U V) + \\ \cos \alpha_x g H \frac{\partial z_b}{\partial x} + \frac{1}{\rho} \left[\tau_{bx} - \frac{\partial(H\tau_{xx})}{\partial x} - \frac{\partial(H\tau_{xy})}{\partial y} \right] = 0 \end{aligned} \quad (2.39)$$

The vertically integrated momentum equation for flow (neglecting Coriolis and wind stress) in the y direction (+ y is to the left when looking downstream) is

$$\begin{aligned} \frac{\partial(HV)}{\partial t} + \frac{\partial}{\partial x} (\beta H V U) + \frac{\partial}{\partial y} \left(\beta H V V + (\cos \alpha_y \cos \alpha_z)^2 \frac{1}{2} g H^2 \right) + \\ \cos \alpha_y g H \frac{\partial z_b}{\partial y} + \frac{1}{\rho} \left[\tau_{by} - \frac{\partial(H\tau_{yx})}{\partial x} - \frac{\partial(H\tau_{yy})}{\partial y} \right] = 0 \end{aligned} \quad (2.40)$$

The continuity equation integrated over depth is

$$\frac{\partial H}{\partial t} + \frac{\partial(HU)}{\partial x} + \frac{\partial(HV)}{\partial y} = q \quad (2.41)$$

An explanation of terms in the previous equations follows:

$$U = \frac{1}{H} \int_{z_b}^{z_s} u \, dz \quad (2.42)$$

$$V = \frac{1}{H} \int_{z_b}^{z_s} v \, dz$$

H = water depth
z = vertical direction
z_b = bed elevation

$$z_s = \text{water surface elevation} = z_b + H \quad (2.43)$$

u = horizontal velocity in the x direction at a point along the vertical coordinate
v = horizontal velocity in the y direction at a point along the vertical coordinate

$$\alpha_x = \arctan\left(\frac{\partial z_b}{\partial x}\right)$$

$$\alpha_y = \arctan\left(\frac{\partial z_b}{\partial y}\right) \quad (2.44)$$

$$\alpha_z = \arccos\left(1 - \cos^2 \alpha_x - \cos^2 \alpha_y\right)$$

g = gravitational acceleration
ρ = water mass density (assumed constant)
τ_{bx}, τ_{by} = bed shear stresses (caused by channel roughness) acting in the x (downstream) and y (cross-stream) directions

$$\tau_{bx} = \rho c_f m_b U \sqrt{U^2 + V^2}$$

$$\tau_{by} = \rho c_f m_b V \sqrt{U^2 + V^2} \quad (2.45)$$

c_f = dimensionless bed friction coefficient

$$c_f = \frac{gn^2}{(\lambda)^2 H^{1/3}} \quad (2.46)$$

$\lambda = 1$ for metric units, 1.49 for English units
 $n =$ Manning's roughness coefficient

$$m_b = \cos\alpha_z \quad (2.47)$$

(The parameter m_b accounts for the increased shear stress caused by a sloping bed.)

$$\beta = \beta_o + c_\beta c_f \quad (2.48)$$

$$c_\beta = 1/\kappa^2 \quad (2.49)$$

$\kappa =$ Von Karman's constant (~ 0.4)

(The parameter β is a momentum flux correction coefficient resulting from the vertical integration of the momentum transport equations that account for the variation of U and V in the vertical direction. When vertical variations in velocity are considered negligible, $\beta_o = 1$ and $c_\beta = 0$.)

$\tau_{xx}, \tau_{xy}, \tau_{yx}, \tau_{yy} =$ depth-averaged lateral shear stresses caused by turbulence.

τ_{xy} is the shear stress acting in the x direction on a plane that is perpendicular to the y direction.

Turbulent *stresses* are *modeled* as proportional to the depth-averaged velocity gradients. Depth-averaged lateral shear stresses caused by turbulence are computed using the eddy viscosity concept. See Chapter 5 for further discussion on eddy viscosity.

$$\tau_{xx} = \rho v_{xx} \left(\frac{\partial U}{\partial x} + \frac{\partial U}{\partial x} \right) \quad (2.50)$$

The depth-averaged kinematic eddy viscosity is modeled as isotropic, i.e., $v_{xx} = v_{xy} = v_{yx} = v_{yy}$. This is likely a source of some error since the cross-channel and along-channel scales of turbulence are different in shallow water flows such as rivers and streams.

When pressure flow conditions exist through a bridge or culvert in FESWMS, the governing equations are modified. The modified governing equations for pressure flow as

given by Froehlich (1996) are listed below. The momentum equation for flow in the x-direction (neglecting Coriolis) becomes:

$$\begin{aligned} H \frac{\partial U}{\partial t} + \frac{\partial}{\partial x} \left(\beta H U U + g H P - \frac{1}{2} g H^2 \right) + \frac{\partial}{\partial y} (\beta H U V) + g P \frac{\partial z_b}{\partial x} \\ - g (P - H) \frac{\partial z_c}{\partial x} + \frac{1}{\rho} \left[\tau_{bx} + \tau_{cx} - \frac{\partial (H \tau_{xx})}{\partial x} - \frac{\partial (H \tau_{xy})}{\partial y} \right] = 0 \end{aligned} \quad (2.51)$$

The momentum equation for flow in the y-direction (neglecting Coriolis) becomes:

$$\begin{aligned} H \frac{\partial V}{\partial t} + \frac{\partial}{\partial y} \left(\beta H V V + g H P - \frac{1}{2} g H^2 \right) + \frac{\partial}{\partial x} (\beta H V U) + g P \frac{\partial z_b}{\partial y} \\ - g (P - H) \frac{\partial z_c}{\partial y} + \frac{1}{\rho} \left[\tau_{by} + \tau_{cy} - \frac{\partial (H \tau_{yx})}{\partial x} - \frac{\partial (H \tau_{yy})}{\partial y} \right] = 0 \end{aligned} \quad (2.52)$$

The continuity equation becomes:

$$\frac{\partial (HU)}{\partial x} + \frac{\partial (HV)}{\partial y} = q \quad (2.53)$$

P = pressure head

z_c = ceiling elevation

$H = z_c - z_b$

τ_{cx} , τ_{cy} = directional components of shear stress at the ceiling

$$\begin{aligned} \tau_{cx} &= \rho C_f m_c U \sqrt{U^2 + V^2} \\ \tau_{cy} &= \rho C_f m_c V \sqrt{U^2 + V^2} \end{aligned} \quad (2.54)$$

$$m_c = \sqrt{1 + \left(\frac{\partial z_c}{\partial x} \right)^2 + \left(\frac{\partial z_c}{\partial y} \right)^2} \quad (2.55)$$

(The parameter m_c accounts for increased resistance caused by a sloping ceiling.)

2.5.3 Application of Two-Dimensional Models

Many studies using two-dimensional finite element hydraulic models have been documented, and some of the pertinent methodologies and findings are summarized in this section. FESWMS has been used to model a variety of two-dimensional flow scenarios.

The FESWMS studies detailed in this literature review were done for bridge hydraulic analyses. No literature was found detailing projects dealing with two-dimensional studies of expansions leading to wide culverts. This absence is likely because state transportation departments do not use two-dimensional models in performing culvert design and analysis, which illustrates the need for the current research. Lessons learned from bridge hydraulic analyses are applicable to wide culverts. There is a difference in the scales of analyses between culverts and bridges, as bridges are built for larger streams and rivers, but the finite element network building process and data analysis process is similar. Both analyses are interested in velocities and water depths and require inputs for the same model parameters. Also, the wide culverts will be modeled with two-dimensional elements in FESWMS, just as a bridge would be.

Thompson and James (1988) used FESWMS to simulate flow at a bridge crossing of a heavily vegetated flood plain. Computational results were compared to field observations and results from HEC-2, a one-dimensional hydraulic model. Lee and Froehlich (1989) used FESWMS to study a multiple opening bridge crossing of a flood plain with a single channel and an expansion downstream of the crossing, a complex dike system, and varying roughness conditions. Kheireldin et al. (1994) used FESWMS to simulate steady flow through a bridge on the Nile River. Ports and South (1995) performed a hydraulic and scour analysis of the Baltimore Street Bridge using FESWMS. A two-dimensional model such as FESWMS was needed because the bridge was located at the middle of a bend in the stream. FESWMS was useful in the analysis of Ports and South (1995) because the model provided parameters for scour analysis: magnitude and direction of velocities and water depth. Froehlich and Trent (1989) used FESWMS to evaluate hydraulic conditions (water surface elevations and depth-averaged velocities) that produced bed scour under pier foundations leading to a bridge failure in New York in 1987. Their model results could then be used to estimate scour depths and design erosion prevention measures.

Several two-dimensional (depth-averaged) finite element hydraulic models exist, and the methodologies of applying the models are similar. HEC (1995) used RMA-2, a two-dimensional finite element system developed by Resource Management Associates, to investigate flow transitions in bridge backwater analysis. The two-dimensional results were compared with the results of a corresponding one-dimensional HEC-RAS model that used expansion and contraction ratios to estimate energy losses through bridges. RMA-2 does not support supercritical flow. Somes et al. (1999) applied MIKE-21, a two-dimensional finite element modeling system developed by the Danish Hydraulic Institute, to simulate wetland hydrodynamics. Knight and Abril (1996) suggested a way to calibrate a finite element river model developed by Abril for overbank flow using three calibration coefficients based on local friction factors, eddy viscosities, and secondary flows. DeVantier (1989) presented finite element formulations of the governing equations for depth-averaged turbulent flow with emphasis on the representation of bottom stress terms and spatially varying eddy viscosity.

3. Physical Model System and Experiment Procedures

3.1 Overview

The main objective of this research is to investigate the hydraulics of channel expansions leading to wide culverts. The investigation uses physical modeling and numerical modeling. This chapter describes the physical model and the equipment and procedures for measuring channel discharge, water depth, water surface elevation, and water velocity during the physical model experiments.

3.2 Design of Physical Model

As a preliminary step towards design of the physical model, consider the culvert system shown in Figures 1.1 to 1.4. For physical-model design purposes, this culvert system is considered as the prototype. Each culvert barrel is 10 feet wide (span $B = 10$ feet) and 6 feet high (rise $D = 6$ feet). At the beginning of this project, the prototype design discharge was unknown, and a design discharge was estimated using the following arguments. The downstream channel shown in Figure 1.3 is wide and should not obstruct the flow (i.e., there is a low tailwater). This suggests that critical flow should occur near the culvert entrance. If it is further assumed that energy losses are small and that the allowable headwater elevation is the same as the culvert height, then one finds

$$HW = E_c = \frac{3}{2} y_c = \left(\frac{v^2}{2g} + y \right)_c = 6 \text{ ft} \quad (3.1)$$

In equation (3.1), E_c is the critical specific energy, v_c is the critical velocity, and y_c is the critical depth. Thus $y_c = 4$ feet, $v_c = \sqrt{2g \times 2 \text{ ft}} = 11.4$ ft/s, and the discharge per barrel is $Q_{\text{barrel}} = B y_c v_c = 10 \text{ ft} \times 4 \text{ ft} \times 11.4 \text{ ft/s} = 456 \text{ ft}^3/\text{s}$. The total design discharge for the 6-barrel culvert system is calculated to be $Q_T = 6 \times Q_{\text{barrel}} = 2,740 \text{ ft}^3/\text{s}$.

For the model delivery system at The University of Texas at Austin, Center for Research in Water Resources (CRWR), the maximum discharge is approximately $10 \text{ ft}^3/\text{s}$. Using equation (2.37), the model to prototype scale ratio L_r is

$$L_r = \left(\frac{Q_m}{Q_p} \right)^{2/5} = \left(\frac{10}{2740} \right)^{0.4} = 0.106 \quad (3.2)$$

Thus a 1:10 scale ratio is required.

The prototype culvert system (culvert barrels plus wingwalls) has a width of about 70 feet (perpendicular to the direction of flow). The model will include an additional width of 25 feet on each side, corresponding to the right-of-way running parallel with the highway embankment. Thus the total prototype width is 120 feet, and the corresponding model width is 12 feet. The prototype design depth of flow upstream of the culvert is 6 feet, which corresponds to a model depth of flow of approximately 7 inches.

The upstream channel is poorly defined, and for the present purposes it is assumed that the upstream channel may be represented as a trapezoidal channel with a bottom width of 10 feet and a side slope of 2:1. The resulting upstream channel width is approximately 30 feet. The length of the highway right-of-way along the channel axis is approximately 50 feet, and most of the channel expansion occurs within the first 30 feet. As measured from the channel centerline and considering only the culvert system width, the channel expands from 15 feet to 35 feet over a distance of 30 feet, giving an expansion ratio of 30:20 or 1.5:1. Considering the entire length of right-of-way, the expansion ratio increases to 2.5:1.

These size characteristics are used to design the model's upstream channel, expansion and culvert system. The physical model is described in the next section.

3.3 Description of the Physical Model

Figure 3.1 details the layout of the physical model. The channel is divided into three sections for the purpose of this description. The upstream section leads from the headbox shown to the left of the figure downstream to the channel expansion. The channel expansion section is a wide section of the channel that contains the culvert model. The third channel section is the tailgate section that contains the tailgate and return channel. Each of these sections and other aspects of the physical model are described below.

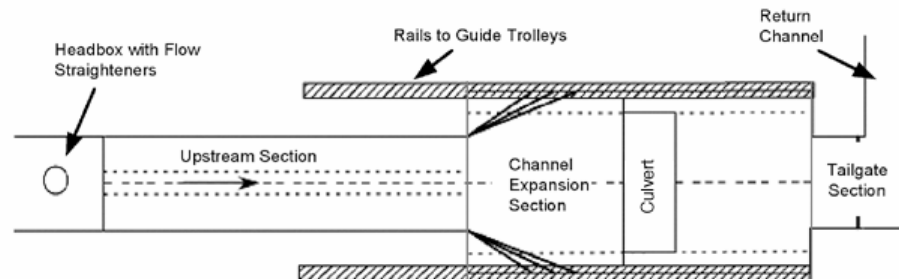


Figure 3.1 Schematic view of the physical model

3.3.2 Water Supply and Upstream Channel Section

The water used for the physical model experiments is pumped into the laboratory through a water distribution system from a half-million gallon reservoir located outside of the laboratory. Figure 3.2 provides a schematic view of the water distribution system. Two water supply lines lead from the distribution reservoir to the channel, each with its own pump. Valves located throughout the system are used to control the magnitude of channel discharge and also to direct the flow to different destinations in the distribution system. As discussed below, there are a number of flow measurement systems available. The standard system consists of two propeller meters, one located in each supply line. These are also shown in Figure 3.2. Not shown in this figure are a number of pipe

branches. One branch from each supply line leads to an outdoor channel that has also been used in these experiments. A second branch leads to a flow measurement tank, which is discussed below.

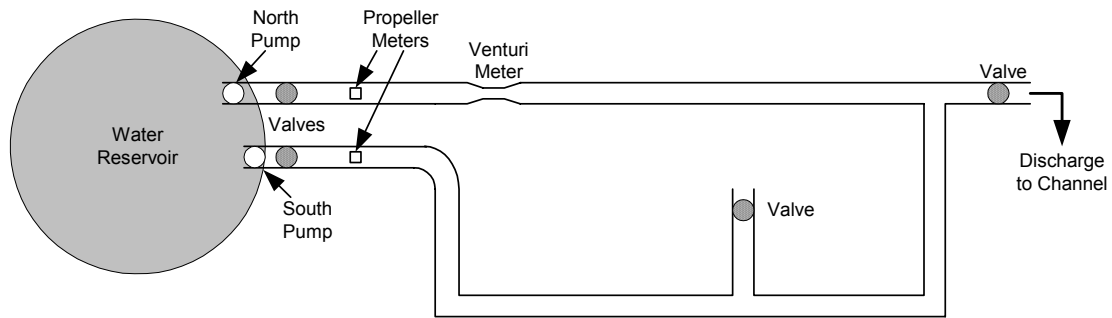


Figure 3.2 Schematic view of the water distribution system

At the head of the upstream section, shown to the left in Figure 3.1, water is pumped into a headbox and then through flow straighteners before entering the channel section. Baffles are located in the headbox to stabilize the flow before entering the upstream channel section. Baffles are made of several layers of cinder blocks that are overlapped so that the water must follow a tortuous path and have significant contact with the blocks before it enters the flow straighteners. The tortuous flow path and contact with cinder blocks helps to stabilize the flow. Flow straighteners, located just downstream of the headbox, are used to eliminate secondary currents as the water enters the upstream section of the channel. The flow straighteners are made from $\frac{1}{8}$ inch-thick plexiglass and extend 2 feet (0.6 meter) in the direction of the flow and across the entire width of the channel. They have a lateral spacing of approximately 0.3 feet (0.09 meter). Figures 3.3 shows the vertical delivery pipe, the downstream end of the set of baffles, and the flow straighteners.



Figure 3.3 Channel headbox and flow straighteners

The cross section of the upstream section is trapezoidal, with top width of 8.4 feet (2.6 meters), and the bottom width 1.8 feet (0.6 meter). The side slope of this portion of the channel is 2.5(H):1(V). The longitudinal slope along the axis of the channel was measured previously by another research team, and determined to be 0.000385, which is effectively flat. The upstream section of the channel is 32.3 feet (9.8 meter) long from the headbox to the channel expansion. This allows development of a natural velocity distribution before the channel expansion is reached. The headbox and this section of the channel remain from a previous research project, and construction details are presented by Tynes (1989).

The model channel roughness was determined in the previous research project, and a detailed description of the process is also presented by Tynes (1989). During experiments, water discharge and depth were measured, and the standard step method (Henderson 1966) was used to determine the roughness coefficient. Using this procedure, the Manning's roughness coefficient was found to be 0.0125 for the model channel. This value corresponds well with literature values for finished concrete, and is assumed for the current research.

3.3.3 Channel Expansion Section

The channel expansion section begins 32.3 feet downstream from the headbox at the channel expansion. The top width of the channel increases from 8.4 feet (2.6 meters) in the upstream channel to a top width of 15.2 feet (4.6 meters) downstream within the channel expansion section. The bottom width of the trapezoidal channel is 11.2 feet (3.4 meters), and the side slopes in this portion of the channel are 2 (H):1(V). The total length of this section along the channel axis is 27.2 feet (8.3 meters). The channel expansion section was surveyed using a surveying level and rod, and longitudinal slope of this section was determined to be 0.0025. The initial design of the channel used an abrupt expansion, as shown in Figure 3.4. The difference in color in the downstream section of this figure shows set and fresh concrete.



Figure 3.4 Abrupt channel expansion looking upstream towards the headbox

Most of the physical model experiments were performed in the channel with an abrupt expansion. Towards the end of the research, the channel expansion was modified to be a smooth, more natural channel transition. The abrupt expansion was first filled in with sand, and then a layer of concrete was applied. This modified transition is shown in Figure 3.5.



Figure 3.5 Modified channel expansion

The indoor channel shown in Figures 3.4 and 3.5 was used in a previous investigation of hydraulics of side-discharge weirs. To construct the channel expansion section, the channel downstream of the upstream section was demolished and removed. New walls were built out of cinder blocks and pre-packaged mortar mix. The inside walls were painted with cement slurry, or a mixture of cement and water that was just thick enough to be applied with a paintbrush and stick to the walls without running. This slurry acted as a wall sealant. Forms for shaping the channel cross section were then made by cutting channel cross sections out of plywood. The forms were placed every 3 feet and filled with sand, leaving about one inch from the top of the forms unfilled. Drains made from perforated PVC pipe were placed throughout the sand to provide drainage and prevent the buildup of hydrostatic forces. The drains were covered with pea gravel to keep sand from clogging the drains. The sand was sprayed with water and allowed to drain twice in order to compact the material and thus prevent the formation of air pockets beneath the channel floor. Concrete was poured on top of the sand to fill the volume that remained above the sand and between the plywood forms. A board was then scraped across the tops of the forms to smooth the concrete and provide a uniform appearance. Concrete was mixed by adding 6 parts of sand to 1 part cement. Water was added until the desired concrete consistency and texture was achieved. The concrete was malleable enough to be smoothed easily within the forms, stiff enough not to run down the sloped sides of the trapezoidal cross section, and strong enough to walk upon when dry. Cement slurry similar to that

used to waterproof the walls was placed on the channel floor and sides to provide waterproofing and a uniform roughness.

3.3.4 Tailgate Section

The tailgate section begins at 59.5 feet (18.2 meters) downstream from the headbox and is an abrupt contraction that leads water into a channel that runs under the laboratory floor, which returns the water to the reservoir from which it came. An important feature contained in this section is the tailwater gate that can be raised and lowered with a crank, cable, and pulley system to control the flow depth upstream. For most of the experiments the tailwater gate was lowered completely since the prototype is assumed to be relatively free of downstream flow obstructions.

The geometry of this channel section is rectangular, rather than trapezoidal, as in the other two sections, thus the bottom and top widths are 8.4 feet (2.6 meters). The tailgate section is 6.5 feet (2.0 meters) long and the slope from 59.5 to 63 feet is 0.0086 while the slope from 63 to 66 feet is 0.057. This section was constructed using the same methods used with the expansion section.

3.3.5 Culvert Model

A model culvert was built at the 1:10 scale that was selected as described in Section 3.2. Thus the rise of the culvert is 0.6 feet (0.2 meter) and the width of each barrel is 1 foot (0.3 meter). The model culvert is a six-barrel, box culvert system made of painted and water treated lumber. The culvert system has a total span (culvert barrels plus wingwalls) of 7 feet (2.1 meters), a 1-foot (0.3-meter) rise, and a headwall of 0.5 feet (0.15 meter). The culvert was constructed so that it could be moved in the longitudinal direction along the channel axis of the channel expansion section as needed. For most experiments it was placed at a location 8 feet (2.4 meters) downstream from the expansion. Removable covers for the culvert barrels were made in order to perform runs with 2, 4, and 6 barrels open. Figure 3.6 shows the model culvert.

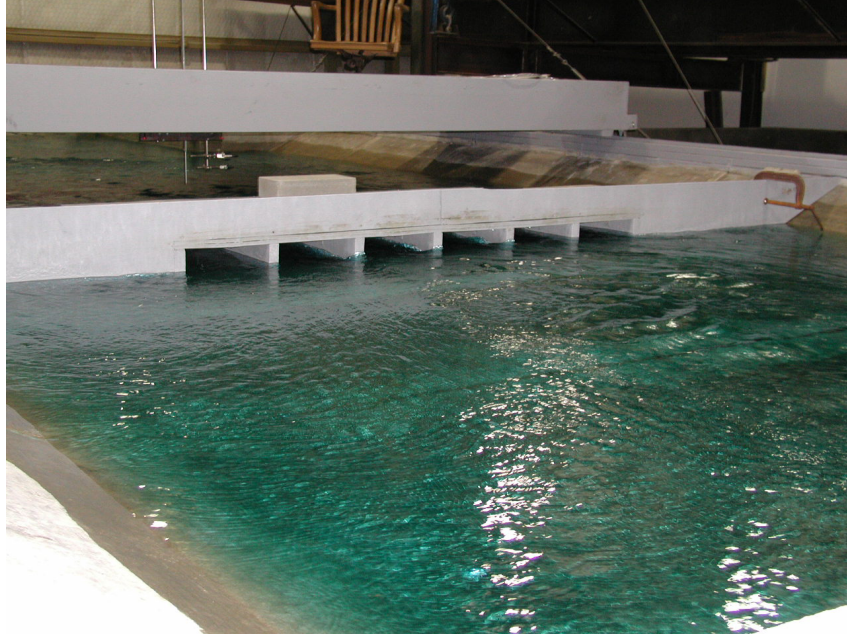


Figure 3.6 Six-barrel culvert model with headwall and wingwalls

3.3.6 Rails and Trolleys

In order to take the measurements needed in the investigation, a system of rails and trolleys was built to carry instruments and provide access to areas of interest in the physical model. Two trolleys were constructed: one for researchers to occupy when performing experiments (person trolley) and the other to mount instruments (measurement trolley). A system of rails was also constructed to provide tracks for guiding the trolleys up and down the channel along the longitudinal channel axis. The rails and tracks are shown crosshatched in Figure 3.1. The trolleys have wheels that allow them to roll in the tracks.

The person trolley, which can be seen in the background of Figure 3.6, is 15 feet (4.6 meters) wide and 4 feet (1.2 meters) long. The trolley was constructed to be strong enough to hold several people.

The measurement trolley, with a length of 1 foot (0.3 meter) and width of 15 feet (4.6 meters) was constructed complete with a carriage and rail system used to move measurement tools in the longitudinal, transverse, and vertical directions. The measurement trolley is shown in Figure 3.7.



Figure 3.7 Measurement trolley

The measurement trolley slides along the length of the rail system and is held in place by bolts that thread through the carriage and press against the rail. A measuring tape, also shown in Figure 3.7, was placed along the width of the trolley, and a pointer is mounted on the carriage to mark its position in the direction transverse to the channel axis. Rods are mounted on the carriage that can move up and down in their mounts so that the vertical instrument position may be varied over the entire water depth. Each rod is held in place with bolts that are threaded through the mount and press against the rod. Marks were made on the rods at every $\frac{1}{2}$ cm to measure rod movement, and thus instrument movement. Instrument holders are mounted on the rods that can grasp measurement tools such as the Acoustic Doppler Velocimeter (ADV) probe or a Pitot tube and hold them in place. A point gauge is also mounted on the carriage to measure water depths. Measurement instruments are described in Section 3.4.

3.4 Data Acquisition

The data collected in this investigation include the channel discharge, water depth, water velocity, depth-averaged water velocity, and specific energy. The following sections describe the methods used to collect these data.

3.4.1 Channel Discharge

Channel discharge was measured with Data Industrial (series 1500) propeller meters. Figure 3.8 shows a picture of a propeller meter. One propeller meter was installed in each of the supply lines, as shown in Figure 3.2.



Figure 3.8 Propeller meter

The propeller meters are inserted into the water supply pipes of the distribution system. Water turns the propeller as it passes through the pipes, and each time the propeller makes a full rotation it generates an electronic pulse. These pulses are recorded by the flow meter, which converts the pulse frequency to a velocity and then uses the known cross-sectional area of the pipe to compute the volume of water that passes the propeller meter. The flow meter device counts every unit volume (metric or English) that passes the propeller, and the flow rate is computed by dividing the total volume of water that has passed the propeller meter by the time elapsed. The time elapsed is recorded with a stopwatch, and recording periods are long enough to reduce the human error involved with delays in starting and stopping the stopwatch at the beginning and end of the volume measurement.

An alternative method of measuring channel discharge was employed to calibrate the propeller meters. This method involves redirecting all channel discharge into the large tank shown in Figure 3.9 with the outlet valve at the bottom left completely open. The water level inside the tank can be viewed through a spyglass mounted on the outside. When the water level in the tank (meniscus in the spyglass) is not moving, the system has reached steady state. Once steady state is achieved, the outlet valve is closed quickly and the elapsed time is recorded for the meniscus in the spyglass to move from the steady state level to a level near the top of the spyglass. Using the change in water level, cross-sectional area of the tank, and the lapsed time, the flow rate is determined. This flow rate was used to calibrate the propeller meters.



Figure 3.9 Large reservoir used for propeller meter calibration

Figure 3.10 shows results from a calibration run. This figure shows the discharge measured in the storage tank from change in water level, versus the discharge measured by the propeller meters. The solid line marks exact one-to-one correspondence.

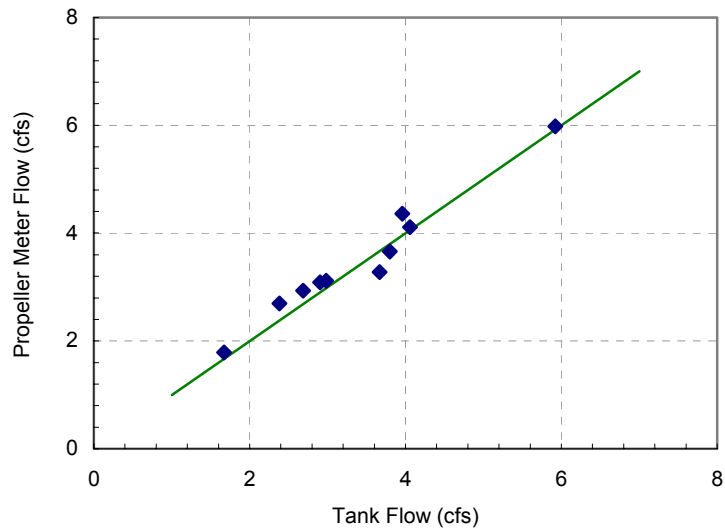


Figure 3.10 Propeller meter calibration

3.4.2 Water Depth

Water depth was typically measured with a point gauge. This tool is a marked pointer that can measure the elevations of the water surface and the channel floor. The difference in these elevations is the water depth.

Pitot tubes connected to a manometer board via flexible plastic tubing were also used to measure water depth in some experiments. A Pitot tube measures both total hydraulic head and static hydraulic head. The static hydraulic head can be used to determine water depth. The static head values measured by a Pitot tube must be referenced to a datum in order to be converted into water depth. A datum was established by creating a level pool in the channel, setting up the Pitot tubes, and marking the static head reading on the manometer board under the level pool condition. Next, the depth was measured at the location of all Pitot tubes with a point gauge. These depths corresponded to the static head reading marked on the manometer board and thus differences in those depths were measured by deviation of the meniscus from the level pool markings on the manometer board. A level pool was created in the channel by passing a very low flow rate through the channel and allowing the system to reach steady state. Velocities in the pool were very low so that, when the level pool condition was achieved, every point on the surface of the pool had the same elevation. A small discharge was required because of leakage through the tailgate and probably through the channel walls.

3.4.3 Water Velocity with ADV

Water velocities were measured with a SonTek Acoustic Doppler Velocimeter (ADV) meter. Two probes, a side-looking probe and a down-looking probe, were used with the ADV meter, and both were used to measure velocity.

The down-looking probe can measure the three velocity components of a flow without being calibrated. This probe uses one transmitter and three acoustic receivers to measure the velocity of the water based on the principle of the Doppler effect. The transmitter emits a short pulse of sound at a known frequency. The pulse propagates through the water along the axis of its beam and acoustic energy is then reflected in all directions by particulate matter as the pulse passes through the sampling volume (which is the point for which the velocity is measured). A portion of the reflected energy passes back along the receiver axis and is sampled and processed by the ADV meter to measure the change in frequency. The velocity of the particles along the bistatic axis, which is located halfway between the center axes of the transmit and receive beams, is proportional to the Doppler shift measured by one receiver. The down-looking probe records three velocity values (v_x , v_y , v_z), three signal strength values, and three correlation values for water moving through the sampling volume, which is located 5 cm from the probe tip. The ADV velocity output can be used directly without any post-processing. Figure 3.11 shows the down-looking probe setup and its in-channel configuration mounted on the measurement trolley. [SonTek web site.]



Figure 3.11 Down-looking ADV probe

Figure 3.12 shows an example output from an ADV measurement. For this figure, the velocity scale (in centimeters per second) has been expanded so that the x-component velocity series is off-scale and not shown. The interesting feature that is shown is the y-component (transverse-horizontal) velocity that has significant amplitude. This reflects the cross-channel wave motion that is established in the basin downstream of the channel expansion and upstream of the culvert. This basin acts as a resonance chamber, and the period of oscillation is well-predicted using Harbor Resonance formula (Ippen, 1960).

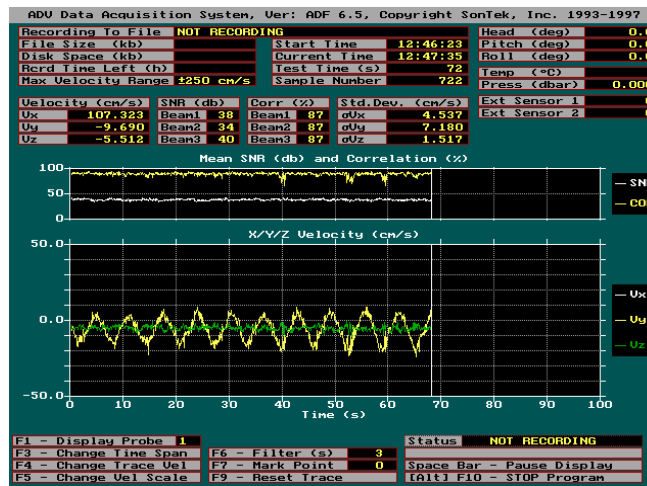


Figure 3.12 ADV velocity output for down-looking probe

The side-looking ADV probe measures velocities using the same principles as the down-looking ADV probe. This probe, however, faces to the side, rather than down, and measures only the x and y components of the water velocity. This feature allows the side-looking ADV probe to measure water velocities at shallower water depths than the down-looking ADV probe. As with the down-looking probe, the sampling volume for this probe

is 5 cm away from the probe tip but the depth of the sampling volume is not reported, as it is with the down-looking probe.

3.4.4 Water Velocity with Pitot Tubes

As mentioned in Section 3.4.2, Pitot tubes measure total head and static head simultaneously. The difference in these head values is the velocity head, which is defined as:

$$h_v = \frac{v^2}{2g} \quad (3.3)$$

Therefore, water velocity can be computed by obtaining readings corresponding to static and total head from a Pitot tube. This method of velocity measurement was useful when water depth was too shallow to use the ADV meter or when water velocities were too high, causing cavitation to occur at the transmitter of the ADV probe.

3.4.5 Depth-Averaged Velocities

In all experiments, depth-averaged velocities are used to show velocity distribution in the transverse and longitudinal directions. Two different methods were used to obtain depth-averaged velocity.

The first method involved measuring velocity at 0.4 times the water depth from the bed. Wanielista et al. (1997) recommends taking one measurement at 0.4 times the water depth (measured from the channel bottom) to approximate the average velocity for watercourses that are 1 to 2 feet deep, which applies to the model channel. If the vertical distribution of velocity is logarithmic, then the average velocity occurs at a depth that is 0.368 times the water depth, measured from the channel bottom (Yalin, 1977).

The second method involved measuring a velocity profile with the ADV and then numerically integrating the depth-averaged velocity as described below. For a typical measurement, the ADV probe was placed in the instrument holders, which were mounted on the measurement trolley. For each profile, the ADV probe tip was positioned as close to the water surface as possible while remaining submerged with the passing of waves during the sampling time period. Velocities were then measured at progressively lower depths until the channel floor interrupted downward movement. A typical velocity profile in the z-direction contained velocities measured at 3 to 7 different depths covering the range of the water depth. Since significant waves and velocity oscillations were present during virtually all of the experiments, sampling periods were chosen that included many periods of the oscillation in an effort to obtain an accurate average velocity. These velocities were plotted versus the corresponding depths and average velocities were computed by calculating the area of the “velocity versus depth” curve using the trapezoidal method and then dividing this area by the total water depth. Due to the varying water surface elevation caused by waves, it was not possible to use the ADV probe to measure water velocity at the water surface. Therefore, the velocity at the water surface was extrapolated manually from the measured velocity profile.

An issue arises in calculation of the average velocity from integration of the velocity profile because the velocity near the bed cannot be measured accurately. However, a

logarithmic extrapolation can be used. A logarithmic velocity profile is fit to measurements from the two lowest data points, and the integral of the resulting velocity profile is evaluated. Figure 3.13 shows a velocity profile with measured values at depths y_1 and y_2 . A logarithmic velocity profile may be fit to these measurements using the following function:

$$u(y) = u_1 + \frac{u_2 - u_1}{\ln(y_2/y_1)} \ln(y/y_1) \quad (3.4)$$

Integrating this function from a lower limit y^* up to the lower measurement depth y_1 , and then taking the limit as $y^* \rightarrow 0$ gives

$$\int_0^{y_1} u(y) dy = \left[u_1 - \frac{u_2 - u_1}{\ln(y_2/y_1)} \right] y_1 \quad (3.5)$$

This value is used to estimate the average velocity using the trapezoidal method of integration.

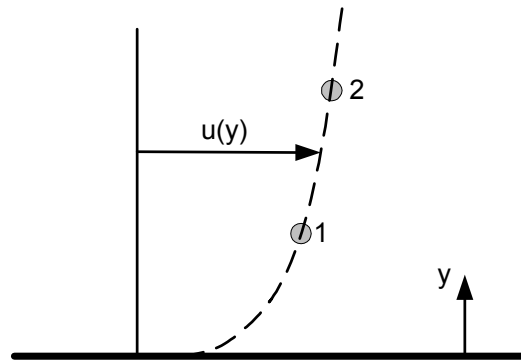


Figure 3.13 Logarithmic velocity profile extrapolation for estimation of the average velocity

3.4.6 Specific Energy

Specific energy, E , is defined as the sum of the water depth, y , and the velocity head:

$$E = y + h_v \quad (3.6)$$

Specific energy was easily measured with the Pitot tube as the total head referenced to a datum. It was also measured as the sum of water depth, measured with a point gauge, and velocity head, computed with the depth-averaged velocity measured with the ADV as described above.

4. Physical Model Experiment Results

4.1 Overview

The physical model, experiments, and measurement procedures were described in Chapter 3. This chapter presents and analyzes the results from these experiments. First, the velocity distribution and flow distribution through the channel expansion are described, as are the distributions of depth and specific energy upstream of the culvert system. It is shown that for low-head culverts, the difference between the upstream water depth and specific energy can be significant for multiple-barrel culverts. The performance curve for box culverts operating under inlet control is developed, based on the experiments performed during this study. The distribution of discharge through different barrels of the multi-barrel culvert system is also discussed.

4.2 Distribution of Velocity

The velocity distribution varies with depth and with location across the channel width. In discussing the latter, it is easier to reference the depth-averaged velocity. This is also the appropriate velocity for comparison with the numerical modeling investigations that are described in Chapter 5. The depth-averaged velocity is discussed first.

4.2.1 Vertical Velocity Distribution

The vertical distribution of velocity in both the upstream channel and within the channel downstream of the expansion has been measured. The length of the upstream channel section, combined with the flow straighteners, allows the effects of the headbox to be dissipated and the flow profiles to become fully developed. Figure 4.1 shows a typical velocity profile along the channel centerline at a station 4 feet (1.22 meters) upstream of the channel expansion. The data point at the water surface is manually extrapolated from the measured data. The depth of flow at this location is 0.804 feet (24.5 cm). Integration of the velocity distribution over depth gives an average velocity of 2.14 ft/s (65.2 cm/s). For comparison, the measured velocity at a fraction depth of 0.368 is approximately 66 cm/s, which shows that both approaches for estimating the depth-averaged velocity discussed in Section 3.4.5 give comparable results, at least in the upstream approach channel.

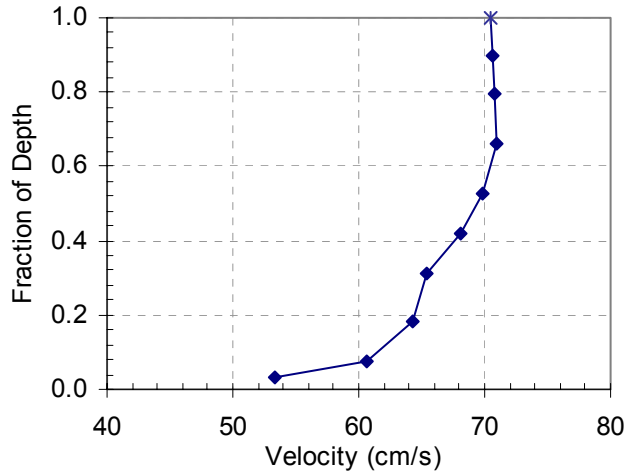


Figure 4.1 Typical velocity profile at 1.22 meters upstream of the channel expansion, where the depth is 24.5 cm and the average velocity is 65 cm/s

For comparison, Figure 4.2 shows the centerline velocity distribution at a location 4 feet (1.22 meters) downstream of the channel expansion. At this location the depth is 0.771 feet (23.5 cm) and the average velocity is 2.34 ft/s (71.2 cm/s). The velocity profile at this location is not as fully developed as in the upstream channel. The velocity at a fraction depth of 0.368 is approximately 76 cm/s, smaller than the average velocity. Vertical velocity profiles within the outer regions of the channel expansion section are poorly developed and irregular, but these velocity profiles are not utilized in this study.

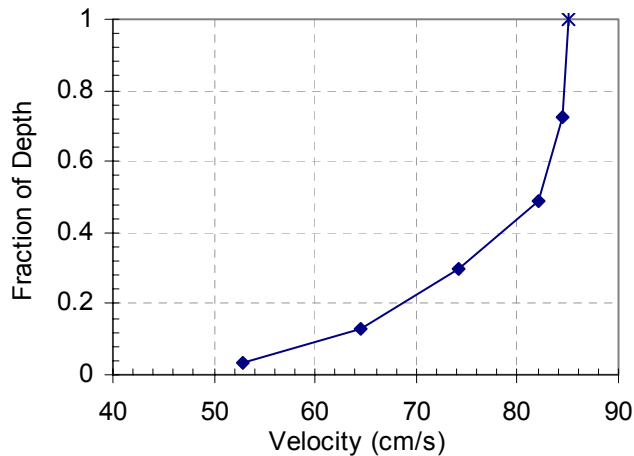


Figure 4.2 Vertical velocity distribution at a centerline location 1.22 meters downstream of the channel expansion where the depth is 23.5 cm and the average velocity is 71.2 cm/s

Figures 4.1 and 4.2 were measured during the same experiment, and the persistence of the velocity profile through the expansion indicates that the momentum associated with

the flow through the channel expansion is quite strong; this strength, in turn, affects the characteristics of the expansion of the jet.

4.2.2 Distribution of Velocity with Cross Section

Ultimately, this research was motivated by a desire to gain a greater understanding of the sediment deposition occurring in channel expansions leading to culverts or bridges. Sediment transport depends in part on water depth and velocity, and the uneven sediment accumulation that is observed in the field suggests that the velocity is not evenly distributed across the channel expansion and the inlets to the multi-barrel box culverts. The velocity distribution across the model culvert system was investigated to evaluate the assumption of equal flow distribution.

The initial experiments investigating the hydraulics of channel expansions were conducted without the culvert in place; this allowed a characterization of the natural expansion ratio of the model channel. As discussed above, the vertical velocity profiles were numerically integrated to obtain an average velocity for each sample station. The model channel did not demonstrate the typical expansion ratio of 4:1 discussed in Section 2.2. Indeed, the model channel's jet expansion was minimal.

Figure 4.3 shows the results from an experiment with discharge of 6.05 ft³/s (0.171 m³/s). The cross sections are located at distances of 2 ft, 8 ft and 16 ft downstream of the abrupt expansion. The channel centerline is located at cross-section station 134 ft. There is evidence of some broadening of the jet in the downstream direction, but no significant decrease in the centerline depth-averaged velocity. Beyond a distance of approximately 3 feet (0.92 meter) from the channel centerline, flow separation from the jet has occurred and there is return flow with a negative (upstream) velocity component.

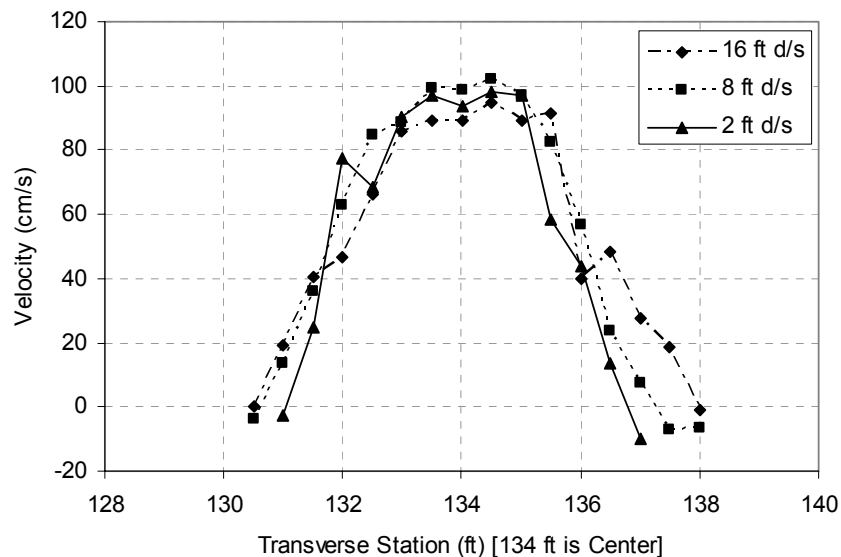


Figure 4.3 Cross-section distribution of depth-averaged velocity as a function of distance downstream of the abrupt channel expansion for a discharge of 6.05 cfs

Having the model culvert present in the channel does not affect the flow distribution shown above. Figure 4.4 shows similar results from an experiment with the culvert in place and located at a distance of 20 feet (6.1 meters) downstream of the expansion. For this experiment the discharge is $6.21 \text{ ft}^3/\text{s}$ ($0.176 \text{ m}^3/\text{s}$). Again there is evidence of broadening of the jet, but no significant decrease in maximum velocity. Note that the velocity entering the barrels (which span from 131 ft to 137 ft) is much greater in the middle barrels than in the outer barrels. Furthermore, the recirculation zones, which appear as negative velocity values, are also apparent.

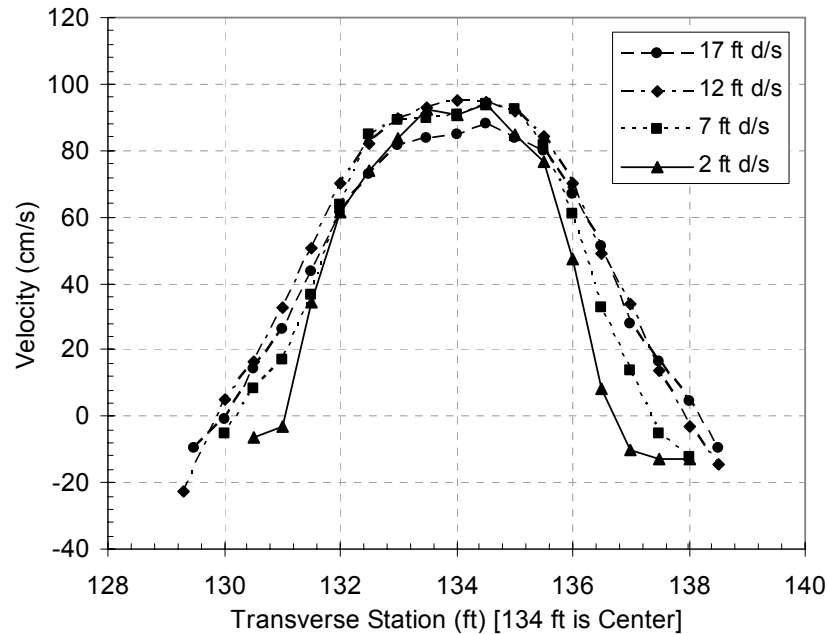


Figure 4.4 Cross-section distribution of depth-averaged velocity as a function of downstream distance from the channel expansion (channel discharge = $6.21 \text{ ft}^3/\text{s}$), with the culvert in place at a distance 20 ft downstream of the expansion

The large difference between velocities in the center of the channel and the sides of the channel is observed during all flow conditions. The majority of data were taken with the culvert located 8 feet (2.44 meters) downstream of the expansion, because this distance scales to 80 ft, which is the estimated extent of the prototype highway right-of-way. Figure 4.5 shows representative velocity distributions as a function of lateral position for runs where the six culvert box inlets were unsubmerged. The centerlines of the inner 4 barrels are located between 132.4 and 135.8 feet. The velocity measurements were taken upstream from and on the centerline of each of the barrels. This is not true of the data points that extend to 130 and 138 feet, which were taken in front of the culvert wingwalls. The most significant feature shown in this figure is the lower velocities in front of the outer culvert barrels, compared with the velocity in front of the central barrels. This confirms that the strong and narrow jet behavior shown in Figure 4.4 continues when the culvert is located 8 feet downstream of the abrupt expansion.

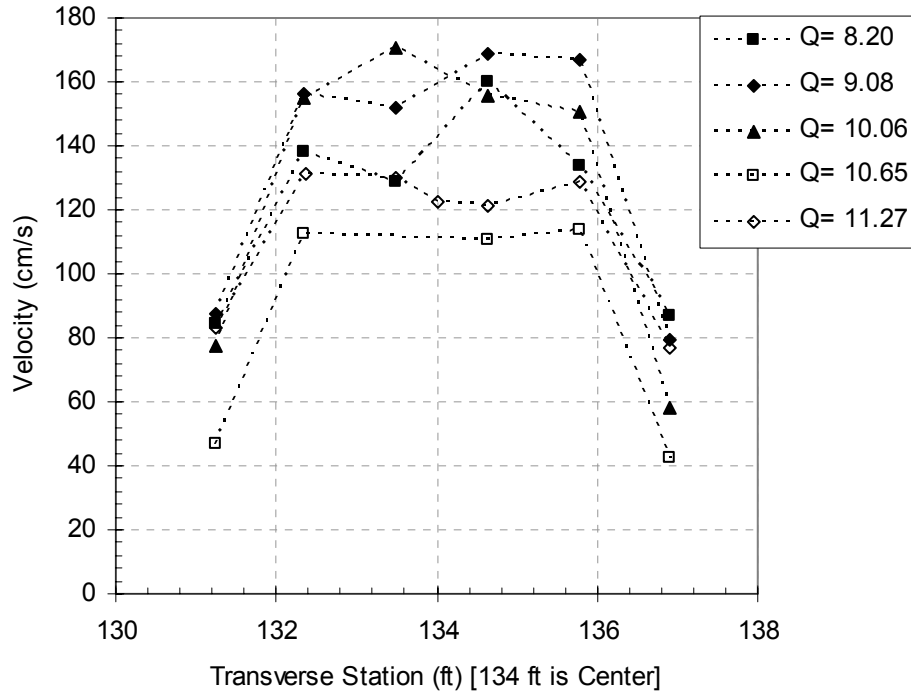


Figure 4.5 Lateral distribution of velocity for a range of channel discharge values with unsubmerged inlet conditions (Q in ft^3/s)

The distribution of depth and velocity, discussed above, both play a part in determining the distribution of specific energy upstream of the culvert, which is discussed in the following section.

4.3 Distribution of Specific Energy Upstream of the Culvert System

The specific energy is the sum of the water depth and the velocity head. As discussed in Section 2.3, water depth is often the only parameter considered in culvert performance because many culverts are designed to function under submerged conditions with a large upstream depth and small approach velocity head. In this section, it is shown that both the depth and velocity head components of specific energy are important in these experiments. Furthermore, it is shown that specific energy is not distributed evenly across the channel.

4.3.1 Variation of Specific Energy with Distance Upstream of the Culvert System

For some of the experiments, two or four of the culvert barrels were blocked, so experiments in the indoor channel had 2, 4 or 6 barrels open. Furthermore, a straight rectangular channel that is 5 feet (1.5 meters) wide was used in additional experiments with a single barrel box culvert. In the 1, 2, 4, and 6-barrel culvert systems investigated, it was found that specific energy did not vary significantly with distance upstream of the culvert. This finding was true both for measurements in the center of the channel and those taken off the centerline of the channel. Figure 4.6 shows representative results from several experiments with 1, 2, 4, and 6-barrel culvert systems. Both submerged and unsubmerged

inlet conditions are included, and the measurements were taken along the channel centerline. The upstream distance extends into the upstream channel section (above the abrupt expansion).

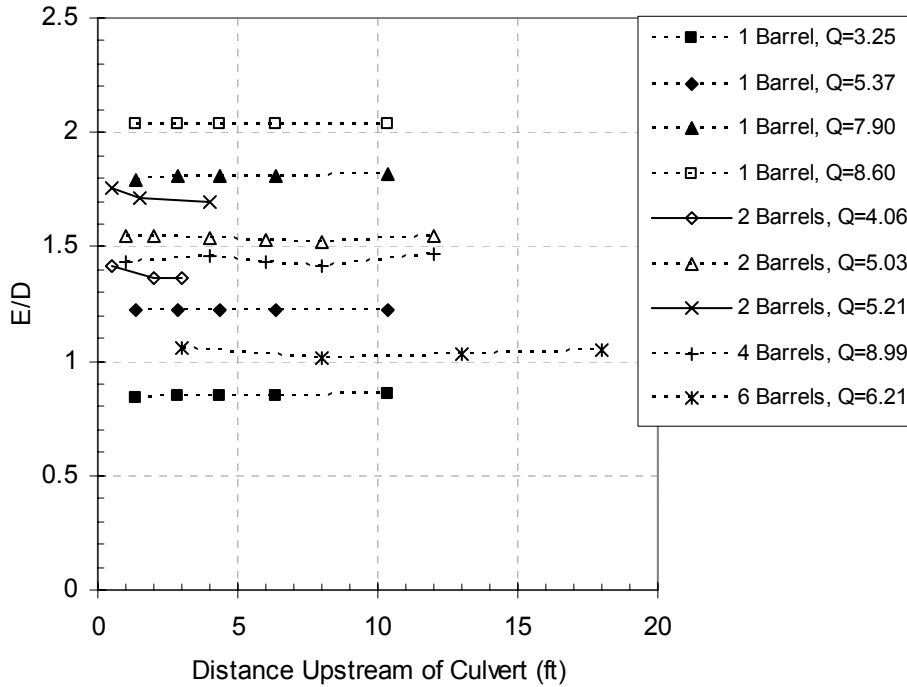


Figure 4.6 Variation of specific energy with distance upstream of the culvert for different discharge values (Q in ft^3/s) and number of barrels

In the above figure, one can see that for some experiments (solid lines) with measurements taken immediately upstream of the culvert system, E/D increases slightly just in front of the culvert. This effect may be a result of the standing wave that develops in front of the inlet to the culvert boxes (see Figure 4.11). In addition, one can see what may be an increase in E/D at large distances upstream of the culvert. This happens because these points are actually measured upstream of the channel expansion. It is reasonable that they have higher specific energies because they have not yet lost energy going through the expansion. Aside from these small and large distances upstream of the culvert, it is clear that E/D does not strongly vary as one moves along the centerline upstream of the culvert. This finding was true also for points not on the channel's centerline, as discussed below.

Figure 4.7 shows E/D values measured at various transverse positions across the channel cross section for an experiment with discharge $6.2 \text{ ft}^3/\text{s}$ ($0.176 \text{ m}^3/\text{s}$) and the culvert located 20 feet downstream of the expansion. Though the data-series curves are not perfectly flat, there is not a consistent relationship between E/D and transverse position. Indeed, depending on the transverse location, E/D values can vary by 25%.

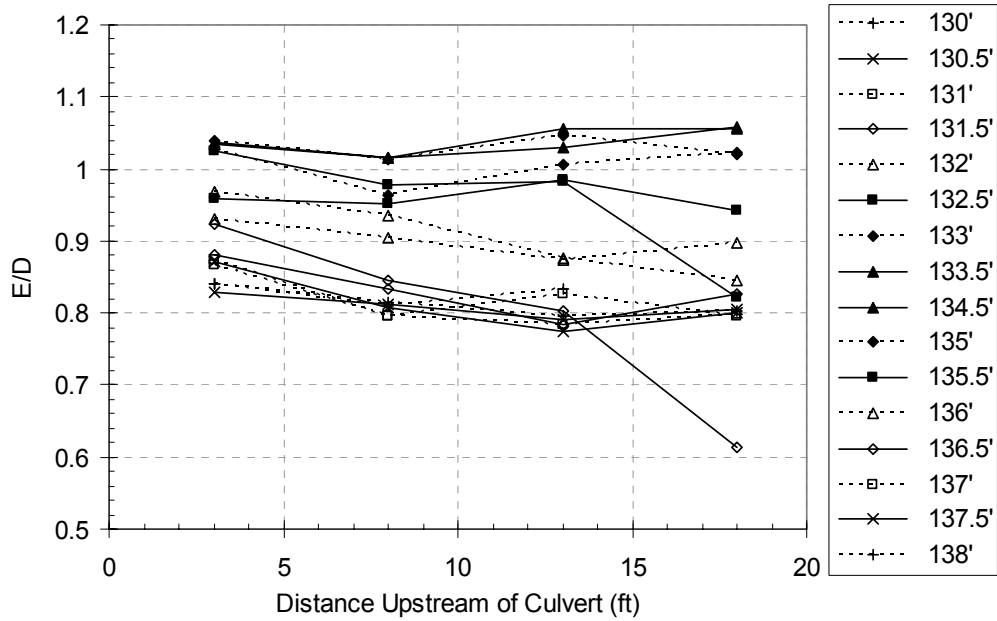


Figure 4.7 Variation of E/D with upstream distance for transverse locations across the channel cross section. Channel centerline is at 134 ft.

Figure 4.8 shows another view of the same data shown in Figure 4.7. Figure 4.8 shows the distribution of specific energy as a function of transverse location for different upstream distances from the culvert. The errant data points are clear, and one can also see there is not one distance upstream that is consistently higher or lower than the others. Nevertheless, the resulting picture of distribution of specific energy is much clearer than in Figure 4.7. The increase in specific energy towards the middle of the channel is associated with the increased velocity of the jet downstream of the expansion.

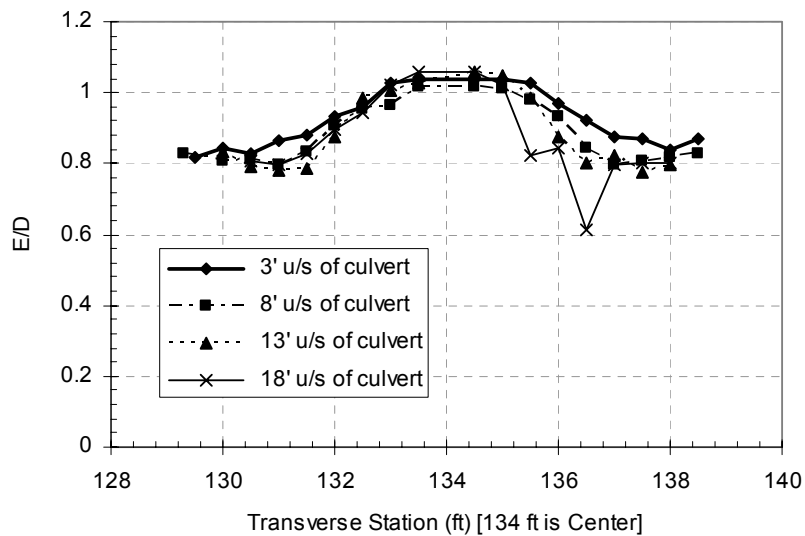


Figure 4.8 Variation in specific energy with transverse location for data set of Figure 4.7

4.3.2 Variation of Specific Energy with Cross-Section

In contrast to the weak dependence of specific energy on distance upstream of the culvert, the data show a strong relationship between lateral position and specific energy. The degree to which specific energy varied depended on the type of culvert flow; for an unsubmerged culvert inlet, this variation was most pronounced. Figure 4.9 shows the lateral variation of specific energy immediately upstream of the culvert for a number of representative experiments with discharge values ranging from 8.20 – 11.27 ft³/s (0.232 – 0.319 m³/s). When experiment results from all runs are considered (discharge values ranging from 3.90 – 11.69 ft³/s (0.111 – 0.331 m³/s)), it is clear that all of the experiments exhibit a marked difference between E/D values for the middle barrels and for the outer barrels. Averaging over all of these runs, the average E/D value for the middle 4 barrels is 37 percent greater than the E/D value associated with the outer 2 barrels.

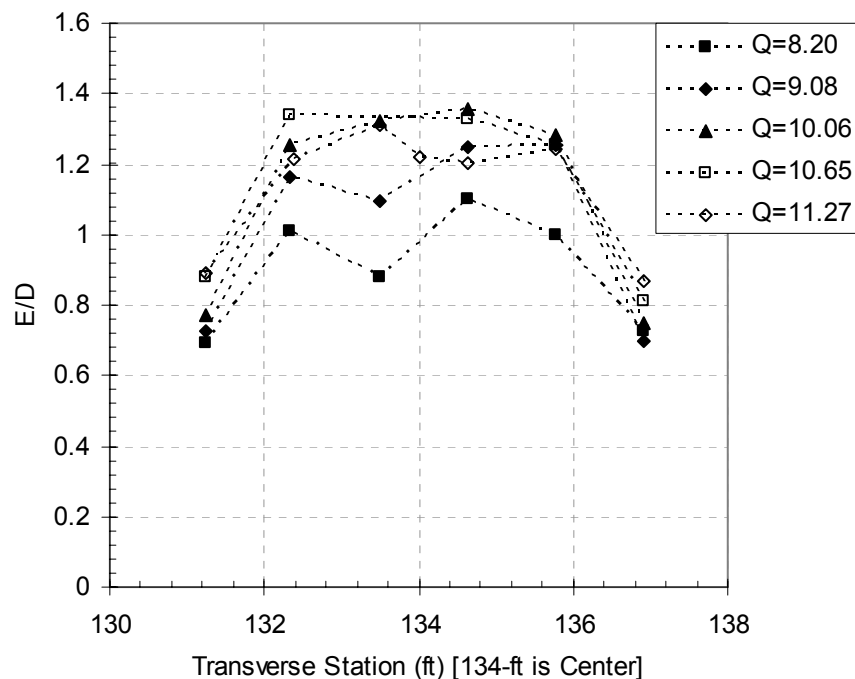


Figure 4.9 Lateral variation of specific energy for unsubmerged inlet experiments (Q in ft³/s)

The dependence of specific energy on lateral location is greatly reduced when the culvert entrance becomes submerged. Figure 4.10 shows that when the depth of water is greater than the barrel rise, the variation of E/D with transverse position is visible but not large. This variation indicates that, even for situations where the barrels span the width of the jet, the energy in the center of the jet is slightly higher than it is on the edges. With the tailgate down, the capacity of the pumps did not allow submergence of the culvert when 6 barrels were open. The tailgate was raised for one of the experiments shown in Figure 4.10 with 6 barrels open, allowing the inlet to be submerged. Data from this experiment demonstrates that lateral variations in E/D are minimal when the culvert inlet is submerged.

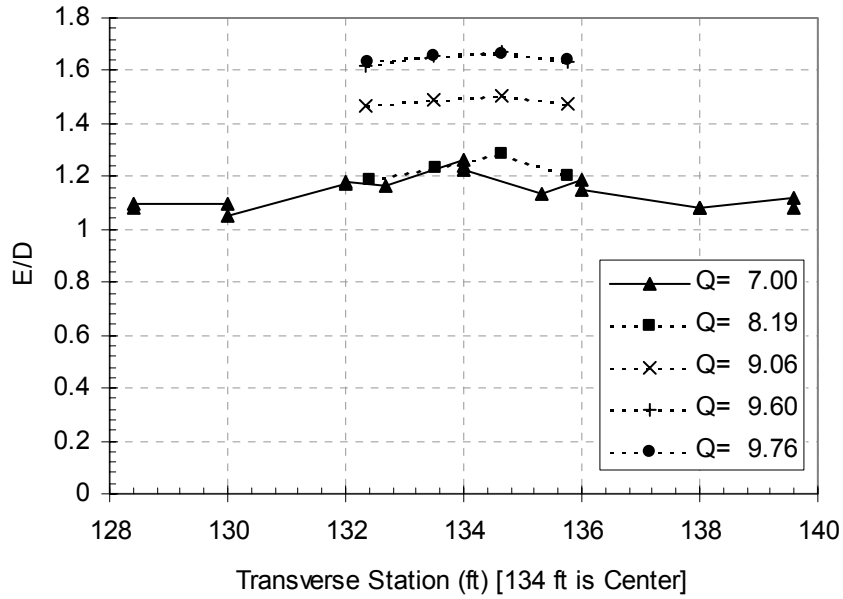


Figure 4.10 Lateral variation of specific energy for submerged inlet conditions with 4 and 6 barrels open

As shown in this section, there is little change in specific energy as one moves upstream of a culvert, while there may be strong dependence of specific energy on lateral position within the channel cross section. This suggests that culvert barrels are not subjected to the same driving energy, and that the distribution of flow among the barrels is not uniform. This is certainly visible in Figure 4.11, which shows the standing wave that develops near the culvert inlet.

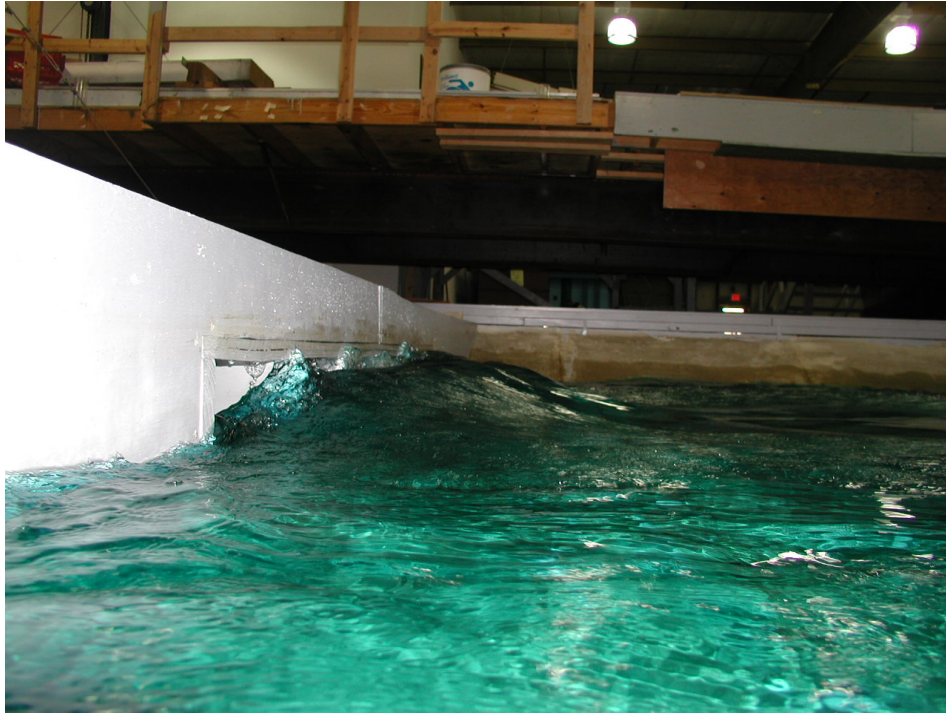


Figure 4.11 Standing wave at culvert inlet

4.4 Performance Curves for Box Culverts

4.4.1 Development of Performance Curve Equations

Experiments have been performed in the CRWR indoor channel with channel expansion and box culvert system for various combinations of 2, 4, and 6 barrels open, and for different flow rates. For the data discussed here, the tailgate was low, causing a drop from subcritical flow upstream of the culvert box to supercritical flow downstream. This resulted in the culvert operating under inlet control. Other experiments were performed in the outdoor channel with a single barrel culvert, also operating under inlet control. Two different barrel spans were evaluated in the single-barrel outdoor channel. For each set of

experiments, the total discharge was measured as well as the depth and velocity upstream of each barrel.

When the experimental data were plotted according to the format shown in Figure 2.3, the data were better fit by the Henderson model equations than the FHWA equations. For this reason, the model form of the equations from Henderson (1966) is re-evaluated. For an unsubmerged culvert operating under inlet control, Henderson assumes that critical flow occurs near the culvert entrance. However, because of width contractions associated with vertical edges of the culvert, the effective width is $C_b B$ (for rounded edges, $C_b = 1$). Thus the barrel discharge is $Q = C_b B y_c v_c$. Since the flow is critical ($Fr = 1$), $v_c = (g y_c)^{1/2}$, and $Q = C_b (g)^{1/2} B (y_c)^{3/2}$. Again, because the flow is critical, $y_c = (2/3) E_c$, where E_c is the specific energy at critical flow (see equation (2.25)). If energy losses between the headwater and critical sections are negligible, and if there is no significant change in elevation, then the energy equation states that $HW = E_c$, where HW is the headwater specific energy. With these assumptions, the discharge for an unsubmerged inlet operating under inlet control is given by

$$Q = C_b \sqrt{g} \left(\frac{2}{3} \right)^{3/2} B (HW)^{3/2} \quad (4.1)$$

Equation (4.1) differs from Henderson's equation (2.19) in that the upstream headwater (specific energy) is used, rather than the upstream water depth. Two alternative and convenient forms for writing equation (4.1) are

$$\frac{Q}{BD \sqrt{gD}} = C_b \left(\frac{2}{3} \right)^{3/2} \left(\frac{HW}{D} \right)^{3/2} \quad (4.2)$$

$$\frac{HW}{D} = \frac{3}{2} \left(\frac{1}{C_b} \right)^{2/3} \left(\frac{Q}{BD \sqrt{gD}} \right)^{2/3} \quad (4.3)$$

Both equations (4.2) and (4.3) represent dimensionless performance curves for an unsubmerged box culvert under inlet control.

When the headwater becomes large compared with the culvert rise, the entrance becomes submerged, and the culvert behaves effectively like a sluice gate. Consider the configuration shown in Figure 4.12. With HW representing the headwater specific energy, application of the energy equation gives

$$HW = \frac{v_{en}^2}{2g} + C_c D \quad (4.4)$$

In equation (4.4), energy losses between the upstream (headwater) station and the culvert entrance have been neglected. Any such losses will be included within the various coefficients. The velocity at the culvert entrance is

$$v_{en} = \sqrt{2g(HW - C_c D)} \quad (4.5)$$

Application of an end contraction coefficient C_b then gives

$$Q = (C_b B)(C_c D)v_{en} = C_b C_c B D \sqrt{2g(HW - C_c D)} \quad (4.6)$$

This equation may be written more conveniently as

$$Q = C_d B D \sqrt{2g(HW - C_c D)} \quad (4.7)$$

According to this formulation, the following relationship should hold between the two contraction coefficients and the discharge coefficient:

$$C_d = C_b C_c \quad (4.8)$$

Equation (4.7) differs from Henderson's equation (2.30) in that the upstream specific energy is used rather than the depth, and the leading coefficient is a discharge coefficient given by equation (4.8), rather than the contraction coefficient. Equation (4.7) may also be written in two alternative and useful forms:

$$\frac{Q}{B D \sqrt{g D}} = C_d \sqrt{2 \left(\frac{HW}{D} - C_c \right)} \quad (4.9)$$

$$\frac{HW}{D} = \frac{1}{2 C_d^2} \left(\frac{Q}{B D \sqrt{g D}} \right)^2 + C_c \quad (4.10)$$

Equations (4.9) and (4.10) represent dimensionless performance curves for submerged box culverts operating under inlet control.

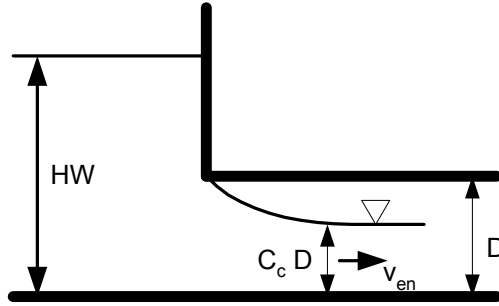


Figure 4.12 Culvert entrance acting as a submerged sluice gate

The models presented by equation (4.1) and (4.7) have interesting characteristics. To find the point where the unsubmerged and submerged equations meet, equations (4.2) and (4.9) are equated, which upon rearrangement gives

$$\left(\frac{HW}{C_c D}\right)^3 - \frac{27}{4}\left(\frac{HW}{C_c D}\right) + \frac{27}{4} = 0 \quad (4.11)$$

It is not difficult to show that the roots of this cubic equation are 3/2 (which is a double-root) and -3. Only the positive root(s) is physically possible, so the condition at which the culvert first becomes submerged with increasing headwater is given by

$$\frac{HW}{D} = \frac{3}{2} C_c \quad (4.12)$$

Furthermore, the slope at this point of contact between the two model equations may be calculated for both curves. From equations (4.2) and (4.9) one finds

$$\frac{d\left(\frac{Q}{BD\sqrt{gD}}\right)}{d\left(\frac{HW}{D}\right)} = C_b \sqrt{\frac{2}{3}} \frac{HW}{D} \quad ; \quad \frac{d\left(\frac{Q}{BD\sqrt{gD}}\right)}{d\left(\frac{HW}{D}\right)} = \frac{C_b C_c}{\sqrt{2\left(\frac{HW}{D} - C_c\right)}} \quad (4.13)$$

Substituting equation (4.12) into (4.13) shows that the slope of both equations is equal to $C_b \sqrt{C_c}$, thus the curves not only touch at this point, they become tangent to each other. This results in a smooth transition within the model between unsubmerged and submerged conditions.

4.4.2 Fitting of the Performance Curves

When fitting the measured data to the performance-curve model equations to estimate the unknown coefficients C_b , C_c , and C_d , one difficulty that arises with the multiple-barrel

culverts is that while the total channel discharge is known, the discharge through each barrel is not. The data from Section 4.3 shows that the headwater is lower for the outer barrels than for those located closer to the channel centerline. It is clear that the discharge is not the same for each barrel. In order to utilize all of the data, the following approach is taken. Using the measured headwater for each barrel, the performance equations are used to predict the barrel discharge. The individual barrel discharge values are then corrected using the following equation:

$$Q_i = Q_i^* \times \frac{Q_T}{\sum_i Q_i^*} \quad (4.14)$$

In equation (4.14), Q_i is the corrected barrel discharge, Q_i^* is the calculated barrel discharge using the measured barrel headwater and the performance equation, and Q_T is the measured channel discharge. The result is a set of data that is consistent with the individual barrel headwater measurements and the measured total channel discharge.

The data that is plotted for each barrel consists of the variables

$$\frac{y_a + \frac{v_a^2}{2g}}{D} = \frac{HW}{D} \quad (4.15)$$

$$\frac{Q_i}{A\sqrt{gD}} \quad (4.16)$$

In equation (4.15), y_a and v_a are the approach depth and velocity near the entrance to the culvert barrel. D is the culvert rise, Q_i is calculated using equation (4.14), and A is the total area of the box culvert barrel ($A = B D$).

The culvert performance data for all of the experiments in the indoor and outdoor channels are plotted as shown in Figure 4.13. The 2, 4, and 6-barrel data sets are for the indoor channel with an abrupt expansion. The 2-barrel (n), 4-barrel (n) and 6-barrel (n) data sets are for the indoor channel with the gradual expansion. The data set labeled 1-barrel is for the outdoor channel, while the set labeled 1-barrel (n) is from the outdoor channel with the culvert barrel having the smaller span.

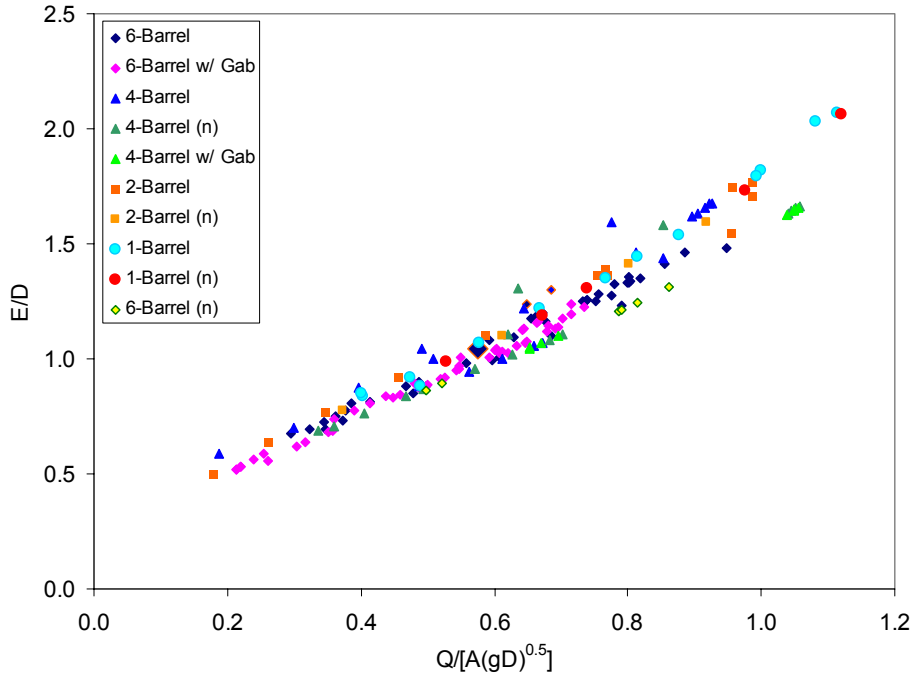


Figure 4.13 Box culvert performance data

The coefficients in the model equations are fit to the data set using the method of least squares. For each measured data-value $(HW/D)_d$, the model equations are used to calculate a model-value $(Q/[A(gD)^{0.5}])_m$. The standard error is then calculated from

$$S.E. = \sqrt{\frac{1}{N} \sum_{i=1}^N \left\{ \left(\frac{Q}{A\sqrt{gD}} \right)_{mi} - \left(\frac{Q}{A\sqrt{gD}} \right)_{di} \right\}^2} \quad (4.17)$$

The first time through, the parameters C_b and C_c were varied manually until a minimum value of the standard error (S.E.) was found. This value gave the parameters $C_b = 1.08$ and $C_c = 0.601$ (which together give $C_d = 0.649$). The corresponding standard error is $S.E. = 0.0376$. The resulting performance curve along with lines located one standard error above and below the mean curve is shown in Figure 4.14. Once the minimum standard error was determined, the relationship $C_d = C_b C_c$ was relaxed, and the magnitude of C_d was varied independently. It was found that either increasing or decreasing C_d resulted in an increase in standard error, thus confirming equation (4.8).

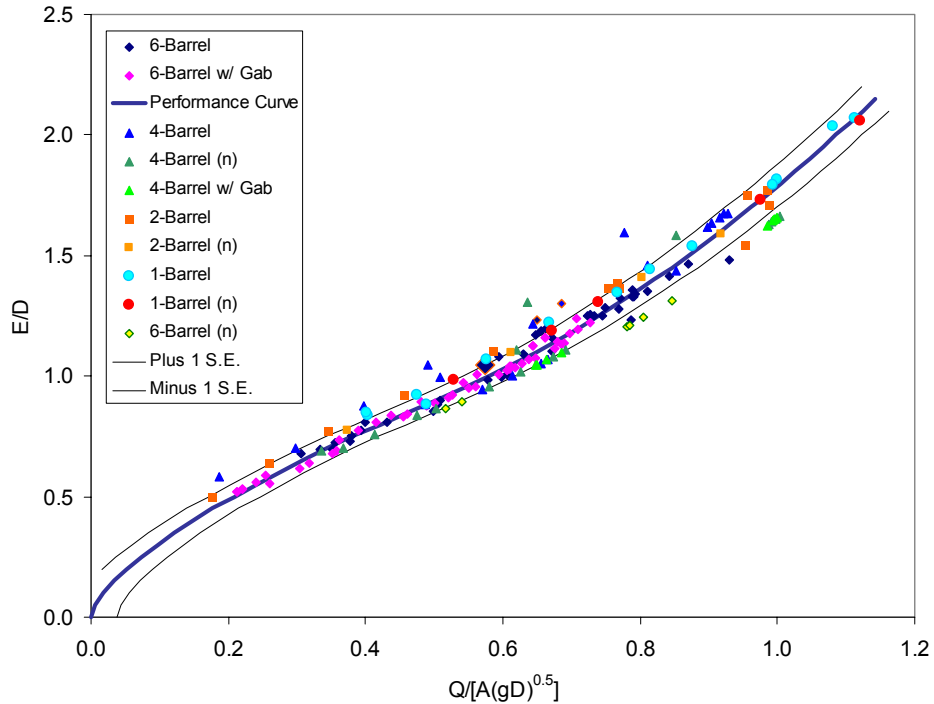


Figure 4.14 Performance curve plus/minus one standard error

One of the difficulties with the model fit shown in Figure 4.14 is the estimated value of the C_b coefficient. As suggested in Section 4.4.1, the physical interpretation of C_b is that it expresses a contraction coefficient that reflects the inward (centerline) momentum associated with flow around the vertical edges of the box culvert. As such, it should have a maximum value of 1.0 for effectively rounded edges. The value of C_c is essentially the same as that suggested by Henderson (1966).

In order to reflect the physical interpretation of C_b , the minimum standard error was again evaluated with a constraint that C_b was equal to (or less than) 1.0. With this constraint, the minimum standard error was found to be $S.E. = 0.0484$, with corresponding parameter values $C_b = 1.0$, $C_c = 0.667$, $C_d = 0.667$. This is an increase in standard error of almost 30%, compared with the unconstrained case. The resulting performance curve is shown in Figure 4.15.

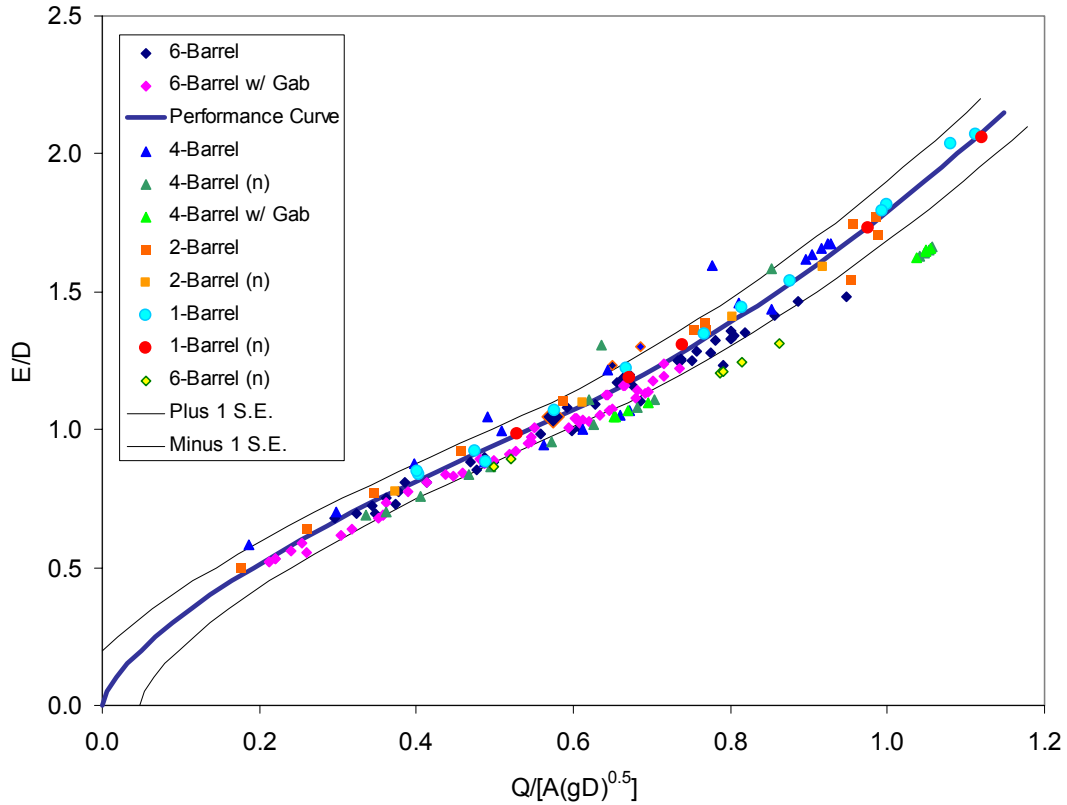


Figure 4.15 Constrained ($C_b = 1$) performance curve with standard error

Figure 4.16 compares these two performance curve models with that presented by Henderson (1966) and discussed in Chapter 2. Henderson's curves use equation (2.19) with $C_b = 0.9$ and equation (2.30) with $C_c = 0.6$. These two curves intersect at $E/D = 1.20$. For a given headwater, both of the curves presented here predict a larger discharge, and comparison with Figure 2.3 shows that the equations presented here also predict a larger discharge than the FHWA equations. Based on physical arguments, the latter form of Figure 4.15 with $C_b = 1$ and $C_c = C_d = 2/3$ is preferred.

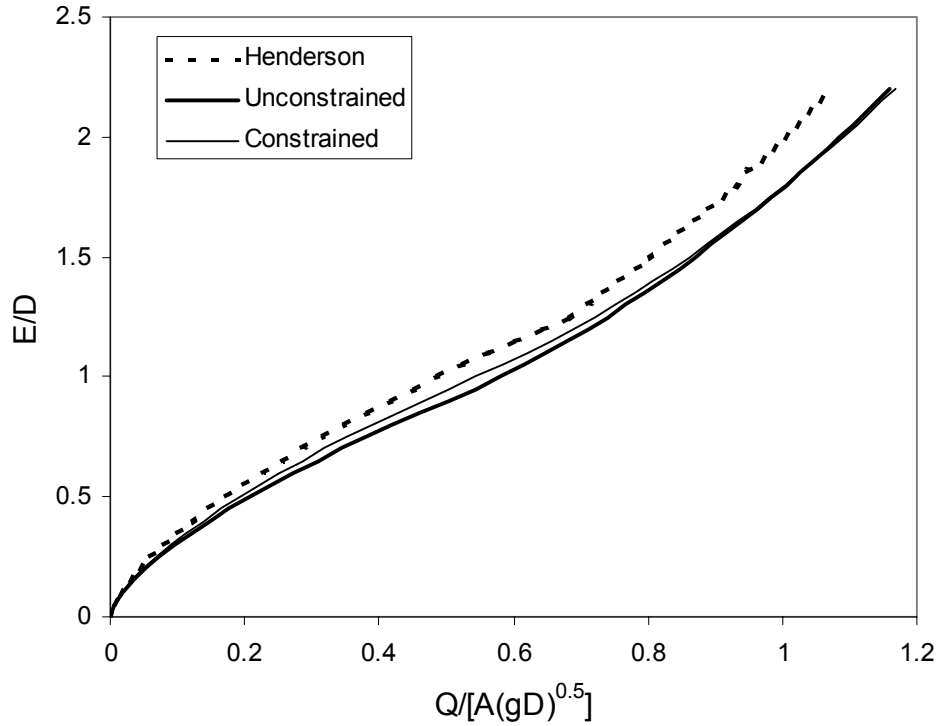


Figure 4.16 Comparison of performance curves

Figure 4.17 shows another view of the culvert performance data developed during the experiments reported herein. This is a normalized plot of the measured depth versus specific energy upstream of the culvert. If all of the data lay near the 1-to-1 line, then culvert performance could be predicted by upstream depth alone. The expression for the specific energy may be written

$$\frac{E}{D} = \frac{y}{D} + \frac{v^2}{2gD} = \frac{y}{D} \left(1 + \frac{Fr^2}{2} \right) \quad (4.18)$$

Using equation (4.18), lines are drawn on Figure 4.17 marking the relationship between depth and specific energy for Froude number values of 1 and 2 (a Froude number value of 0 corresponds to the 1-to-1 line). A number of the data points for the 4 and 6-barrel culvert systems fall between the $Fr = 1$ and $Fr = 2$ lines, showing that the approach flow is supercritical. This suggests that the performance curves are valid for both subcritical and supercritical flow conditions upstream of the culvert system.

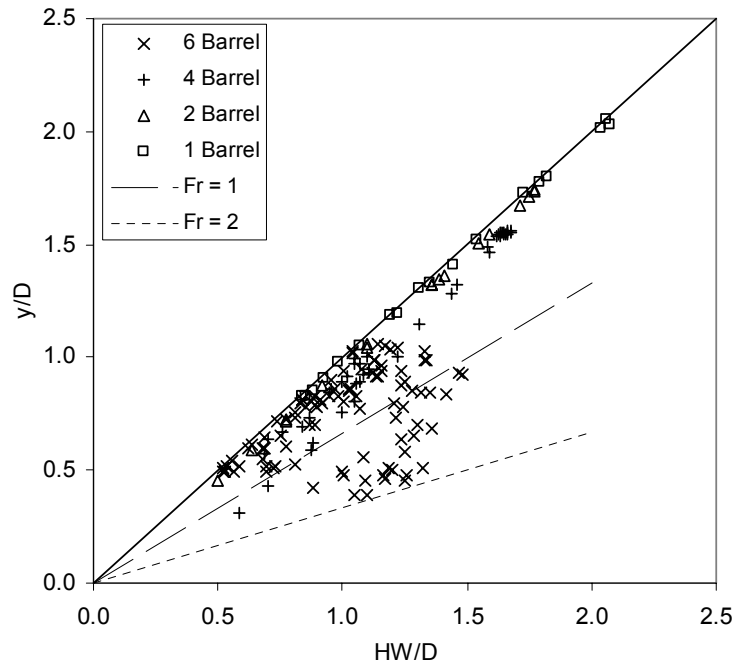


Figure 4.17 Performance data showing depth versus specific energy and that data includes both subcritical and supercritical flow conditions

5. FESWMS Modeling

5.1 Introduction

The major steps in the process of developing a model for a hydraulic system include data collection, network design, model debugging, model testing/calibration/verification, and finally model application. This chapter describes the application of this process to the physical model basin described in Chapter 3. Following model calibration, the model is applied for different channel configurations to investigate the effects of changing the channel expansion ratio.

5.2 Data Collection

Numerical modeling relies heavily on data such as measured flow rates, velocities, water depths, channel bathymetry, material properties, and other characteristics. In developing a model for the physical channel described in Chapter 3, the finite element mesh is built with the same dimensions and bathymetry as the physical model.

The FESWMS numerical model requires boundary condition data on the flow rate entering the system, the water surface elevation at the downstream end of the region being modeled, and the amount of shear stress to be applied at the closed boundaries of the system. The closed boundaries are the channel and culvert walls where no flow enters or exits the system. A good calibration also requires several water depth and velocity measurements in the area of interest. The research team collected discharge, velocity, and water depth data from the physical model. Several sets of physical model data were taken at different flow rates. Two sets of data were taken with no culvert in the channel so numerical model construction and calibration techniques could be practiced on a simple scenario. Three sets of data were taken with the culvert in the channel at locations 20 ft, 10 ft, and 12 ft downstream of the expansion. Murdock (2002) describes these data sets.

While the actual velocity in an open channel varies with depth, FESWMS uses depth-averaged velocities. The horizontal components of velocity and water depth were measured at calibration points for three cross sections in the channel. Figure 5.1 shows the calibration point locations for the experiment with the culvert 12 feet downstream of the expansion. Numerical model results for these calibration points can be compared to measured data for velocity and water depth.

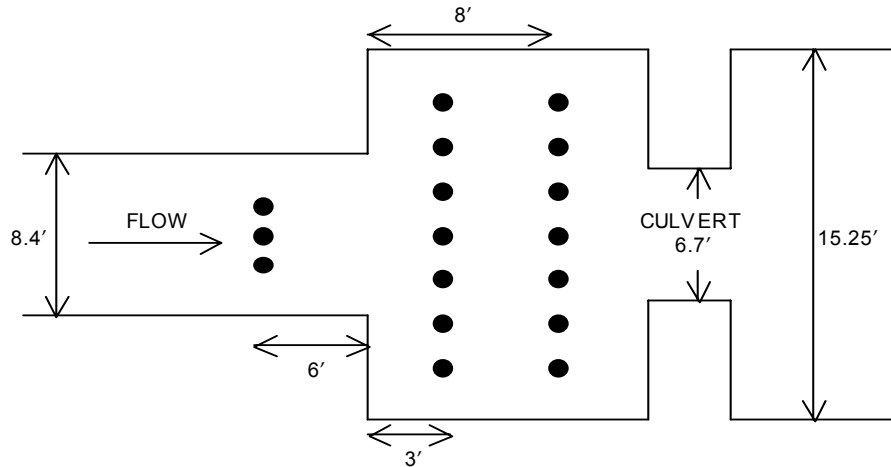


Figure 5.1 Calibration point locations in physical model

Two-dimensional models can accurately simulate surface water flows when the vertical (z) component of velocity is small compared to the horizontal (x and y) components. Figure 5.2 illustrates the average x, y, and z velocity components at the cross section 8 feet downstream of the expansion that is shown in Figure 5.1. The downstream (x) component of velocity clearly dominates the flow in the channel. At each station, the magnitude of z-velocity components is small compared to the magnitude of the x-velocity component. The magnitude of y-velocity is larger than the z-velocity for all but one station along the cross section. The direction of the velocity components changes for the outside locations that are in the recirculation zone. Observations and data taken from the physical model show that a one-dimensional model would not be appropriate for this channel with expansion and culvert due to the presence of recirculation near the outer edges of the expansion area. The data also show that the vertical velocity component is small compared to the horizontal components, and therefore a three-dimensional model is not needed. The two-dimensional modeling approach taken here is appropriate for modeling channel expansions leading to wide culverts.

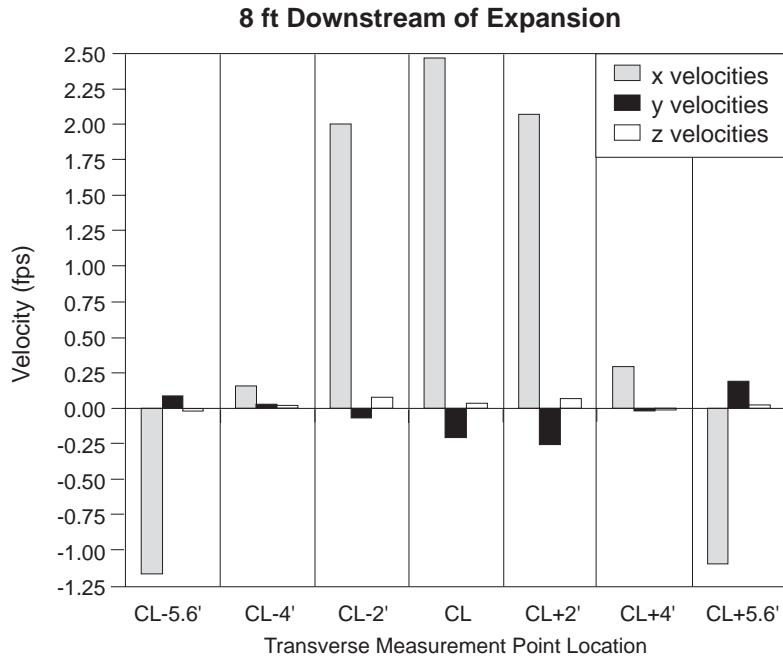


Figure 5.2 Velocity component comparisons for physical model data

5.3 Numerical Model Network Design

In finite element modeling, the physical system to be modeled is divided into subregions called elements. Elements have a set of points called nodes associated with them. Nodes are computation points where the model solves for the unknowns (U, V, H). The modeler specifies the location of the corner nodes; midside and center nodes may be created automatically by SMS to provide more computation points for better solution detail. Figure 5.3 shows an example element. Elements are typically quadrilateral or triangular. A finite element network, also called a mesh, is a group of elements assembled to represent the domain of the physical system. A picture of the finite element mesh for the physical model of the expansion and culvert system is shown in Figure 5.6 at the end of this section.

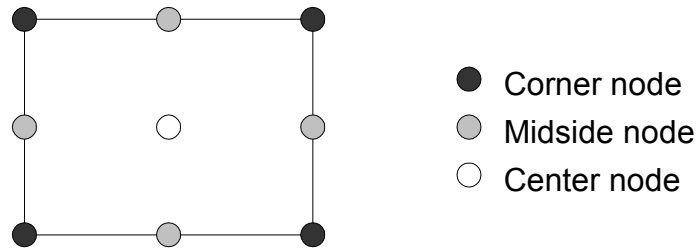


Figure 5.3 Example of a two-dimensional finite element with node points

Network development is the process of planning and building a finite element network or mesh. ASCE (2001) and Froehlich (1996) suggest general guidelines to aid finite element modelers in developing a network that will run properly. The guidelines

include network layout planning, element shape rules, and mesh guidelines. The layout of the network, including the necessary number of elements, should be planned before starting construction of the mesh. Regions of the domain that are of special interest should be identified.

Quadrilateral elements should be used wherever possible and practical. For quadrilateral elements, interior angles should be between 30°-150° to avoid computation problems. For triangular elements, interior angles should be between 10°-150°. Aspect ratio is the ratio of the length of the longest element side to the shortest element side. The aspect ratio should be greater than unity and less than 10 in the expected flow direction. If the flow direction is not known, elements should have an aspect ratio close to unity. In other words, elements should be elongated in the direction of the flow if the direction is known, but not too much so. Slope should be consistent within each element so problems associated with ambiguous direction of drainage will not occur. SMS includes tools to identify and fix problematic elements. These element shape rules should be checked in the mesh editing process.

Elements need to be consistent with each other. When the size of elements transition from larger to smaller, it is important for the size change to be gradual. A general rule is that an element should be between one-half to twice the size of its adjacent elements. The mesh must contain enough elements to model the detail and location of geometric features such as changes in channel cross section (channel transitions). An increased number of elements can give better answers if all of the nodes are well-formed, but having too many elements increases the computation time and increases the likelihood of having ill-formed elements (ASCE, 2001).

5.3.1 Network Development Process

The first step in the network development process is to establish a conceptual model of the domain. The conceptual model is a description of the site, including geometric features such as banks, the boundary of the domain to be modeled, flow rates and water surface elevations of boundary conditions, and different material zones. The SMS pre-processing capabilities may be used to set up the conceptual model of the channel and convert it into a finite element mesh. Feature arcs are created to form the boundaries and sections of the model. The vertices along the arcs are redistributed to the desired finite element density, allowing grid spacing of the mesh to be specified. A relatively uniform distribution of vertices is desirable so the elements are close to rectangular. Figure 5.4 shows a conceptual model of the physical model channel, where vertices have been redistributed along the arcs. Generally, in this channel the direction of flow is known, and it is desirable to have rectangular elements elongated in this direction of flow. However, the recirculation zones at the outer edges of the physical model expansion section exhibit flow in a circular pattern, so elongation of the elements in the downstream direction is limited. For the present modeling effort, the conceptual model was initially set up to create elements 2 feet long in the direction of the channel axis and 1 foot wide in the transverse direction in the expansion area, resulting in an aspect ratio of 2:1. The size of the elements was later altered to provide finer resolution.

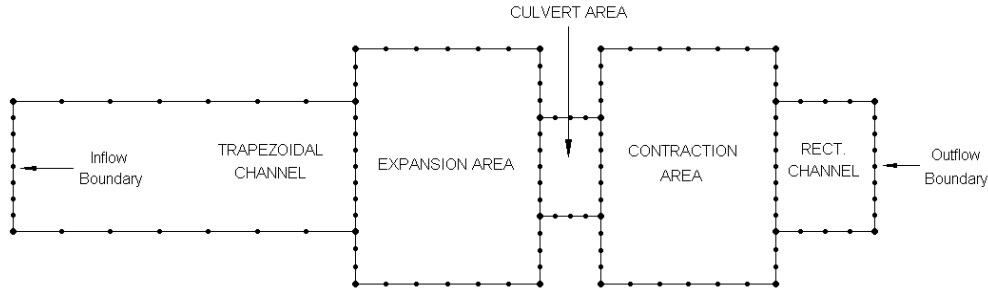


Figure 5.4 Setup of conceptual model

After the conceptual model is built, a mesh or grid network is automatically constructed to fit the conceptual model and the model data are converted from the conceptual model to the elements and nodes of the mesh network. Polygons are automatically created in SMS from the groups of arcs forming the model boundaries and sections. Material types and meshing parameters are then assigned to each polygon. The entire physical model surface is concrete, so that is the only material type specified in the mesh.

Meshing parameters control the shape and distribution of elements by specifying how the vertices along the edges of polygons will be connected inside the polygons to form elements. In SMS the user chooses an automatic finite element mesh generation method for each polygon. Two options are Coons Patch and Tessellation, and Figure 5.5 shows the difference between these mesh generation methods as applied on the conceptual model polygon representing the expansion section. This project uses the Coons Patch for all elements, requiring a three- or four-sided polygon (for this application, four-sided polygons that create rectangular elements are used).

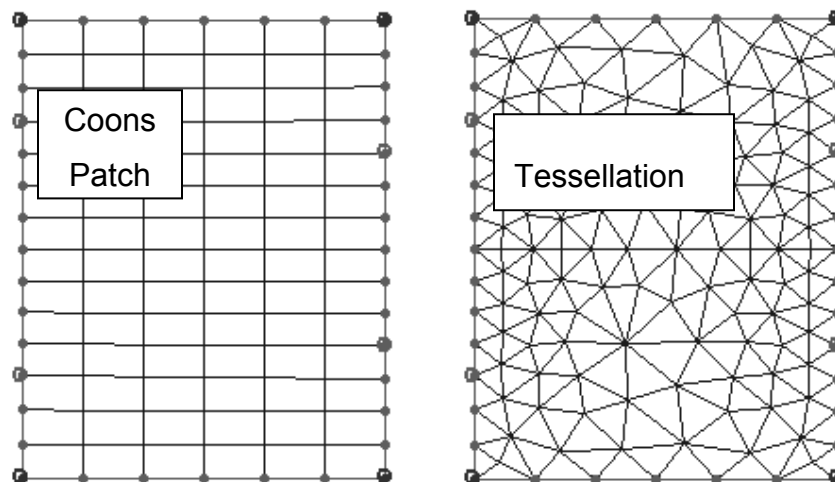


Figure 5.5 Coons Patch and Tessellation mesh generation techniques

Inflow and outflow boundary conditions need to be located where the flow is stable and approximately one-dimensional. Figure 5.4 shows the locations of inflow and outflow

boundary conditions in the conceptual model. Boundary conditions must be applied along the whole cross section. For all the modeling runs, the flow rate entering the system is the inflow boundary condition (located at the upstream boundary) and the water surface elevation just upstream of the tailgate is the outflow boundary condition (located at the downstream boundary). The flow is subcritical in the trapezoidal channel upstream and in the rectangular channel downstream. The flow rate is specified to enter perpendicular to the boundary and is applied along the entire inflow boundary. Boundary conditions will be discussed further in the next section.

Elevation points can be interpolated onto the finite element mesh to assign channel bottom elevation values to the nodes. As noted in Chapter 3, the physical model was surveyed to obtain detailed elevation data for the numerical model. An elevation point file was constructed from the survey points and interpolated onto the mesh. Since the mesh is relatively small, one could alternatively assign elevations to each node point individually. When more than one point have the same elevation, all of the points can be selected at the same time and elevation assigned accordingly.

5.3.2 Culvert Representation in FESWMS

FESWMS allows users to specify culverts as either one-dimensional or two-dimensional elements. One-dimensional elements act as one-dimensional links between node points on the upstream and downstream sides of the culvert. Each culvert barrel can be modeled as a separate culvert using a separate one-dimensional link. Information on culvert material, shape, inlet type, entrance loss coefficient, roughness, height, width, length, and upstream and downstream invert elevations are input to FESWMS.

When culverts are represented with one-dimensional elements in FESWMS, the flow rate (Q_c) through a culvert with inlet control is computed using

$$Q_c = C_d A_c \sqrt{2g(z_{s_{up}} - z_{inv_{up}})} \quad (5.1)$$

$$C_d = \frac{1}{\sqrt{1+k_e}} \quad (5.2)$$

For outlet control in FESWMS the culvert discharge is calculated from

$$Q_c = C_d A_c \sqrt{2g(z_{s_{up}} - z_{s_{down}})} \quad (5.3)$$

$$C_d = \frac{1}{\sqrt{1+k_e + \frac{2gn_c^2 L_c}{\phi^2 R_c^{4/3}}}} \quad (5.4)$$

In equations (5.1) to (5.4) the following parameters and variables are defined:

- C_d = culvert discharge coefficient
- A_c = cross-section area of culvert barrel
- $Z_{s_{up}}$ = upstream water-surface elevation
- $Z_{inv_{up}}$ = upstream invert elevation
- $Z_{s_{down}}$ = downstream water-surface elevation
- g = acceleration of gravity
- k_e = entrance loss coefficient (depends on entrance type)
- n_c = Manning's roughness coefficient of the culvert
- R_c = hydraulic radius
- L_c = culvert barrel length
- ϕ = 1 for metric units, 1.49 for English units

There are a couple of factors that make use of one-dimensional culvert elements inappropriate for this work. Both equations (5.1) and (5.3) require that the entrance be submerged and at least the upstream part of the culvert flow full. In addition, the headwater is taken as the upstream depth of the water surface above the culvert invert, rather than the upstream specific energy. As the experiment results in Chapter 4 show, the upstream kinetic energy of the approaching flow can be significant for low-head culverts. For these reasons, one-dimensional elements were not used.

In this project the culverts take up a significant portion of the expanded channel and the ratio of the culvert width to the channel width is larger than in most culvert systems. Therefore two-dimensional culverts are best suited for this analysis since two-dimensional flow may occur in the culverts. ASCE (2001) guidelines state that "Bridges and culverts need to be modeled with two dimensional elements when they span large stream channels or are large in comparison to floodplain elements." Two-dimensional culvert representations allow the user to see velocity vectors and depths inside the culverts while the one-dimensional culverts do not. Two-dimensional culverts are represented by elements that are given a *ceiling elevation* based on the soffit height. A six-box culvert was modeled, so each culvert box was represented by separate groups of elements. This approach may be better suited for box culverts than for circular culverts with multiple barrels.

In order to represent the culvert more accurately, elements were inserted into the mesh to represent the walls of the culvert boxes. The way that the culvert walls are represented is similar to the way that bridge piers are modeled in FESWMS. Ports and South (1995) explained objects such as bridge piers may be modeled by creating an element that is the size and shape of the pier, and then assigning an element type of zero to that element. By specifying an element type of zero, FESWMS treats that element as a boundary through which flow cannot pass.

The culvert wall elements are disabled (turned off) so FESWMS will not simulate water flowing through them. Adding the culvert walls slows down the computed velocities at the calibration points along the centerline of the channel by 5 to 10 % (depending on distance from the culvert), and caused some numerical error and instability for eddy viscosities below 0.3 ft²/s. The model simulation velocity results along the centerline of

the channel in the expansion section were 4 to 8 % closer to the measured values in an early simulation when the culvert walls are not included in the mesh. However, further efforts showed that changing the culvert by adding walls does not change the eddy viscosity needed to calibrate the model. The finite element mesh that experienced numerical stability problems after adding the culvert walls needed to be refined upstream of and in the culvert to get better results.

Mesh refinement took place after the model had performed several simulations at the initial resolution. The mesh was also refined after the original mesh was constructed to show more detail in the expansion section. This update was incorporated into the mesh by doubling the resolution, creating elements in the expansion area 0.5 feet wide x 1 foot long. The sensitivity of the calibration results to the mesh refinement is discussed below.

Figure 5.6 shows the refined finite element mesh including elements for the culvert walls. It is contoured by bed elevation. The datum for the channel elevations is taken at the downstream end of the channel (on the right side in Figure 5.6). The physical model has an abrupt expansion, so the numerical model is similarly constructed to allow comparison and calibration to the physical model data.

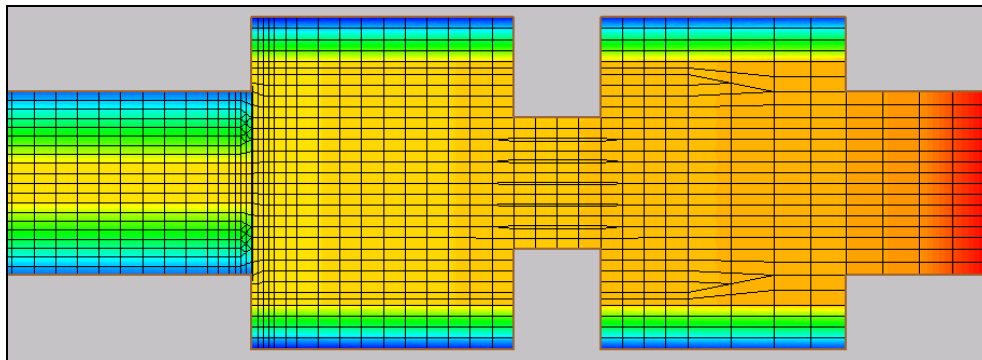


Figure 5.6 Completed version of finite element network

5.4 Model Debugging

Model debugging is the process of assigning parameters and boundary conditions to the model, specifying model control options and parameters, running the FESWMS model, inspecting the model layout and results, determining if refinement is needed. The main material properties include Manning's n , which is a roughness parameter used in the calculation of bed shear stresses appearing in the depth-averaged momentum equations, and parameters for the eddy viscosity model.

Chow (1959) listed Manning's n values for a variety of channel types, but these values have been determined assuming one-dimensional flow, and account for turbulence effects and transverse velocity variation along a cross section. These roughness values may be slightly larger than necessary since the depth-averaged flow equations account directly for horizontal variations of velocity and the effects of turbulence (Froehlich 1996). A Manning's n value of 0.0125 is used in the numerical model of the concrete channel. Tynes (1989) found Manning's n to be 0.0125 in his hydraulics experiments using the channel that was modified to build the current physical model. Chow (1959) gives a normal n value of 0.013 for trowel-finished concrete. The concrete slurry used in the

physical model contained no aggregate larger than sand, so the slightly smaller value is consistent with Chow (1959).

Eddy viscosity is another key parameter that needs to be specified in the model to represent the turbulent exchange of momentum. A more detailed discussion of eddy viscosity will be given during the discussion of model calibration in the next section. HEC (1995) found that turbulence terms damp numerical oscillations and higher values of eddy viscosity lead to greater stability in the solution. However, higher values of eddy viscosity also artificially flatten velocity gradients. Parameters of the eddy viscosity model are left to calibration.

FESWMS allows the user to select from several model control options and parameters that provide methods and data used to compute solutions for U, V, and H. A steady-state hydrodynamic simulation is selected with bottom stresses calculated using Manning's roughness. Coriolis forces are neglected because the rotation of the earth does not have a significant effect in the flows in small-scale channels. Wind stresses are not included in the steady-state model.

The water density is set to 1.937 slug/ft³. Water depth and velocity convergence are set to 0.001-0.01 ft and 0.001-0.01 ft/s, respectively. The maximum number of iteration allowed is 15. When combined with the "incremental loading" strategy that is described below, this approach was found to work satisfactorily. The momentum flux correction coefficients are $\beta_o = 1$ and $c_\beta = 0$ (see equation (2.48)), which results in the treatment of vertical variations in horizontal velocity as negligible.

Boundary conditions are required along all boundaries of the solution domain. The inflow and outflow boundaries are known as open boundaries. In this project, flow rate and direction are specified for the inflow boundary and water surface elevation and flow direction are specified for the outflow boundary. The inflow boundary condition specified for the model calibration run is 7 ft³/s, which is the flow rate in the physical model experiment used for calibration. The inflow is applied along the entire upstream cross section of the model. The outflow boundary condition specified is a downstream water surface elevation of 0.917 feet, which was also measured in the physical model experiment.

Slip conditions need to be specified for all closed boundaries, which in the present numerical model are the walls of the channel and culvert. The choices for closed boundaries are (1) slip boundary, (2) no-slip boundary, and (3) semi-slip boundary. Figure 5.7 illustrates the treatment of velocities near a closed boundary for all of the slip condition options. When *slip* is chosen, zero shear stress is applied to the closed boundaries, so water can slip along the mesh boundaries (channel walls). *Slip* conditions are typically used where flow depths are shallow and lateral shear stresses are negligible at the closed boundary (Froehlich, 1996). *No-slip* means that the shear stress along the closed boundaries causes the tangential velocity to equal zero. *No-slip* boundary conditions should only be specified for individual nodes. *No-slip* boundary conditions are applied when velocities along a boundary are known to be very small and a group of node points is created to resolve any large velocity gradients that may exist close to the boundary (Froehlich, 1996). *Semi-slip* applies zero shear stress at closed boundaries, just as for a *slip* condition, except for flow along a vertical wall. Using this condition, FESWMS applies a tangential shear stress, caused by friction, along a vertical wall. The only vertical walls in the mesh are the culvert walls and the walls of the downstream rectangular channel.

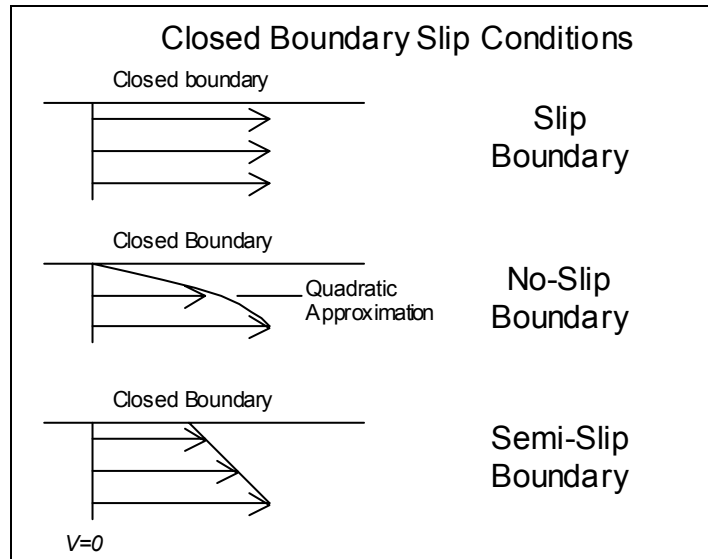


Figure 5.7 Closed boundary slip conditions

The option chosen for the present model was *semi-slip*. This choice was made because the closed boundaries represent channel walls that are actual physical boundaries. Froehlich (1996) states that “Semi-slip conditions are usually applied when the closed boundary represents an actual physical boundary such as a wall that is vertical or nearly vertical. Increased frictional resistance caused by the wall will then be considered.” The equation used by FESWMS to calculate the vertical wall friction when *semi-slip* is chosen is (Froehlich, 1996):

$$\tau_w = c_f \rho U_w^2 \quad (5.5)$$

τ_w = vertical wall friction (shear stress)
 c_f = vertical wall shear coefficient
 ρ = water density
 U_w = velocity tangent to the wall

The parameter c_f should be much less than one, and a value of $c_f = 0.003$ was selected to represent the physical model. To evaluate the sensitivity of this parameter on the model results, values between 0 and 1 were specified for c_f , and it was found that different vertical wall shear coefficients used did not change the solution. More detail on the effects of the vertical wall shear coefficient is discussed in the model calibration section.

At the beginning of the modeling process, appropriate initial conditions are unknown. Depth-averaged velocities in the x and y directions (U, V) as well as water depth (H) need to be specified at all nodes as initial conditions (an initial guess for the steady-state solution). The approach taken is called a *cold start*. For a *cold start*, the downstream water surface elevation boundary condition is specified higher than any elevation in the mesh. Thus, the entire network is covered with water. This is referred to as *bathtub* conditions: a

flat water surface with zero velocity. When results from a previous simulation are available, they can be used as the initial conditions, an approach called a *hot start*.

The depth-averaged flow equations are nonlinear, so an iterative solution is needed. Using the *cold start* solution as an initial condition for the next step, loads can be increased gradually over a number of steps to the desired value. In the incremental loading strategy, *loads* consist of hydrostatic pressures and mass flow rates along the mesh boundaries (Froehlich, 1996). The converged solutions found at each *incremental* step are used as initial conditions for the following step. It is very important to take small enough steps or the solution will not converge. This process is where the number of iterations and convergence criteria are involved. Another effective method to obtain convergence when starting the incremental loading process is temporarily increasing the eddy viscosity for a few iterations, which virtually thickens the water. Large eddy viscosities facilitate convergence due to their dissipative effect when large velocity gradients exist (Froehlich, 1996).

The incremental loading strategy is applied to obtain converged solutions for the numerical modeling experiments. Combinations of incremental loading are used, including incremental decrease in the downstream depth boundary condition, incremental increase in the upstream flow rate boundary condition, and adjustment of the parameters in the eddy viscosity model.

5.5 Model Testing/Calibration/Validation

5.5.1 Overview

One of the main objectives of the research is to assess the validity and usability of FESWMS in representing two-dimensional flow at highway crossings. Calibration and validation are key parts of the assessment of the model. If the numerical model is able to produce results closely matching the measured data, it can be applied to other channel geometries and culvert alignments to get reasonable results that would take much longer to obtain in the laboratory. The numerical model geometry is based on the physical model, so the correct geometry is known quite precisely. With the correct geometry, the main parameters to be evaluated are roughness and eddy viscosity. The eddy viscosity is the most significant model parameter in the calibration runs. The roughness parameter (Manning's n) is the same for all channel sections and is left constant.

5.5.2 Eddy Viscosity Model

Eddy viscosity is not a real property of the fluid, but it is a way of modeling the Reynolds stresses. The Reynolds stresses are the turbulent momentum transport terms. Kundu (1990) explained that the Reynolds stress is a “stress exerted by the turbulent fluctuations on the mean flow...[I]t is the rate of mean momentum transfer [per unit area] by turbulent fluctuations.” As such, it is the eddy viscosity coefficient for expressing the turbulent exchange of momentum. The depth-averaged eddy viscosity is assumed to be isotropic ($\nu_{xx} = \nu_{xy} = \nu_{yx} = \nu_{yy}$) in FESWMS.

The eddy viscosity has a significant effect on velocity gradients. A smaller value for eddy viscosity will allow larger horizontal velocity gradients, while a larger value for eddy viscosity will result in larger lateral shear stresses for smaller velocity gradients, and the horizontal velocity profile will be smoothed. Eddy viscosity is significant because of the

large velocity gradients in the channel expansion area. Although the eddy viscosity is not actually isotropic, the longitudinal variations in velocity and turbulence usually are smaller than in the transverse direction. As a result, FESWMS is not very sensitive to v_{xx} .

Eddy viscosity simulates turbulence by assuming turbulent stresses are proportional to the horizontal gradients of depth-averaged velocity, which is similar to diffusion. Mass transport by diffusion is proportional to concentration gradients. Eddy viscosity represents the diffusion of momentum. Eddy viscosity in open channels can be related to the bed shear velocity and depth. In the FESWMS code, eddy viscosity is calculated according to the following formula (ASCE, 2001):

$$v_t = v_o + c_{\mu 1} u^* H \quad (5.6)$$

v_t = total eddy viscosity

v_o = base kinematic eddy viscosity

$c_{\mu 1}$ = turbulence model coefficient

u^* = shear velocity ($u^* = \sqrt{\frac{\tau_{bed}}{\rho}}$)

H = water depth

Constant eddy viscosity was used in initially calibrating the numerical model to physical model data. A constant eddy viscosity produces reasonable results with a large horizontal velocity gradient, as the lateral shear stresses caused by turbulence will still be affected by the gradients in the horizontal flow field (see equation (2.50)). Using a constant eddy viscosity, calibration results were within 15% of the measured velocity values for the points in the middle region of the channel, but the comparisons on the edges show 30-80% error (depending on the data set). Initial meshes without a culvert calibrate slightly more accurately using the constant eddy viscosity than meshes with a culvert. These calibration results are fair, but there is no consistent pattern in the relationship between the eddy viscosity and the other data being calibrated; different data sets, with different flow rates and tail waters, require significantly different values of eddy viscosity for calibration. This may be because different flow rates produce different bed shears and turbulence characteristics and different tailwater depths produce different upstream depths.

Using a spatially varying eddy viscosity makes more intuitive sense than a constant value, as the mixing length model increases turbulent diffusion nonlinearly with increasing shear. The mixing length model gives more consistent results between calibrations for different data sets. A spatially varying eddy viscosity is specified in FESWMS by assigning a value for the turbulence coefficient $c_{\mu 1}$. In FESWMS, a second turbulence coefficient can be used to account for large-scale vorticity in the flow, but this coefficient is not used. In the model simulations $c_{\mu 1}$ is adjusted (along with v_o) to calibrate the model. In natural open channels the value for $c_{\mu 1}$ is in the range 0.3-0.9 (Froehlich, 1996). DeVantier (1989) also found that using a spatially varying eddy viscosity representation gave better results than a constant turbulent viscosity in calibrating to measured velocity and depth data. Somes et al. (1999) compared calibration results using a constant eddy viscosity term and a time-varying function of the local velocity gradients in their two-dimensional wetland

model. They found the formulation based on the local velocity gradients produces a more accurate simulation than a constant value for the turbulent exchanges in a wetland.

5.5.3 Calibration Process

The calibration process is straightforward, but evaluating the results proves more difficult. The idea is to adjust the eddy viscosity by adjusting $c_{\mu 1}$ in each model run in order to match the computed velocities and depths as closely as possible to the measured data. The base kinematic eddy viscosity (ν_o) is also adjusted slightly. Final calibration values for ν_o and $c_{\mu 1}$ are presented in later in this section.

Two important questions in model calibration concern locations for calibration data and required closeness of fit between model simulation and measured variable values. Selection of locations for calibration data is based on research objectives that were focused on hydraulics of channel expansions leading to wide culverts. Locations for calibration data were taken along one cross section upstream of the channel expansion and two cross sections downstream of the expansion, as shown in Figure 5.1. This includes the region with largest velocity gradients.

With regard to required closeness of fit, specific criteria were not developed. However, it is felt that it is more important to calibrate to the data points taken in the middle region of the channel; the low-velocity points in the recirculation zones at the outer edge are not as important to calibrate accurately if calibration to all points does not seem to be possible. The calibration points in the middle of the recirculation zones at the outer edges of the channel have much smaller velocities, so calibration based on a percentage error will be misleading. Calibration for the smaller velocities is more difficult because their values are sometimes 1-2 orders of magnitude smaller than the velocities in the middle of the channel. Kheireldin et al. (1994) submit that a good agreement between the measured and the computed results is within a 15% range.

A *semi-slip* boundary condition was applied along the closed boundaries (channel walls), so a vertical wall shear coefficient (c_f) was specified. This coefficient has a value on the order of 0.003 for the small-scale physical model. In order to examine the sensitivity of the results for changing c_f , it was applied at values ranging from 0 to 1. As discussed in section 5.4, *semi-slip* applies no shear stress at closed boundaries, just as for a *slip* condition, except for the flow along a vertical wall. So changing the *vertical wall shear coefficient* from 0 to 1 in this boundary condition had no velocity-decreasing effect near the walls in the expansion area because the longitudinal expansion channel walls are not vertical. Flow through the culvert is of interest and walls inside of the culvert boxes are vertical. However, changing c_f from 0 to 1 did not make any difference in the velocities or depths inside of the culvert. This is a different result from what was expected; adjusting the vertical wall shear coefficient should change the shear stress applied along the walls inside the culvert boxes, thus changing velocities and depths there.

The mesh resolution was also examined as part of the calibration process. The resolution of elements in the area of interest needs to be fine enough to represent the flow phenomena. The initial mesh had elements in the expansion area that were 2 feet long (downstream) by 1 feet wide (cross-stream). The mesh resolution in the expansion and culvert was refined two times after the original mesh was constructed, halving the size of each dimension each time. The final mesh refinement used for calibration has an element size in the expansion area of 1 feet by 0.5 feet, and was able to characterize the two-

dimensional velocity vectors. This is the mesh shown in Figure 5.6. Use of the finest mesh (0.5 ft by 0.25 ft) did not represent the recirculation zones or velocity vectors and depths in the middle of the channel more accurately (visually or numerically) and required significantly longer model computation times in comparison to the selected mesh.

In the data set used for the model calibration, the culvert was located 12 feet (3.66 meters) downstream of the expansion, the flow rate was 7 ft³/s (0.198 m³/s), and the downstream water depth (which is the same as the downstream water surface elevation since the downstream end of the channel was taken as the datum) was measured to be 0.917 feet (0.280 meters). Upon lowering the water surface elevation through incremental loading, 0.917 feet is used as the downstream boundary condition. The estimated uncertainty in the flow measurement is $\pm 4\%$ (± 0.25 ft³/s) and the estimated uncertainty in the downstream water surface elevation measurement is ± 0.02 feet.

The eddy viscosity parameters determined through model calibration are $\nu_0 = 0.05$ ft²/s and $c_{\mu 1} = 0.9$. Figures 5.8 to 5.10 show visual representations of the velocity and depth calibration results. Figure 5.8 compares the measured and calculated velocity magnitudes for locations marked by the “X”. The computed velocity magnitudes are shown to the left of the symbol with the measured values to the right in parentheses.

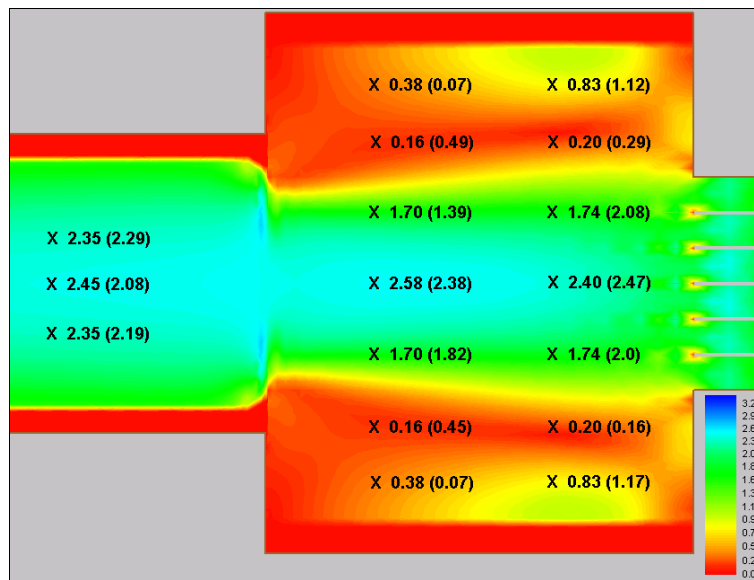


Figure 5.8 Calibration of velocity magnitude (ft/s) values

Figure 5.9 shows the velocity vectors in the calibration solution near the location of the abrupt channel expansion. The decrease in water surface elevation as the transition is approached combined with the upstream trapezoidal channel result in the inward component to the velocity vectors, towards the channel centerline. The lack of expansion of the resulting “jet” is evident.

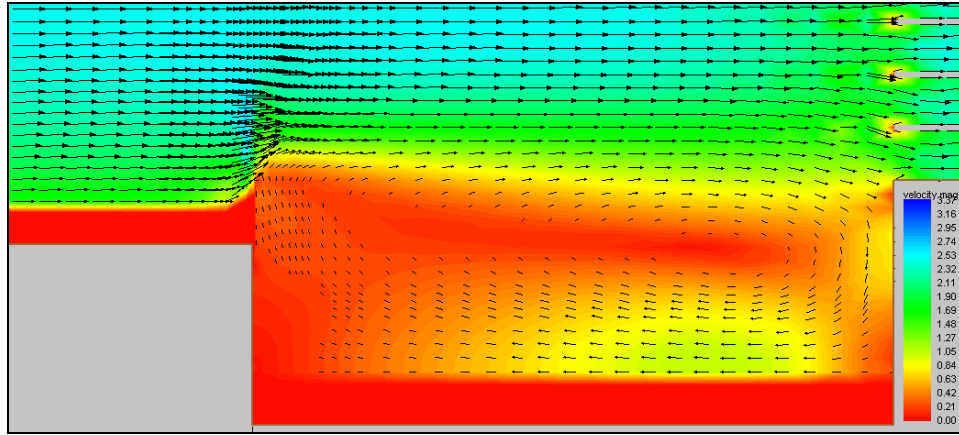


Figure 5.9 Velocity vectors near abrupt expansion in calibration solution, with the upper boundary of the figure representing the channel centerline

Figure 5.10 compares the corresponding water depths, where again the symbol “X” marks the measurement location, the computed depths are listed to the left, and the measured depths are shown to the right in parentheses.

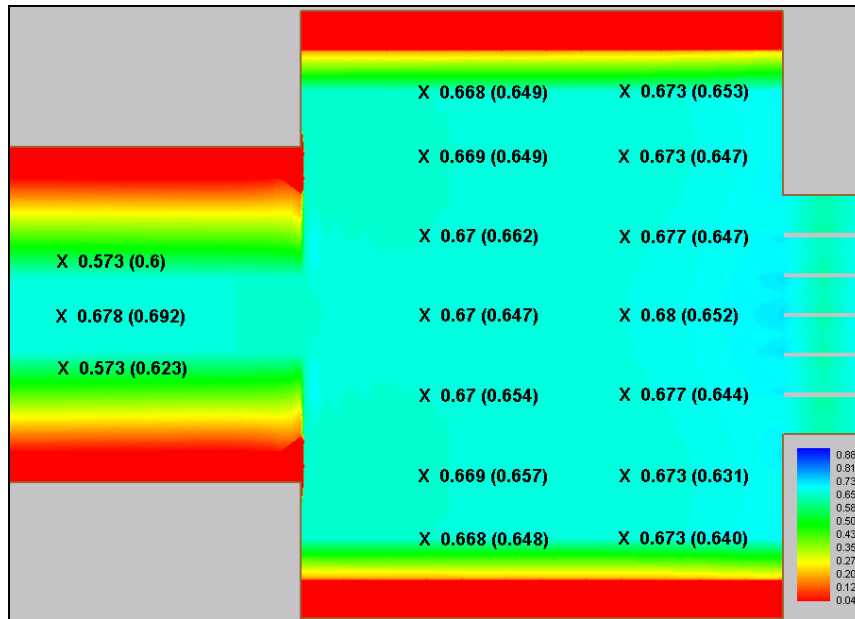


Figure 5.10 Comparison of water depths (feet) in the calibration solution

Table 5.1 provides a quantitative comparison of the calibration results for water depth. The computed values upstream of the expansion are smaller than the measured values, while the computed depth values downstream of the expansion are larger than measured values. The largest percent difference is less than 8%.

Table 5.1 Calibration results for water depth magnitudes (CL = centerline)

	calibration point location	measured depth (ft)	avg. measured depth of symmetrical points (ft)	computed depth (ft)	% error: (avg. measured - computed) / avg. measured	difference: avg measured - computed (ft)
6 ft upstream of expansion	CL - 1.33'	0.623	0.612	0.573	6.4%	0.039
	CL	0.692	0.692	0.678	2.0%	0.014
	CL + 1.33'	0.601	0.612	0.573	6.4%	0.039
3 ft downstream of expansion	CL- 5.6'	0.648	0.649	0.699	-7.8%	-0.051
	CL- 4'	0.657	0.653	0.699	-7.0%	-0.046
	CL- 2'	0.654	0.658	0.670	-1.8%	-0.012
	CL	0.647	0.647	0.670	-3.6%	-0.023
	CL + 2'	0.662	0.658	0.670	-1.8%	-0.012
	CL + 4'	0.649	0.653	0.699	-7.0%	-0.046
8 ft downstream of expansion	CL- 5.6'	0.636	0.645	0.673	-4.4%	-0.028
	CL- 4'	0.631	0.639	0.673	-5.3%	-0.034
	CL- 2'	0.644	0.646	0.677	-4.9%	-0.032
	CL	0.652	0.652	0.680	-4.3%	-0.028
	CL + 2'	0.647	0.646	0.677	-4.9%	-0.032
	CL + 4'	0.647	0.639	0.673	-5.3%	-0.034
	CL + 5.6'	0.653	0.645	0.673	-4.4%	-0.028

Table 5.2 presents a quantitative comparison of calibration results for water velocity magnitudes. For all but the outer calibration points in the expansion section (that have been problematic to calibrate accurately for all of the data sets), the calculated velocities are within 15% of the average measured values. It is difficult to evaluate calibration results for small velocities based on a percent error. A better calibration summary for the outside points downstream of the expansion is to note that the computed values were within 0.3 ft/s of the measured velocity values, which is 12% of the mean velocity in the middle of the expansion.

Table 5.2 Calibration results for water velocity magnitudes

	calibration point location	measured velocity (fps)	avg. measured velocity mag. of symmetrical points (fps)	computed velocity magnitude (fps)	% error: (avg. measured - computed) / avg. measured	difference: avg measured - computed (fps)
6 ft upstream of expansion	CL - 1.33'	2.19	2.24	2.35	-4.9%	-0.11
	CL	2.08	2.08	2.45	-17.8%	-0.37
	CL + 1.33'	2.29	2.24	2.35	-4.9%	-0.11
3 ft downstream of expansion	CL- 5.6'	0.07	0.07	0.38	-442.9%	-0.31
	CL- 4'	0.45	0.47	0.16	66.0%	0.31
	CL- 2'	1.82	1.61	1.70	-5.6%	-0.09
	CL	2.38	2.38	2.50	-5.0%	-0.12
	CL + 2'	1.39	1.61	1.70	-5.6%	-0.09
	CL + 4'	0.49	0.47	0.16	66.0%	0.31
	CL + 5.6'	0.07	0.07	0.38	-442.9%	-0.31
8 ft downstream of expansion	CL- 5.6'	1.17	1.14	0.83	27.5%	0.31
	CL- 4'	0.16	0.22	0.20	10.5%	0.02
	CL- 2'	2.00	2.04	1.74	14.7%	0.30
	CL	2.47	2.47	2.40	2.8%	0.07
	CL + 2'	2.08	2.04	1.74	14.7%	0.30
	CL + 4'	0.29	0.22	0.20	10.5%	0.02
	CL + 5.6'	1.12	1.14	0.83	27.5%	0.31

Based on the calibration tolerance of 15% given by Kheireldin et al. (1994), an acceptable calibration was obtained for this data set. It is the best example of the calibration process because it has a good density of calibration points along each cross section and used a spatially varying eddy viscosity.

For further comparison, Table 5.3 shows results for the measured and computed Froude numbers at the calibration points. All of the Froude numbers are less than 1, so the flow is subcritical at all of the calibration point locations. The largest difference between measured and computed Froude number is 0.08, so the FESWMS model was able to compute the Froude numbers with reasonable accuracy.

Table 5.3 Froude number comparison for calibration model

	calibration point location	measured Froude no.	computed Froude no.
6 ft upstream of expansion	CL - 1.33'	0.50	0.55
	CL	0.44	0.52
	CL + 1.33'	0.50	0.55
3 ft downstream of expansion	CL- 5.6'	0.02	0.08
	CL- 4'	0.10	0.03
	CL- 2'	0.35	0.37
	CL	0.52	0.54
	CL + 2'	0.35	0.37
	CL + 4'	0.10	0.03
	CL + 5.6'	0.02	0.08
8 ft downstream of expansion	CL- 5.6'	0.25	0.18
	CL- 4'	0.05	0.04
	CL- 2'	0.45	0.37
	CL	0.54	0.51
	CL + 2'	0.45	0.37
	CL + 4'	0.05	0.04
	CL + 5.6'	0.25	0.18

5.5.4 Model Validation

Model validation (also called model verification) is the process of demonstrating that the calibrated model is an adequate representation of the physical system. Since the primary interest in application of the model is to evaluate performance of different channel geometries, the validation data set consisted of measured water depth and velocity along three cross sections (one upstream of the expansion and two downstream of the expansion and upstream of the culvert), but the channel geometry was different than for the calibration data set. For model validation, the culvert was located 8 feet (2.44 meters) downstream of the expansion, rather than 12 feet (3.66 meters), and the expansion was smoothed, rather than abrupt (see the difference between Figures 3.4 and 3.5). The geometry of the simulation model was changed accordingly, but none of the model parameters were modified from the calibration runs. The resulting comparison between measured and simulated values is presented in Table 5.4.

Table 5.4 Validation results for water depth and velocity (CL = centerline)

Station	Point Location	Measured Depth (ft)	Simulated Depth (ft)	% Depth Difference	Measured Velocity (ft/s)	Simulated Velocity (ft/s)	% Velocity Difference
6 ft Upstream of Expansion	CL-1.74'	0.50	0.535	-7.0	2.09	1.96	6.2
	CL	0.67	0.742	-10.8	1.98	2.12	-7.1
	CL+1.74'	0.46	0.535	-16.3	2.29	1.96	14.4
5 ft Upstream of Culvert	CL-5.3'	0.63	0.640	-1.6	0.83	0.53	36.1
	CL-4'	0.62	0.639	-3.1	0.24	0.49	-104.
	CL-2'	0.62	0.642	-3.6	2.08	1.37	34.1
	CL	0.57	0.638	-11.9	2.27	3.28	-44.5
	CL+2'	0.58	0.642	-10.7	2.11	1.37	35.1
	CL+4'	0.60	0.639	-6.5	0.20	0.49	-145.
	CL+5.3'	0.63	0.640	-1.6	0.94	0.53	43.6
2 ft Upstream of Culvert	CL-5.3'	0.63	0.641	-1.7	0.83	0.97	-16.9
	CL-4'	0.63	0.634	-0.6	0.24	0.13	45.8
	CL-2'	0.64	0.645	-0.8	2.08	1.77	14.9
	CL	0.65	0.662	-1.8	2.27	2.99	-31.7
	CL+2'	0.62	0.645	-4.0	2.11	1.77	16.1
	CL+4'	0.61	0.634	-3.9	0.20	0.13	35.0
	CL+5.3'	0.63	0.641	-1.7	0.94	0.97	-3.2

The computed depths are larger than the measured depth values both upstream and downstream of the expansion, though generally the values are quite close. This is especially true immediately upstream of the culvert. The differences between measured and computed velocity values are much greater. In particular, the computed centerline velocity is much larger than the measured value, suggesting that the eddy viscosity might be too small. However, the general features including the width of the jet downstream of the expansion and the size of the recirculation zones are well represented by the model, and the model is adequately validated for investigation of other channel geometries.

5.6 Model Application to Expansion Ratio Effects

After the model is calibrated and validated, it can be applied with some confidence to a new set of conditions. This section presents summary results on application of the model to investigate the effects of different channel expansion ratios in the transition leading to the culvert system. Calibration was performed for the channel with an abrupt expansion. Changing the expansion ratio of the numerical model allows analysis of the changes in flow distribution through the culvert boxes, the location and size of the recirculation zones, and the contraction of the jet at the interface between the upstream channel and the expansion for various expansion ratios. One of the objectives of applying the model is to determine which expansion ratio (if any) distributes the flow most evenly through the culvert barrels, thus reducing or eliminating the sediment deposition in the outer barrels.

The simulations of channel performance for different expansion ratios were performed with the culvert located 8 feet (2.44 meters) downstream of the expansion because this location scales better to expected field conditions. The same set of model parameters for the calibration and validation runs were used to evaluate hydraulic

performance of various expansion ratios, with focus on the flow distribution through the culvert barrels and trends in stagnation zones. The stagnation zone is the center of the recirculation zone where the flow is essentially still or very slowly rotating. This area was studied because it is one of the locations where sediment may begin to deposit.

Representing an abrupt expansion in the finite element mesh was much simpler than changing the geometry for the other expansion ratios. The mesh editing for the different expansion ratios was done one element at a time. The expansion ratios (expansion length:width increase of one side) modeled and analyzed were: abrupt (rectangular), 0.5:1, 1:1, 2:1, and 4:1. Due to the width of the 6-barrel box culvert, a 4:1 expansion was the most gradual one that could be represented with the given upstream channel width and culvert location. Figure 5.11 shows the five expansion ratios that were modeled.

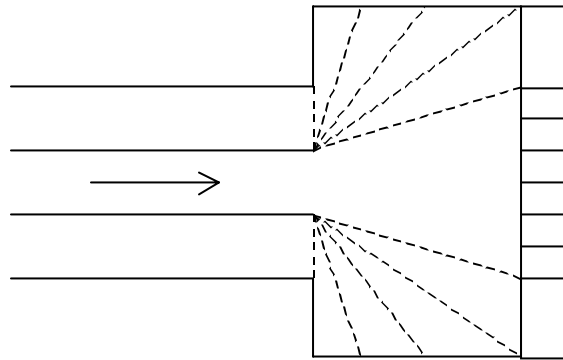


Figure 5.11 Varying expansion ratio schematic

The flow distribution near the abrupt expansion and within the recirculation zone are shown in Figure 5.12 for the case with the culvert box located 8 feet downstream from the expansion. The channel discharge is $7 \text{ ft}^3/\text{s}$ and the maximum velocity is 2.70 ft/s . The flow distribution shown in this figure does not differ significantly from that shown in Figure 5.9 with the culvert box located 12 feet downstream of the expansion.

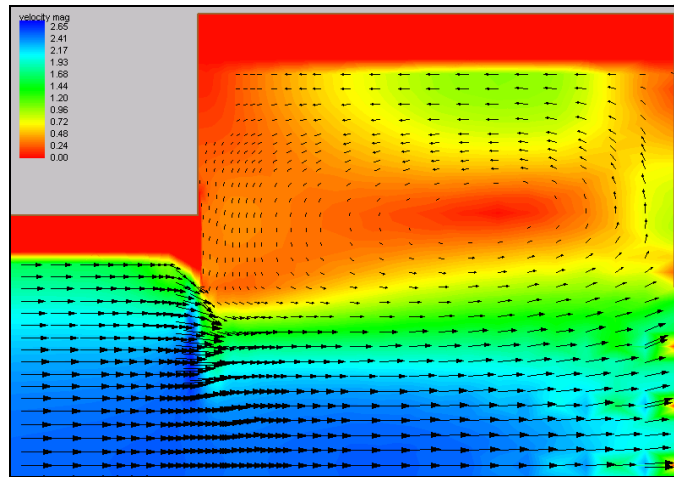


Figure 5.12 Velocity vectors and contours for abrupt expansion

In order to identify the stagnation zone, the velocity magnitudes that are less than 6% of the maximum velocity were contoured and are shown in Figure 5.13. The value of 6% does not have any particular significance, but it produces contoured stagnation zone representations that coincide best with the center of the recirculation zones.

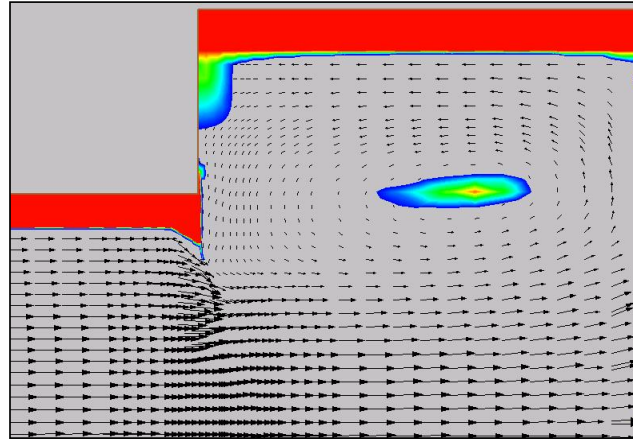


Figure 5.13 Stagnation zone for abrupt expansion

In comparing all of the expansion ratio simulations, the changes in expansion ratio have no significant effect on the magnitude of the velocities, but the size and location of the stagnation zone changes as the expansion ratio increases. For all but one simulation, the flow contractions at the entrance to the channel expansion are similar. For a reason that is unclear, the 0.5:1 expansion produces a different jet contraction that is more gradual and starts further upstream. Perhaps changes in the contraction would be better represented if the mesh were refined further in that area.

With increasing expansion ratio, the stagnation zone becomes elongated and moves closer to the centerline of the channel, nearly paralleling the extension of the upstream channel, and the size of the recirculation decreases significantly. Figure 5.14 shows the velocity vector diagram for the 4:1 expansion ratio. The small size of the recirculation zone is evident, as are the small return velocities.

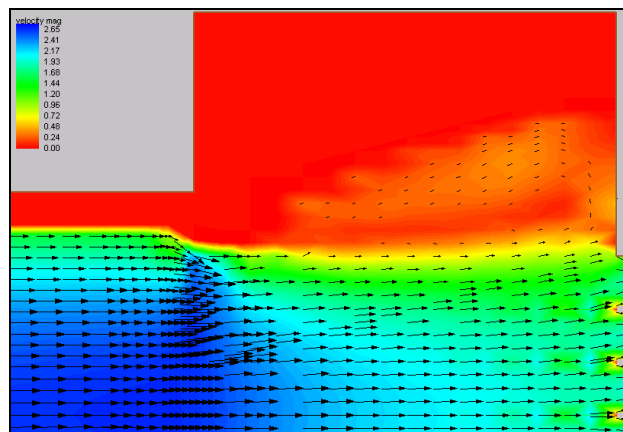


Figure 5.14 Velocity vectors and contours for 4:1 expansion ratio

Flow distribution through the culvert barrels under design conditions is of major importance in this research. Standard design procedures assume an equal distribution of flow through the culvert barrels, but physical model observations and measurements, as well as numerical model results, have shown that the middle boxes carry more flow than the outer boxes, especially with an abrupt expansion. This is a likely contributor to the increased sedimentation in the outer boxes.

Calculation of the culvert barrel discharge from the numerical model requires analysis of the simulation model output. FESWMS provides values of water depth (H) and horizontal velocity (U, V) at each node point of the model. Mathematically, the discharge through the culvert box would be calculated from

$$Q_{\text{box}} = \int_{\text{width}} UHdy \quad (5.7)$$

The node point values of U and H, and the finite element basis functions can be used to evaluate this integral. Figure 5.15 shows the form of the basis functions $\phi_i(\eta)$ along the side of the element for the three side node points. The variable h is the local coordinate for the element with range -1 to 1 (the local coordinate pair are ξ and η , and the side of the element corresponds to $\xi = -1$). The weights w_i are calculated from

$$w_i = \int_{-1}^1 \phi_i(\eta) d\eta \quad (5.8)$$

The weights for the five node points along the sides of the two elements (the culverts box is two elements wide) are also shown in Figure 5.15, with the middle node point having weight 1/6 from each element. The barrel discharge is calculated from

$$Q_{\text{box}} = \left(\sum_{i=1}^5 w_i U_i H_i \right) \frac{B_{\text{box}}}{2} \quad (5.9)$$

In equation (5.9) B_{box} is the width of the culvert barrel.

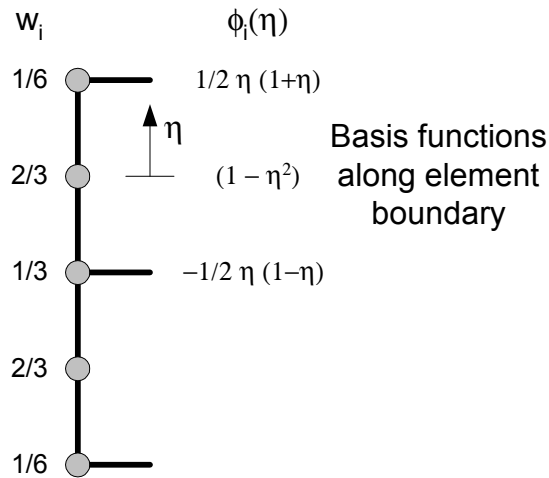


Figure 5.15 Basis functions and weights for calculation of barrel discharge

Figure 5.16 illustrates the magnitudes of the simulated flow rates in each of the culvert boxes with all of the expansion ratios modeled. It shows the 4:1 expansion has the most even distribution of flow rates through the culvert barrels (with a 9% difference between the maximum and minimum flow rates), while the abrupt expansion has the greatest difference (20%) between the flow rates in the middle culvert boxes versus the outer ones (approximately 0.2 ft³/s). Construction of a 4:1 channel expansion does provide a more uniform flow distribution. However, this would be an expensive remedy. Alternative (and less expensive) remedies are investigated in the following chapter.

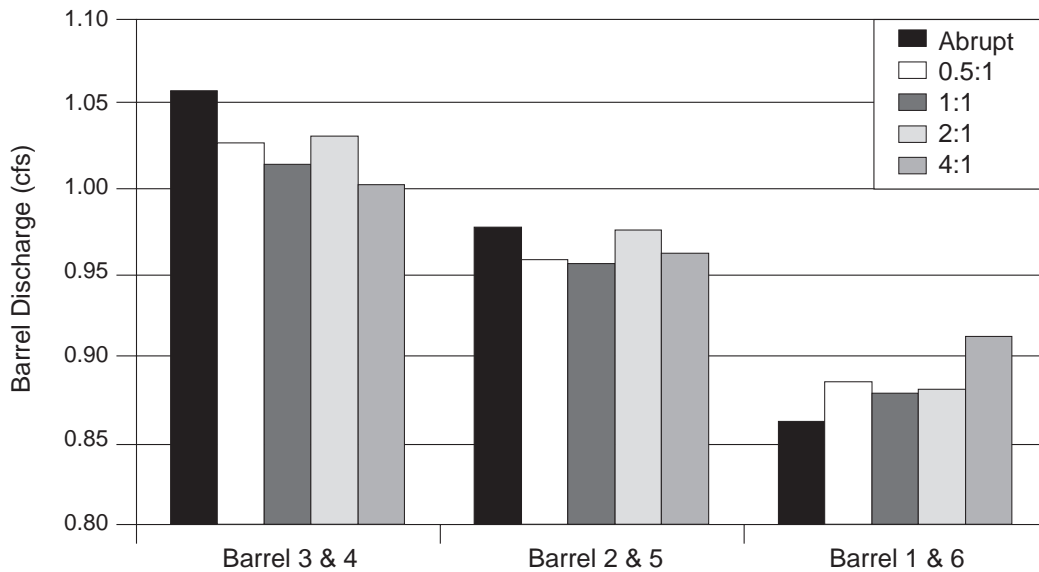


Figure 5.16 Flow distribution through culvert boxes for all expansion ratios

6. Design Procedures and Remedies

6.1 Introduction

The performance curves that were developed in Chapter 4 and fit to the experiment data from the physical model may be used to develop design equations for low-head box culverts. These equations provide the total culvert span required for a total culvert design discharge and limiting headwater. The design equations are presented in Section 6.2.

Section 6.3 presents data from physical model and FESWMS numerical model experiments on hydraulics of channel expansions with gabions present within the expansion section. Gabions may be used to develop a uniform flow distribution through the culvert barrels.

6.2 Design of Box Culverts for Inlet Control

6.2.1 Development of Design Equations

The performance curves for box culverts are specified by equations (4.2) and (4.9), with parameter values $C_b = C_c = 2/3$. These equations are written

$$\frac{Q}{BD\sqrt{gD}} = \left(\frac{2}{3}\right)^{3/2} \left(\frac{HW}{D}\right)^{3/2} \quad (6.1)$$

$$\frac{Q}{BD\sqrt{gD}} = \frac{2}{3} \sqrt{2 \left(\frac{HW}{D} - \frac{2}{3}\right)} \quad (6.2)$$

According to equation (4.12), the transition between these performance curves occurs at $HW/D = 1.0$.

For design of low-head highway culverts, the culvert rise D is usually determined by roadway elevation constraints, and specification that the upstream water depth under design conditions is equal to the culvert rise will allow for the thickness of the roadway above the culvert to act as freeboard. As an initial assumption, one may use $y_D = y_a = D$ so that $y_a/D = 1$. Thus $HW/D > 1$ for design of box culverts, and equation (6.2) provides the design performance curve. If it is further assumed that $v_a = Q/(BD)$, then equation (6.2) gives

$$\frac{v_a^2/2g}{D} = \frac{1}{2} \left(\frac{Q}{BD\sqrt{gD}} \right)^2 = \frac{4}{9} \left(\frac{HW}{D} - \frac{2}{3} \right) \quad (6.3)$$

With equation (6.3) one finds

$$\frac{y_a + v_a^2/2g}{D} = \frac{HW}{D} = 1 + \frac{4}{9} \left(\frac{HW}{D} - \frac{2}{3} \right) = \frac{4}{9} \frac{HW}{D} + \frac{19}{27}$$

This equation gives

$$\frac{HW}{D} \Big|_D = \frac{19}{15} \quad (6.4)$$

Using this value in equation (6.2) gives the design relationship

$$\frac{Q}{BD\sqrt{gD}} \Big|_D = \frac{2}{3} \sqrt{2 \left(\frac{19}{15} - \frac{2}{3} \right)} = \frac{2}{3} \sqrt{\frac{18}{15}} = \sqrt{\frac{72}{135}} \cong 0.73 \quad (6.5)$$

Equation (6.5) may be used to support design calculations for highway culverts that are limited by upstream headwater depths. The usual design situation has the design discharge known, along with the maximum culvert rise that is fixed by highway design. Equation (6.5) may then be used to calculate the total culvert span for the design discharge Q_T :

$$B|_D = \frac{Q_T}{0.73\sqrt{g}(D)^{3/2}} \quad (6.6)$$

6.2.2 Example Problem

Problem Statement: Determine the required size for a (multiple-barrel) box culvert if the design discharge is 3000 ft³/s and the culvert rise is limited to 6 feet.

Solution:

Using equation (6.6) the required culvert span is

$$B|_D = \frac{3000}{0.73 \times \sqrt{32.2} \times (6)^{1.5}} = 49.3 \text{ feet}$$

This result suggests that a 5-barrel system is required, with each barrel having a rise of 6 feet and span of 10 feet. For a uniform distribution of flow, each barrel will carry a design discharge of 600 ft³/s.

Discussion:

The design results should also be checked for outlet control.

For comparison with standard equations, the FHWA design equations that are presented in Chapter 2 are used. Two different assumptions are used to calculate the culvert span.

1. It is assumed that the design headwater is given by equation (6.4). Using this in equation (2.31) with $c = 0.040$, $Y = 0.80$, and $S = 0.02$ (which is used in the FHWA design nomographs), one finds $B = 59.1$ feet. This value suggests a 6-barrel culvert system with each barrel having a rise by span equal to 6×10 feet.
2. It is assumed that the upstream depth (rather than headwater) is used for design purposes, and that $y_a = 6$ feet. Using y_a/D in equation (2.31) in place of HW/D , one finds $B = 89.1$ feet. This value suggests using six barrels (6×15 feet) or nine barrels (6×10 feet).

Comparison of these results shows the importance of considering the upstream specific energy (headwater) in design calculations, rather than the upstream water depth.

6.3 Use of Gabions as Remedy for Hydraulic Performance

6.3.1 Physical Model Experiments

The physical model experiment results presented in Chapter 4 show that the concentrated flow (jet) downstream of the expansion does not diffuse outward to any significant extent, and this results in larger velocity values and specific energy in front of the central barrels of a multiple-barrel culvert system, compared with the outer barrels. Under inlet control, the barrel discharge is determined by its upstream headwater (specific energy). As confirmed by FESWMS numerical modeling, this results in the flow distribution across the culvert barrels not being uniform. It is likely that this nonuniform distribution of flow is responsible for the sedimentation problems observed in the field and shown in Figure 1.4.

A possible remedy for the concentrated flow is to disturb the jet by placing an obstacle in its path, and an inexpensive obstacle would be a rock gabion. Experiments were performed using the physical model to investigate this potential remedy. Cinder blocks (concrete blocks) were used to represent the gabions. The blocks were generally placed midway between the expansion and the culvert (with the culvert located 8 feet downstream of the expansion), and with spacing between pairs of block of about 1.4 feet (0.43 meter). Pairs of blocks were used so that the resulting gabion model measured 1.33 feet by 1.33 feet, with one pair on each side of the centerline. Some of the data that was derived from these experiments was used to evaluate the culvert performance curve and is shown in Figures 4.14 and 4.15.

Figure 6.1 shows experiment results of specific energy across the channel for various flow rates. In each case, the depth and velocity were measured on the centerline of the barrels, and for some of the experiments, only four barrels were open. The results shown in this figure should be compared with Figure 4.9. It is clear that the distribution of energy

is much more uniform with the gabions in place, which suggests that the distribution of discharge through the culvert barrels is also more uniform.

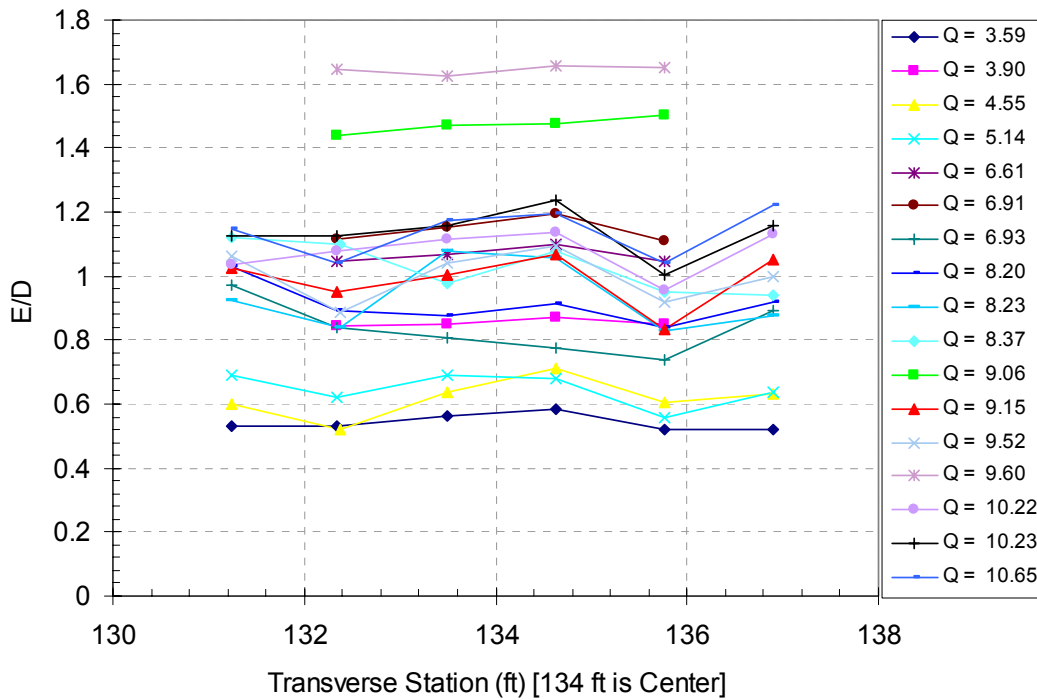


Figure 6.1 Specific energy distribution across culvert barrels (discharge in ft^3/s)

Figure 6.2 shows similar results from pairs of runs with the same discharge for conditions with and without the gabions present. Again, it is clear that the presence of the gabions increases the specific energy on the outer barrels, thus increasing the discharge through these barrels.

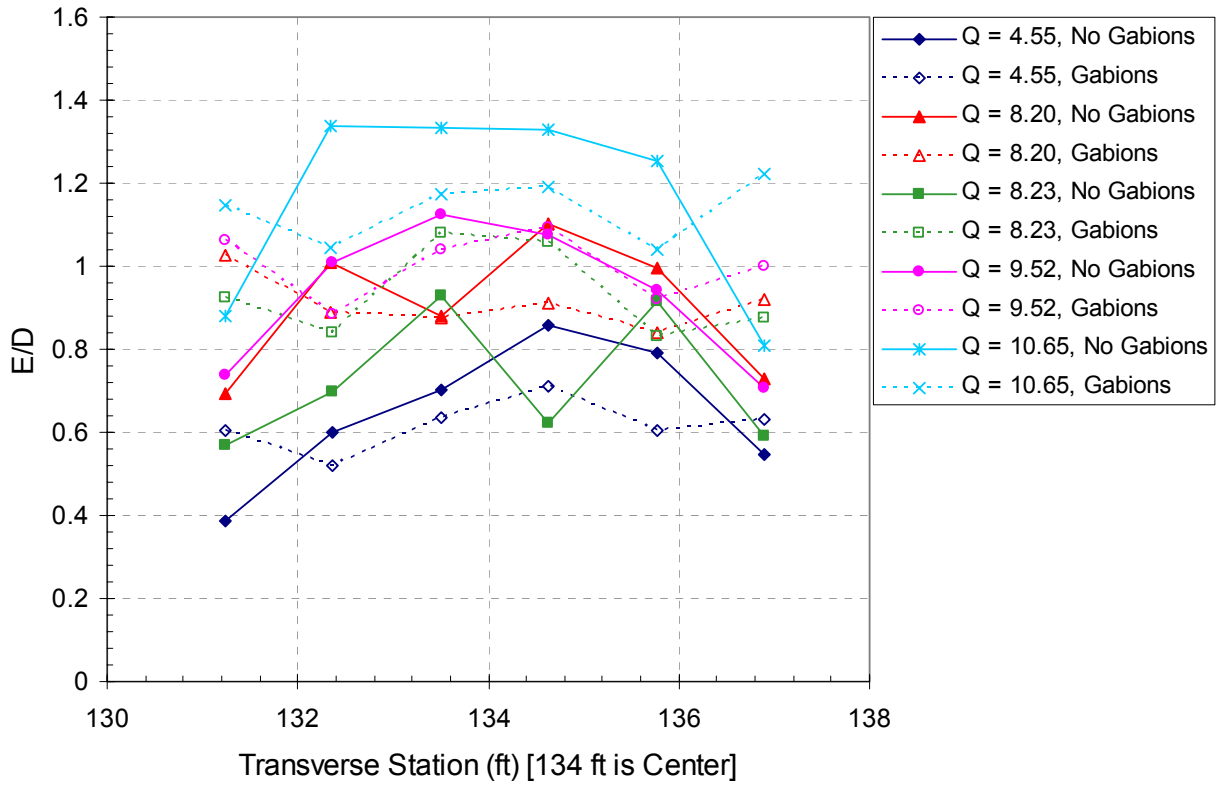


Figure 6.2 Distribution of specific energy with and without gabions present

There might be some concern that the presence of gabions would adversely affect the specific energy in a situation where the flow is already evenly distributed. The data in Figure 6.3 shows that this is not the case. This figure shows data from runs with four barrels open and for different flow rates. Pairs of data are for the same discharge, but with and without the gabions present. The presence of gabions does not significantly impact the flow distribution.

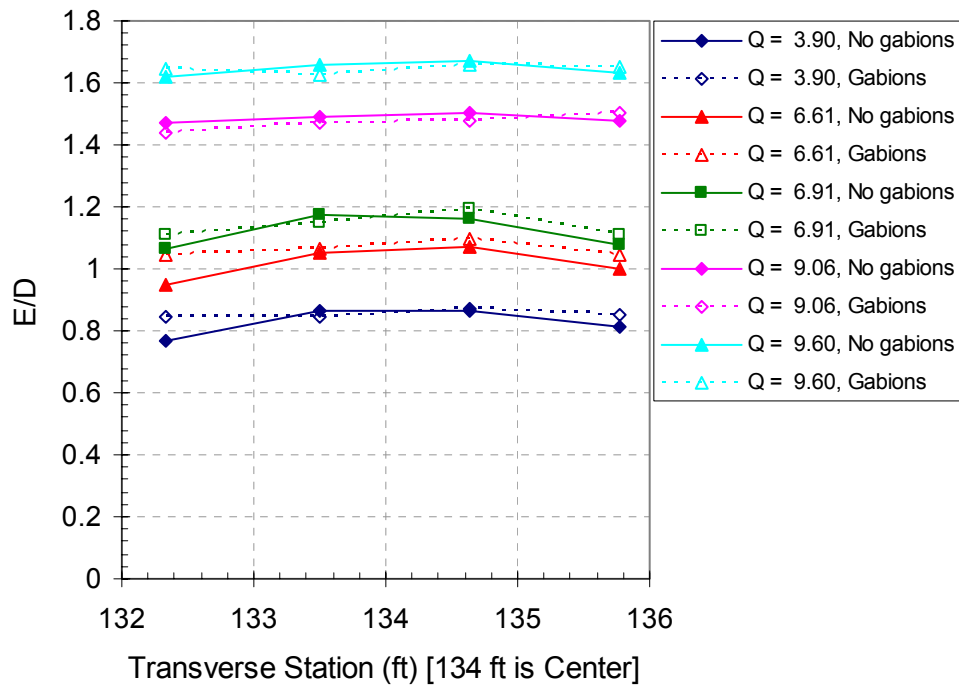


Figure 6.3 Lack of impact of gabions on flow distribution

Finally, it is noted that the presence of gabions did create an increase in the upstream water depth (backwater). Measurements with a discharge of $8.9 \text{ ft}^3/\text{s}$ ($0.25 \text{ m}^3/\text{s}$) show a depth of 0.480 feet (0.146 meter) at a station located 15 feet (4.6 meters) upstream of the culvert when the gabions were not present. This station is located in the upstream channel. At the same discharge, and with the gabions in place, the backwater was measured as 0.512 feet (0.156 meter). While backwater affects of the gabions are present, they appear to be small.

6.3.2 Numerical Model Experiments

The hydraulic performance of the channel expansion with gabions present may also be investigated using the FESWMS numerical model. For this purpose that data set from the model validation runs was used. Gabions are simulated by disabling the elements that represent the gabions. This means that no flow can go through these elements. As a rough representation of the cinder blocks used in the physical model experiments, the gabions are represented as elements that are one-half foot wide by one foot long in the direction of flow. For example, Figure 6.4 shows a representation of a square gabion (one-by-one foot) located four feet upstream of the culvert system, along the channel centerline. This is the representation shown as the Gabion 1 model. The Gabion 2 and Gabion 3 models have the gabion located 3 feet and 5 feet upstream of the culvert, respectively. Locating the gabion along the channel centerline effectively breaks up the fluid jet, but it results in too much flow into the outer culvert barrels.

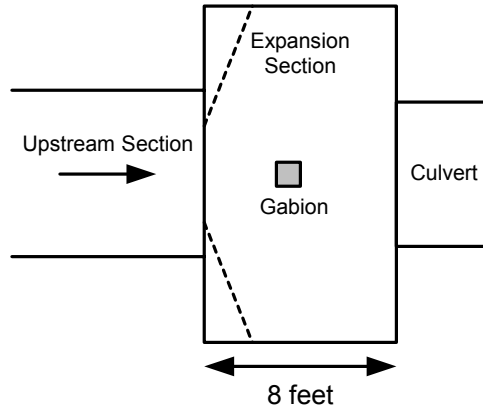


Figure 6.4 Gabion located along the channel centerline

Figure 6.5 shows an alternative location for a gabion pair. Two sets of gabions are shown located 4 feet upstream of the culvert system and 1 foot apart, with each set representing a one-by-one foot gabion. This corresponds to the Gabion 4 model. Gabion 5 model uses two ½ by 1-foot gabions located 4 feet upstream of the culvert and 1 foot apart, while the Gabion 6 model has the gabions located 2 feet apart. Locating a pair of gabions off-centerline allows part of the jet to continue down the channel unimpeded, while sending the remainder of the jet towards the outer barrels.

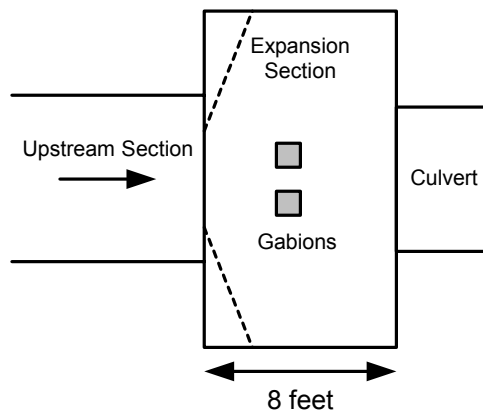


Figure 6.5 Gabion pair located off-center

The results from this set of numerical experiments are summarized in Figure 6.6. With no gabions present the central barrels receive nearly twice the discharge of the outer barrels. Model runs Gabion 1 through Gabion 3 have a single gabion located along the channel centerline (see Figure 6.4). For these cases, the outer four barrels receive almost 80 percent of the channel discharge. There does appear to be some advantage to moving the gabion further upstream from the culvert system. The best alternative appears to use two gabions located off-center. If the spacing is too great (Gabion 6 model run) then there is too much flow concentrated on the central barrels. Gabion 5 model run has the best distribution of flow (flow fractions are 38%, 32%, and 29% for the outer, middle, and

central culvert boxes). However, comparison between the model runs Gabion 5 and Gabion 6 shows that spacing between 1 foot and 2 feet should provide the best results in terms of uniform distribution of discharge between the culvert barrels. This was also suggested by the physical model experiments where a cinder block spacing of approximately 1.5 feet gave a uniform distribution of specific energy across the culvert entrance.

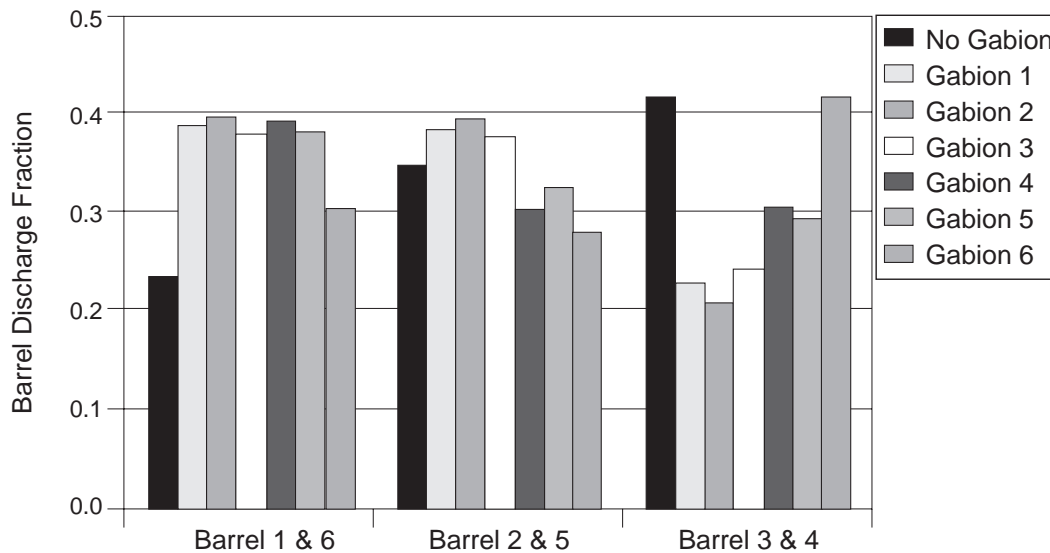


Figure 6.6 Flow distribution from FESWMS model simulations with and without gabions present

7. Summary and Conclusions

7.1 Summary

The overall goal of this research was to develop an improved understanding of the hydraulics of channel expansions leading to low-head, wide culverts; to develop design recommendations for new low-head culverts; and to identify potential remedies for existing culvert systems that are performing poorly due to sediment accumulation. These goals were achieved through a combination of literature review, physical modeling studies, and numerical modeling studies.

The research objectives are listed in Section 1.2. The first objective was to evaluate the hydraulic performance of the channel expansion from a trapezoidal (nonrectangular) channel. While laboratory channels are often rectangular, natural channels frequently vary from trapezoidal to parabolic in cross section, and these natural cross-section shapes strongly influence the flow characteristics in the downstream expansion. For subcritical flow, the water level drops in the upstream channel as the expansion is approached. Because of this decreasing water level and the channel side slopes, the flow near the banks has an inward (centerline) component to its momentum as it enters the expansion. This results in a fluid jet that separates from the channel walls in the expansion section, and the jet does not expand to any significant degree as the water moves downstream. This is shown most clearly in Figures 4.3 and 4.4, and with the velocity distribution shown in Figure 5.9. The conclusion is that because of the natural side slope in the approach channel, the flow distribution in the channel expansion region will not show the expected 4:1 expansion ratio, and the width of the water jet may not increase to any significant degree.

The second objective was to determine the hydraulic performance of box culverts for single and multiple-barrel systems. This objective was met through literature review and through physical model experiments in an indoor channel with 2, 4 and 6 barrels of a box culvert model open, and in a single-barrel box culvert model located in an outdoor channel, where multiple barrel sizes were investigated. The physical modeling results are shown in Figures 4.14 and 4.15. The consistency of the proposed model is superior to other models suggested in the literature (compare with the curves shown in Figure 2.3, where the curves for unsubmerged and submerged conditions do not cross, or they cross with an abrupt change in slope). While the statistical fit in Figure 4.14 has a smaller standard error, physical interpretation of the model coefficients suggests that the model fit shown in Figure 4.15 is preferred. The resulting performance model is presented in equation (6.1) for unsubmerged conditions and equation (6.2) for submerged conditions.

The third objective was to determine the distribution of discharge and specific energy through different barrels of a multiple-barrel culvert system. This distribution was determined experimentally using the physical model and confirmed by the FESWMS numerical model simulations. The data presented in Section 4.3.2 show that the specific energy is fairly uniform across the central four barrels of the 6-barrel culvert. The average specific energy of the middle 4 barrels exceeds that of the outer barrels by more than 35 percent. For experiments with 4 and 2 barrels open, the specific energy is uniform across the barrels. The discharge per barrel was not measured in the physical model experiments, but is related to the upstream specific energy through the nonlinear performance curves

presented in Section 4.4. Based on the measured specific energy distribution and the performance curves, the discharge per barrel for the middle 4 barrels of the 6-barrel culvert is larger than for the outer barrels. As shown in Chapter 5, the same result was found in all numerical simulations of the 6-barrel culvert without gabions present.

The fourth objective was to calibrate the FESWMS numerical simulation model to existing physical model conditions. As described in Sections 5.5.3 and 5.5.4, this was successfully accomplished for sets of data with the model having different physical characteristics (distance of the culvert downstream from the expansion and shape of the channel expansion). Calibration and validation data included velocity and depth values for cross sections at three stations (one upstream of the expansion and two downstream).

Objective five was to apply the calibrated model to investigate and identify potential remedies for the existing culvert systems. This objective is addressed in Sections 5.6 and 6.3.2. It is shown that increasing the expansion ratio will improve the flow distribution through the culvert barrels, but that even with a 4:1 expansion ratio, the discharge through the central barrels remains significantly greater than through the outer barrels. The FESWMS results presented in Chapter 6 show that a combination of two gabions located upstream of the culvert system with one on each side of the channel centerline will significantly modify the distribution of discharge through the culvert barrels, and can result in a uniform distribution of barrel discharge.

The sixth objective was to evaluate the applicability of FESWMS for practical application to the class of problems addressed through this research. Application of FESWMS requires a significant learning curve in understanding the hydraulic system, its model representation, the finite element method, and specific components within the model formulation. The literature review and experience in this research effort suggest that FESWMS is applicable to analysis of culvert and bridge hydraulics, including channel transitions. The model provides reasonable representation of recirculation zones in expansion areas, and it did simulate the standing wave that develops immediately upstream of the culvert entrance. The FESWMS model also provides reasonable estimates of culvert flows, water depths and velocities, and barrel discharges for multiple-barrel culvert systems. Use of the implicit culvert representation models for FESWMS described in Section 5.3.2 are not recommended for low-head culvert analysis. The overall assessment is that the FESWMS model is applicable to the class of problems dealing with channel transitions near highway structures.

7.2 Conclusions and Recommendations

A number of conclusions and recommendations have been drawn from this research. For low-head highway culverts, the headwater should include both the upstream depth and the approach velocity head. For design purposes it is assumed that the approach velocity is equal to the quotient of the barrel discharge and the barrel cross-section area. The resulting velocity head can be a significant fraction of the upstream depth, and neglect of the approach velocity head can result in under prediction of barrel discharge.

The hydraulic performance of the channel expansion was found to be contrary to what was expected based on literature review. The literature suggests that the natural expansion ratio (longitudinal:transverse) is about 4:1. However, neither the physical modeling experiments nor the numerical simulations of this research support this value for the expansion ratio. It is concluded that the combination of the upstream channel cross

section (trapezoidal) and the decrease in water depth immediately upstream of the expansion result in the regions of the channel flow having an inward (centerline) momentum component. The resulting water jet expands only slightly over the relatively short distance between the expansion and the culvert system.

The box culvert performance curve developed through this research predicts a larger barrel discharge as a function of headwater, than is predicted by other literature and FHWA performance curves. In design applications, this results in a smaller required culvert barrel size for a specified design discharge. The design example presented in Chapter 6 suggests that use of channel expansions may not be necessary, even for low-head culvert systems. It is recommended that any culvert design calling for expanding the natural channel width receive special attention and review.

Investigation of potential remedies for existing low-head, wide culvert systems suggests that placement of rock-filled gabions upstream of the culvert, within the highway right-of-way, can be a cost effective solution to problems of nonuniform flow distribution and sedimentation. Both physical and numerical model studies suggest that appropriately-placed gabions can redistribute the flow evenly across the culvert barrels. Furthermore, these studies suggest that sedimentation that may occur will occur immediately downstream of the gabions, within the wake, rather than within the culvert barrels. This would greatly simplify required field maintenance.

References

- Albertson, M.L., Dai, Y.B., Jensen, R.A. and Rouse, H. (1950): Diffusion of Submerged Jets. *Transactions, American Society of Civil Engineers*, 115, pp. 639-664.
- [ASCE] American Society of Civil Engineers (2001): Two Dimensional Hydraulic Modeling of Complex Waterways Using SMS: Training Manual.
- [ASCE/WEF] American Society of Civil Engineers/Water Environment Federation (1992): *Design and Construction of Urban Stormwater Management Systems*, ASCE Manuals and Reports of Engineering Practice No. 77/WEF Manual of Practice FD-20, New York/Alexandria, VA.
- Chow, V.T. (1959): *Open-Channel Hydraulics*, McGraw-Hill, New York.
- DeVantier, B.A. (1989): A Comparison of Primitive Variables and Streamfunction-Vorticity for FEM Depth-Averaged Modeling of Steady Flow, *International Journal for Numerical Methods in Fluids*, Vol. 9, No. 11, pp. 1369-1379.
- Ferguson, B.K. and Deak, T. (1994): Role of Urban Storm-flow Volume in Local Drainage Problems, *Journal of Water Resources Planning and Management*, Vol. 120, No. 4, pp. 523-530.
- [FHWA] Federal Highway Administration (1986): Bridge Waterways Analysis Model: Research Report, Report No. FHWA-RD 86-108, McLean, Virginia.
- French, J.L. (1955): First Progress Report on Hydraulics of Culverts; Hydraulic Characteristics of Commonly Used Pipe Entrances, *NBS Report 4444*, National Bureau of Standards, Washington, D.C.
- French, J.L. (1966): Fifth Progress Report on Hydraulics of Culverts; Nonenlarged Box Culvert Inlets, *NBS Report 9327*, National Bureau of Standards, Washington, D.C.
- Froehlich, D.C. and Trent, R.E. (1989): Hydraulic Analysis of the Schoharie Bridge, Hydraulic Engineering: Proceedings of the 1989 National Conference, ASCE, New York, pp. 887-892.
- Froehlich, D.C. (1996): Finite Element Surface-Water Modeling System: Two-Dimensional Flow in a Horizontal Plane, Version 2, Draft Users Manual, Federal Highway Administration, McLean, VA.
- [HEC] Hydrologic Engineering Center (1995): Flow Transitions in Bridge Backwater Analysis, Research Document No. 42, U.S. Army Corps of Engineers, Hydrologic Engineering Center, Davis, CA.
- [HEC] Hydrologic Engineering Center (1998): HEC – River Analysis System (HEC-RAS), Hydraulic Reference Manual, Version 2.2, U.S. Army Corps of Engineers, Hydrologic Engineering Center, Davis, CA.
- Henderson, F.M. (1966): *Open Channel Flow*, Macmillan, New York.
- Herr, L.A. and Bossy, H.G. (1965): Hydraulic Charts for the Selection of Highway Culverts, Hydraulic Engineering Circular No. 5 (HEC-5), Federal Highway Administration, U.S. Department of Transportation, Washington, D.C.

- Hinds, J. (1928): The Hydraulic Design of Flume and Siphon Transitions, *Transactions, American Society of Civil Engineers*, 92, p. 1423.
- Ippen, A.T. (1950): Channel Transitions and Controls, in *Engineering Hydraulics*, H. Rouse (Ed.), John Wiley and Sons, New York.
- Ippen, A.T. (1960): *Estuarine and Coastline Hydrodynamics*, Engineering Societies Monographs, McGraw-Hill, New York.
- Jones, N.L., Zundel, A.K. and Wallace, R.M. (1995): A Comprehensive Graphical Environment for Surface Water Flow Modeling, Proceedings of the First International Conference on Water Resources Engineering, ASCE, New York, pp. 405-409.
- Kheireldin, K., Fahmey, A. and Gasser, M. (1994): Application of the FESWMS-2DH Software to Solve the Navigation Problem at EL-Menya Bridge in Egypt, *Computing in Civil Engineering*, Proceedings of the First Congress, ASCE, New York, pp. 1244-1250.
- King, I.P. (1994): *RMA-2V Two-Dimensional Finite Element Hydrodynamic Model*, Resource Management Associates, Lafayette, CA.
- Knight, D.W. and Abril, J.B. (1996): Refined Calibration of a Depth-Averaged Model for Turbulent Flow in a Compound Channel, *Proceedings of the Institution of Civil Engineers: Water, Maritime, and Energy*, Vol. 118, No. 3, pp. 151-159.
- Kundu, P.K. (1990): *Fluid Mechanics*, Academic Press, San Diego, CA.
- Langlinais, S.J. (1992): DRAINCALC Release 4.0: A Computer Model for Culvert and Open Channel Design, *Land Reclamation: Advances in Research & Technology*, ASAE Publication 14-92, American Society of Agricultural Engineers, St. Joseph, MI.
- Lee, J.K. and Froehlich, D.C. (1989): *Two-Dimensional Finite-Element Hydraulic Modeling of Bridge Crossings: Research Report*, FHWA-RD-88-146, Federal Highway Administration (FHWA), McLean, VA.
- Liriano, S.L. and Day, R.A. (2001): Prediction of Scour Depth at Culvert Outlets Using Neural Networks, *Journal of Hydroinformatics*, Vol. 3, No. 4, pp. 231-238.
- Mavis, F.T. (1943): The Hydraulics of Culverts, Bulletin No. 56, The Pennsylvania State College, pp. 1-34.
- Metzler, D.E. and Rouse, H. (1959): Hydraulics of Box Culverts, Bulletin 38, State University of Iowa Studies in Engineering, pp. 1-31.
- Murdock, R.C. (2002): Two-dimensional Finite Element Hydraulic Modeling of Channel Expansions Leading to Wide Culverts, M.S. Thesis in Engineering, The University of Texas at Austin.
- Normann, J.M., Houghtalen, R.J. and Johnson, W.J. (2001): Hydraulic Design of Highway Culverts, Second Edition, Hydraulic Design Series No. 5, Federal Highway Administration, U.S. Department of Transportation, Washington, D.C.

- Ports, M.A. and South, N.R. (1995): A Practical Application of Two-Dimensional Hydraulic Analysis for the Baltimore Street Bridge Rehabilitation Project, Proceedings of the First International Conference on Water Resources Engineering, ASCE, New York, pp. 1051-1055.
- Saleh, R.S. and Hwang, R. (1992): Analytical Hydraulic Modeling of Road Culverts, Water Resources Planning and Management: Proceedings of the 1992 National Conference, ASCE, New York, pp. 798-803.
- Scobey, F.C. (1933): The Flow of Water in Flumes, U.S. Department of Agriculture Technical Bulletin 393, December.
- Somes, N.L.G., Bishop, W.A. and Wong, T.H.F. (1999): Numerical Simulation of Wetland Hydrodynamics, *Environment International*, Vol. 25, No. 6, pp. 773-770.
- SonTek web site: <http://www.sontek.com/princop/adv/advpo.htm>
- Streeter, V.L. and Wiley, E.B. (1985): *Fluid Mechanics*, Eighth Edition, McGraw-Hill, New York.
- Thompson, J.C. and James, W.P. (1988): Two-Dimensional Modeling of Buckhorn Creek, Hydraulic Engineering: Proceedings of the 1988 National Conference, ASCE, New York, pp. 1220-1225.
- Tynes, K.A. (1989): Hydraulics of Side-channel Weirs for Regional Detention Basins, M.S. Thesis in Engineering, The University of Texas at Austin.
- Wanielista, M., Kersten, R. and Eaglin, R. (1997): *Hydrology: Water Quantity and Quality Control*, Second Edition, John Wiley and Sons, New York.
- Warnock, J.E. (1950): Hydraulic Similitude, in *Engineering Hydraulics*, H. Rouse (Ed.), John Wiley and Sons, New York.
- Yalin, M.S. (1977): *Mechanics of Sediment Transport*, Second Edition, Pergamon Press, Oxford.
- Yarnell, D.L., Nagler, F.A., and Woodward, S.M. (1926): Flow of Water through Culverts, Bulletin 1, State University of Iowa Studies in Engineering.

